Available online at www.sciencedirect.com
SCIENCE DIRECT®
Physics Reports 419 (2005) 1–64
PHYSICS REPORTS
www.elsevier.com/locate/physrep

Cellular automata models of road traffic

Sven Maerivoet*, Bart De Moor

Department of Electrical Engineering ESAT-SCD (SISTA), Katholieke Universiteit Leuven, Kasteelpark Arenberg 10, 3001 Leuven, Belgium

Accepted 22 August 2005

editor: I. Procaccia

Abstract

In this paper, we give an elaborate and understandable review of traffic cellular automata (TCA) models, which are a class of computationally efficient microscopic traffic flow models. TCA models arise from the physics discipline of statistical mechanics, having the goal of reproducing the correct macroscopic behaviour based on a minimal description of microscopic interactions. After giving an overview of cellular automata (CA) models, their background and physical setup, we introduce the mathematical notations, show how to perform measurements on a TCA model's lattice of cells, as well as how to convert these quantities into real-world units and vice versa. The majority of this paper then relays an extensive account of the behavioural aspects of several TCA models encountered in literature. Already, several reviews of TCA models exist, but none of them consider all the models exclusively from the behavioural point of view. In this respect, our overview fills this void, as it focusses on the behaviour of the TCA models, by means of time–space and phase-space diagrams, and histograms showing the distributions of vehicles' speeds, space, and time gaps. In the report, we subsequently give a concise overview of TCA models that are employed in a multi-lane setting, and some of the TCA models used to describe city traffic as a two-dimensional grid of cells, or as a road network with explicitly modelled intersections. The final part of the paper illustrates some of the more common analytical approximations to single-cell TCA models.

PACS: 02.50.−r; 45.70.Vn; 89.40.−a

Keywords: Cellular automata; Traffic flow modelling; Tempo-spatial behaviour; Phase-space diagrams

Contents

* Corresponding author. Tel.: +32 16 32 17 09; fax: +32 16 32 19 70.
E-mail addresses: sven.maerivoet@esat.kuleuven.be (S. Maerivoet), bart.demoor@esat.kuleuven.be (B. De Moor).
URL: http://www.esat.kuleuven.be/scd (S. Maerivoet).

0370-1573/$ - see front matter © 2005 Published by Elsevier B.V.
doi:10.1016/j.physrep.2005.08.005

0. Introduction

In the field of traffic flow modelling, microscopic traffic simulation has always been regarded as a time consuming, complex process involving detailed models that describe the behaviour of individual vehicles. Approximately a decade ago, however, new microscopic models were being developed, based on the *cellular automata* programming paradigm from *statistical physics*. The main advantage was an *efficient and fast performance* when used in computer simulations, due to their rather low accuracy on a microscopic scale. These so-called *traffic cellular automata* (TCA) are dynamical systems that are discrete in nature, in the sense that time advances with discrete steps and space is coarse-grained (e.g., the road is discretised into cells of 7.5 m wide, each cell being empty or containing a vehicle). This coarse-graininess is fundamentally different from the usual microscopic models, which adopt a semi-continuous space, formed by the usage of IEEE floating-point numbers [1]. True to the spirit of statistical mechanics, all the TCA models discussed in this report do not have a realistic microscopic description of traffic flows as their primary intent, but are rather aimed at obtaining a correct macroscopic behaviour through their crude microscopic description. Such an approach would involve more human-oriented aspects such as those found in socio-economic, behavioural, and psychological sciences. Due to large lack of knowledge about the manner in which human beings operate in a traffic system, traffic engineers currently stick with this higher-level scientific approach. As such, they are able to positively capture the first- and second-order macroscopic effects of traffic streams. TCA models are very flexible and powerful, in that they are also able to capture all previously mentioned basic phenomena that occur in traffic flows [2,3]. In a larger setting, these models describe *self-driven, many-particle systems, operating far from equilibrium*. And in contrast to strictly gaseous analogies, the particles in these systems are intelligent and able to learn from past experience, thereby opening the door to the incorporation of behavioural and psychological aspects [4–6].

The cellular automata approach proved to be quite useful, not only in the field of vehicular traffic flow modelling, but also in other fields such as pedestrian behaviour, escape and panic dynamics, the spreading of forest fires, population growth and migrations, cloud formation, material properties (corrosion, cracks, creases, peeling, etc.), ant colonies and pheromone trails, etc. [7–11]. It is now feasible to simulate large systems containing many ‘intelligent particles’, such that is it possible to observe their interactions, collective behaviour, self-organisation, etc. [12,13,7,6,14–17].

In this report, we provide a detailed description of the methodology of cellular automata applied to traffic flows. We first discuss their background and physical setup, followed by an account of the mathematical notations we adopt. The remaining majority of this report extensively discusses the behavioural aspects of several state-of-the-art TCA models encountered in literature (our overview distinguishes between single-cell and multi-cell models). The report concludes with a concise overview of TCA models in a multi-lane setting, and TCA models used to describe two-dimensional traffic (e.g., a grid for city traffic). We end with a description of several common analytical approximations to single-cell TCA models.

Note that aside from our phenomenological discussion of different TCA models, we refer the reader to the work of Chowdhury et al. [3], Santen [18], and Knospe et al. [19] for more theoretically and quantitatively oriented overviews.

1. Background and physical setup for road traffic

In this section, we give a brief overview of the historic origins of cellular automata, as they were conceived around 1950. We subsequently describe which main ingredients constitute a cellular automaton: the physical environment, the cells’ states, their neighbourhoods, and finally a local transition rule. We then move on to a general description on how cellular automata are applied to vehicular road traffic, discussing their physical environment and the accompanying rule set that describes the vehicles’ physical propagation.

1.1. Historic origins of cellular automata

The mathematical concepts of cellular automata (CA) models can be traced back as far as 1948, when Johann Louis von Neumann introduced them to study (living) biological systems [20]. Central to von Neumann’s work, was the notion of *self-reproduction* and theoretical machines (called *kinematons*) that could accomplish this. As his work progressed, von Neumann started to cooperate with Stanislaw Marcin Ulam, who introduced him to the concept of *cellular spaces*. These described the physical structure of a cellular automaton, i.e., a grid of cells which can be either ‘on’ or ‘off’

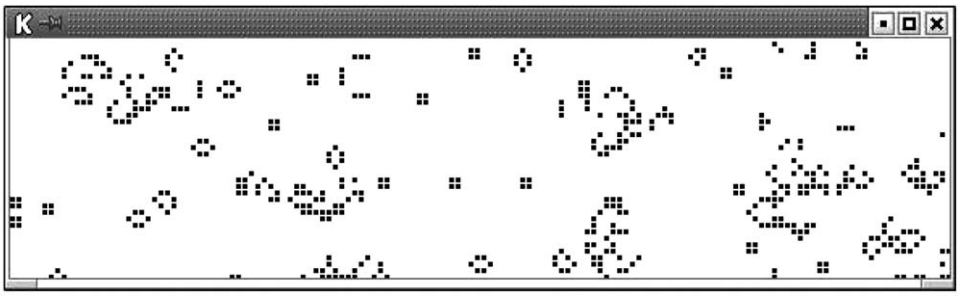

Fig. 1. An example of the Game of Life, with a rectangular grid of cells. Live cells are coloured black, whereas dead cells remain white. The image shows a snapshot during the game's course, illustrating many different shapes to either die out, or live indefinitely by remaining stationary or moving around (image adapted from [143]).

[21,22]. Interestingly, Alan Mathison Turing proposed in 1952 a model that illustrated reaction–diffusion in the context of *morphogenesis* (e.g., to explain the patterns of spots on giraffes, of stripes on zebras, . . .). His model can be seen as a type of continuous CA, in which the cells have a direct analogy with a simplified biological organism [23].

In the 1970s, CA models found their way to one of the most popular applications called 'simulation games', of which John Horton Conway's "*Game of Life*" [24] is probably the most famous. The game found its widespread fame due to Martin Gardner who, at that time, devoted a Scientific American column, called "*Mathematical Games*", to it. Life, as it is called for short, is traditionally 'played' on an infinitely large grid of cells. Each cell can either be 'alive' or 'dead'. The game evolves by considering a cell's all surrounding neighbours, deciding whether or not the cell should live or die, leading to phenomenon called 'birth', 'survival', and 'overcrowding' (or 'loneliness'). An example of a Life game board can be seen in Fig. 1. Typical of Life, is the spawning of a whole plethora of patterns or shapes, having illustrious names such as gliders, guns, space ships, puffers, beehives, oscillators, . . . The Game of Life is now all about how these shapes evolve, and whether or not they die out or live indefinitely (either by remaining stationary or moving around).

The widespread popularisation of CA models was achieved in the 1980s through the work of Stephen Wolfram. Based on empirical experiments using computers, he gave an extensive classification of CA models as mathematical models for self-organising statistical systems [21,25]. Wolfram's work culminated in his mammoth monograph, called *A New Kind of Science* [25]. In this book, Wolfram related cellular automata to all disciplines of science (e.g., sociology, biology, physics, mathematics, . . .). Despite the broad range of science areas touched upon, Wolfram's book has received its share of criticism. As an example of this, we mention the comments of Gray, who points out that Wolfram's results suffer from a rigorous mathematical test. As a consequence, the physical examples in his book are deemed either uncheckable or unconvincing. Gray's final critique is that "*. . . he* [*Wolfram*] *has helped to popularise a relatively little-known mathematical area* (*CA theory*), *and he has unwittingly provided several highly instructive examples of the pitfalls of trying to dispense with mathematical rigour*" [26]. However, with respect to their computational power, CA models can emulate universal Turing machines within the theories of computation and complexity. Recently, Chua took Wolfram's empirical observations one step further, proving that some of the CA models are capable of Turing universal computations. He furthermore introduced the paradigm of *cellular neural networks* (CNN), which provide a very efficient method for performing massive parallel computations, and are a generalisation of cellular automata [27].

Finally, an important step in this direction, is Bill Gosper's proof that the Game of Life is computationally universal, i.e., it can mimic arbitrary algorithms [28]. Notably, one of the most profound testimonies related to this concept, is the work of Konrad Zuse and Edward Fredkin at the end of the 1960s. Their Zuse–Fredkin thesis states that "*The Universe is a cellular automaton*", and is based on the assumption that the Universe's physical laws are discrete in nature [29–31]. This latter statement was also conveyed by Wolfram in his famous CA compendium [25].

1.2. Ingredients of a cellular automaton

From a theoretical point of view, four main ingredients play an important role in cellular automata models [32,22,33]:

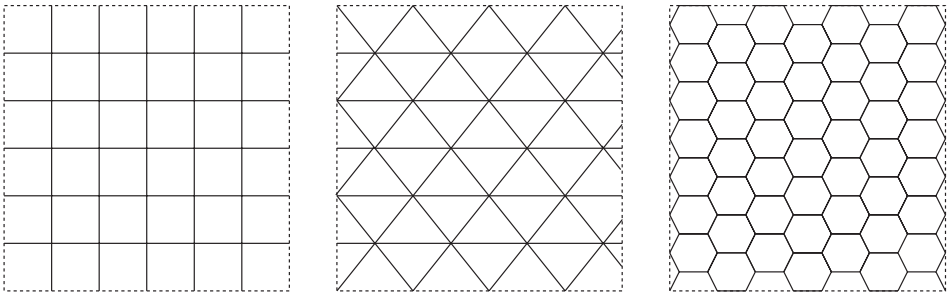

Fig. 2. Some examples of different Euclidean lattice topologies for a cellular automaton in two dimensions. *Left*: rectangular. *Middle*: triangular/isometric. *Right*: hexagonal.

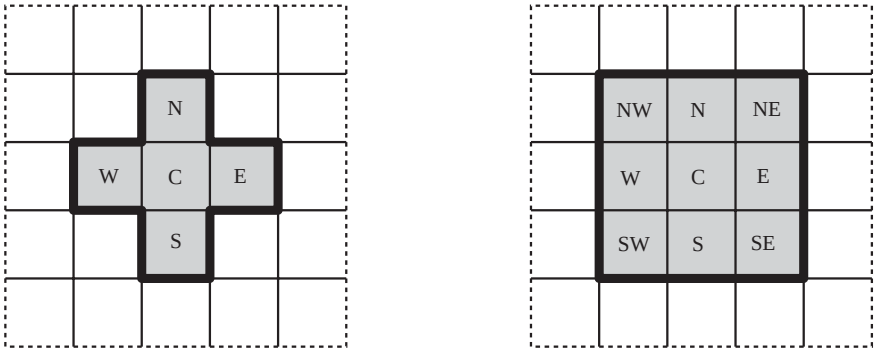

Fig. 3. Two commonly used two-dimensional CA neighbourhoods with a radius of 1: the von Neumann neighbourhood (left) consisting of the central cell itself plus 4 adjacent cells, and the Moore neighbourhood (right) where there are 8 adjacent cells. Note that for one-dimensional CA's, both types of neighbourhoods are the same.

1.2.1. The physical environment

This defines the *universe* on which the CA is computed. This underlying structure consists of a *discrete lattice of cells* with a rectangular, hexagonal, or other topology (see Fig. 2 for some examples). Typically, these cells are all equal in size; the lattice itself can be finite or infinite in size, and its dimensionality can be 1 (a linear string of cells called an *elementary cellular automaton* or ECA), 2 (a grid), or even higher dimensional. In most cases, a common—but often neglected—assumption, is that the CAs lattice is embedded in a *Euclidean space*.

1.2.2. The cells' states

Each cell can be in a certain state, where typically an integer represents the number of distinct states a cell can be in, e.g., a binary state. Note that a cell's state is not restricted to such an integer domain (e.g., $\mathbb{Z}_2$), as a continuous range of values is also possible (e.g., $\mathbb{R}^+$), in which case we are dealing with *coupled map lattices* (CML) [34,35]. We call the states of all cells collectively a CAs *global configuration*. This convention asserts that states are local and refer to cells, while a configuration is global and refers to the whole lattice.

1.2.3. The cells' neighbourhoods

For each cell, we define a neighbourhood that locally determines the evolution of the cell. The size of neighbourhood is the same for each cell in the lattice. In the simplest case, i.e., a one-dimensional lattice, the neighbourhood consists of the cell itself plus its adjacent cells. In a two-dimensional rectangular lattice, there are several possibilities, e.g., with a radius of 1 there are, besides the cell itself, the four north, east, south, and west adjacent cells (*von Neumann neighbourhood*), or the previous five cells as well as the four north–east, south–east, south–west, and north–west diagonal cells (*Moore neighbourhood*); see Fig. 3 for an example of both types of neighbourhoods. Note that as the dimensionality of the lattice increases, the number of direct neighbours of a cell increases exponentially.

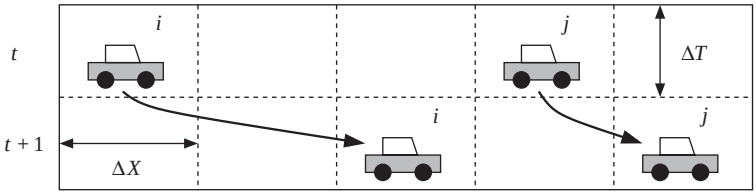

Fig. 4. Schematic diagram of the operation of a single-lane traffic cellular automaton (TCA); here, the time axis is oriented downwards, the space axis extends to the right. The TCA's configuration is shown for two consecutive time steps t and $t+1$, during which two vehicles i and j propagate through the lattice.

1.2.4. A local transition rule

This rule (also called function) acts upon a cell and its direct neighbourhood, such that the cell's state changes from one *discrete time step* to another (i.e., the system's iterations). The CA evolves in time and space as the rule is subsequently applied to all the cells *in parallel*. Typically, the same rule is used for all the cells (if the converse is true, then the term *hybrid* CA is used). When there are no stochastic components present in this rule, we call the model a *deterministic* CA, as opposed to a *stochastic* (also called *probabilistic*) CA.

As the local transition rule is applied to all the cells in the CAs lattice, the global configuration of the CA changes. This is also called the CAs *global map*, which transforms one global configuration into another. This corresponds to the notion of *computing a function* in automata theory, see also Section 2.1. Sometimes, the CAs evolution can be reversed by computing past states out of future states. By evolving the CA backwards in time in this manner, the CAs *inverse global map* is computed. If this is possible, the CA is called *reversible*, but if there are states for which no precursive state exists, these states are called *Garden of Eden* (GoE) states and the CA is said to be *irreversible*.

Finally, when the local transition rule is applied to all cells, its global map is computed. In the context of the theory of dynamical systems, this phenomenon of *local simple interactions* that lead to a *global complex behaviour* (i.e., the spontaneous development of order in a system due to *internal* interactions), is termed *self-organisation* or *emergence*.

Whereas the previous paragraphs discussed the classic approach to CA models, the following sections will exclusively focus on vehicular traffic flows, leading to traffic cellular automata (TCA) models: Section 1.3 discusses the physical environment on which these TCA models are based, and Section 1.4 deals with their accompanying rule set that determines the vehicular motion.

1.3. Road layout and the physical environment

When applying the cellular automaton analogy to vehicular road traffic flows, the physical environment of the system represents the road on which the vehicles are driving. In a classic single-lane setup for traffic cellular automata, this layout consists of a one-dimensional lattice that is composed of individual cells (our description here thus focuses on unidirectional, single-lane traffic). Each cell can either be empty, or is occupied by *exactly* one vehicle; we use the term *single-cell models* to describe these systems. Another possibility is to allow a vehicle to span several consecutive cells, resulting in what we call *multi-cell models*. Because vehicles move from one cell to another, TCA models are also called *particle–hopping models* [36].

An example of the tempo-spatial dynamics of such a system is depicted in Fig. 4, where two consecutive vehicles i and j are driving on a one-dimensional lattice. A typical discretisation scheme assumes $\Delta T = 1\,\mathrm{s}$ and $\Delta X = 7.5\,\mathrm{m}$, corresponding to speed increments of $\Delta V = \Delta X/\Delta T = 27\,\mathrm{km/h}$. The spatial discretisation corresponds to the average length a conventional vehicle occupies in a closely jam packed (and as such, its width is neglected), whereas the temporal discretisation is based on a typical driver's reaction time and we implicitly assume that a driver does not react to events between two consecutive time steps [37].

With respect to the layout of the system, we can distinguish two main cases: closed versus open systems. They correspond to periodic (or cyclic) versus open boundary conditions. The former is usually implemented as a closed ring of cells, sometimes called the *Indianapolis scenario*, while the latter considers an open road. This last type of system, is also called the *bottleneck scenario*. The name is derived from the fact that this situation can be seen as the outflow from a jam, where vehicles are placed at the left boundary whenever there is a vacant spot. Note that, in closed systems,

the number of vehicles is always conserved, leading to the description of *number conserving cellular automata* (NCCA) [38].

1.4. Vehicle movements and the rule set

The propagation of the individual vehicles in a traffic stream, is described by means of a rule set that reflects the car-following and lane-changing behaviour of a traffic cellular automaton evolving in time and space. The TCAs local transition rule actually comprises this set of rules. They are consecutively applied to all vehicles in parallel (called a *parallel update*). So in a classic setup, the system's state is changed through *synchronous position updates* of all the vehicles: for each vehicle, the new speed is computed, after which its position is updated according to this speed and a possible lane-change manoeuvre. Note that there are other ways to perform this update procedure, e.g., a random sequential update (see Section 3.2.4). Because time is discretised in units of ΔT seconds, an *implicit reaction time* is assumed in TCA models. It is furthermore assumed that a driver does not react to events between consecutive time steps.

For single-lane traffic, we assume that vehicles act as *anisotropic particles*, i.e., they only respond to frontal stimuli. So typically, the car-following part of a rule set only considers the direct frontal neighbourhood of the vehicle to which the rules are applied. The radius of this neighbourhood should be taken large enough such that vehicles are able to drive collision-free. Typically, this radius is equal to the maximum speed a vehicle can achieve, expressed in cells per time step.

From a microscopic point of view, the process of a vehicle following its predecessor is typically expressed using a *stimulus–response relation* [1]. Typically, this response is the speed or the acceleration of a vehicle; in TCA models, a vehicle's stimulus is mainly composed of its speed and the distance to its leader, with the response directly being a new (adjusted) speed of the vehicle. In a strict sense, this only leads to the avoidance of accidents. Some models however, incorporate more detailed stimuli, such as anticipation terms. These forms of 'anticipation' only take leaders' reactions into account, *without predicting* them. When these effects are taken into account together with a safety distance, strong accelerations and abrupt braking can be avoided. Hence, as the speed variance is decreased, this results in a more stable traffic stream [39–41].

To conclude this section, we note that a TCA model can also be derived from a so-called Gipps car-following model. All speeds in this Gipps model are directly computed from one discrete time step to another [1]. If now the spatial dimension is also discretised (a procedure called *coarse graining*), then this will result in a TCA model.

2. Mathematical notation

In this section, we give an overview of the mathematical notation adopted throughout this report. The focus will be on the variables in TCA models, the measurements that can be done on a TCA model's lattice, and their conversion to real-world units. We first take a look at the notation that is commonly used in automata theory, from which cellular automata sprung.

2.1. Classic notation based on automata theory

Let us first briefly present the notation for cellular automata models, adopted in spirit of *automata theory*. As mentioned in Section 1, a CA model represents a discrete dynamic system, consisting of four ingredients:

$$\mathrm{CA} = (\mathscr{L}, \Sigma, \mathscr{N}, \delta) \ , \tag{1}$$

where the physical environment is represented by the discrete lattice $\mathscr{L}$ and the set of possible states denoted by Σ. Each ith cell of the lattice, has at time step t a state $\sigma_i(t) \in \Sigma$. Furthermore, the associated neighbourhood with this cell is represented by $\mathscr{N}_i(t)$, i.e., a (partially) ordered set of cells. Finally, the local transition rule is represented as

$$\delta : \Sigma^{|\mathscr{N}|} \longrightarrow \Sigma : \bigcup_{j \in \mathscr{N}_i(t)} \sigma_j(t) \longmapsto \sigma_i(t+1) \ . \tag{2}$$

Eq. (2) shows that the state of the ith cell at the next time step $t+1$ is computed by δ based on the states of all the cells in its neighbourhood at the current time step t. In the previous equation, $|\mathcal{N}|$ represents the number of cells in this neighbourhood, which is taken to be invariant with respect to time and space. Note that the local transition rule is commonly given by a *rule table*, where the output state is listed for each possible input configuration of the neighbourhood. Given the sizes of Σ and $\mathcal{N}$, the total number of possible rules equals:

$$|\Sigma^{\Sigma^{\mathcal{N}}}| \ , \tag{3}$$

where each of the $|\Sigma^{\mathcal{N}}|$ possible configurations of a cell's neighbourhood is mapped to the number of possible states a cell can be in.

Considering the ordered set of all the states of all cells collectively at time step t, a CAs global configuration is obtained as

$$\mathscr{C}(t) = \bigcup_{j \in \mathscr{L}} \sigma_j(t) \ , \tag{4}$$

with $\mathscr{C}(t) \in \Sigma^{\mathscr{L}}$ where the latter refers to the set of all possible global configurations a CA can be in (also called its *phase space*). Sometimes, such a global configuration $\mathscr{C}(t)$ is also represented by its characteristic polynomial (i.e., generating function) [42]:

$$\mathscr{C}(t) = \sum_{j=0}^{|\mathscr{L}|} \sigma_j(t) x^j \ . \tag{5}$$

If we now apply the local transition rule to all the cells in the CAs lattice, the next configuration of the CA can be computed by its induced global map:

$$G : \Sigma^{\mathscr{L}} \longrightarrow \Sigma^{\mathscr{L}} : \mathscr{C}(t) \longmapsto \mathscr{C}(t+1) \ . \tag{6}$$

Note that if the CA is reversible, the inverse global map G^{-1} can be computed. As the CA evolves in time and space, the global map is iterated from a certain initial configuration $\mathscr{C}(0)$ at $t=0$, leading to the following sequence of configurations:

$$\mathscr{C}(0) \to G(\mathscr{C}(0)) \to G^2(\mathscr{C}(0)) \to G^3(\mathscr{C}(0)) \to \cdots \tag{7}$$

The above sequence is called the *trajectory* of the initial configuration $\mathscr{C}(0)$ under the global map G, and we denote it by

$$\mathscr{T}_{\mathscr{C}(0)|G} = \{G^n(\mathscr{C}(0)) | n \in \mathbb{N}\} \ . \tag{8}$$

When this trajectory is periodic or chaotic, we use the terminology *forward orbit* and denote it by $\mathscr{O}^+_{\mathscr{C}(0)|G}$. Similarly, the *backward orbit* (i.e., the reverse trajectory) is denoted by $\mathscr{O}^-_{\mathscr{C}(t)|G^{-1}}$, where we specify a certain global configuration $\mathscr{C}(t)$ at time step t under the inverse global map G^{-1}.

2.1.1. Classification of CA rules

Computing the global map G is rather difficult, as it may require many or even an infinite amount of iterations in order to obtain the trajectories. In practice, the system's lattice size should be taken infinitely large, but even only considering 1000 cells of a binary elementary cellular automaton (ECA) would increase the size of the search space of global configurations to $2^{1000} \approx 10^{300}$.

A more intuitive methodology, is to observe a CAs tempo-spatial behaviour, i.e., its evolution on the lattice in the course of time. To this end, Stephen Wolfram empirically studied many configurations of binary ECA rules, with a neighbourhood of three cells. According to Eq. (3), this amounts to $2^{2^3} = 256$ different rules. In 1984, based on this research, Wolfram conjectured four distinct *universality classes* [43]:

Class I: These CA evolve after a finite number of iterations to a unique homogeneous state, i.e., a *limit point*.

Class II: These CA generate regular, periodic patterns, i.e., entering a *limit cycle*.

Class III: CAs in this class evolve to a periodic patterns, independent of the initial configuration; their trajectories in the configuration space lie on a *chaotic attractor*.

Class IV: This class encompasses all the CAs that seem to behave in a *complex* way, with features such as propagating structures, long transients; they are thought to have the capability of universal computation.

Although Wolfram's classification scheme is widely adopted, it still remains a tentative result as he himself states [25]. Note that the type of classification he provides is *phenotypic*, in the sense that it is based on observed behaviour, whereas a *genotypic* classification would be based on the intrinsic structure of the rules in each class.

Despite these observations, classification still remains a difficult task as is evidenced by the ongoing research in dynamical systems. Other attempts at classification of ECA rules include the following. Firstly, Čulik and Yu gave a formalisation of Wolfram's classes [44]. Secondly, Li and Packard studied the structure of the ECA rule space according to a certain distance metric, resulting in five classes [45]. Then, Braga et al. identified three classes based on the growth of patterns observed in CA models [46]. Next, Wuensche used a whole arsenal of local measures to automatically create complex rules, thereby classifying the rule space for the CAs' dynamics [47]. Furthermore, Dubacq et al. classified CA models based on their algorithmic complexity by measuring the information content of the local transition rule [48]. And finally, Fatès who used a macroscopic parameter, i.e., the density of 1's, to separate chaotic ECA rules from non-chaotic ones [49].

2.1.2. An example of a CA

To end this section, let us give some definitions of a one-dimensional, infinitely large, binary state CA with a neighbourhood of radius 1:

$$\mathscr{L} = \mathbb{Z}^d \quad (\text{with } d = 1)\ , \tag{9}$$

$$\Sigma = \mathbb{Z}_2 = \{0, 1\}\ , \tag{10}$$

$$\mathscr{N}_i = \{i-1, i, i+1\}\ , \tag{11}$$

$$\begin{aligned} \delta(i,t) &: \mathbb{Z}_2^3 \longrightarrow \mathbb{Z}_2 \\ &: \{\sigma_{i-1}(t), \sigma_i(t), \sigma_{i+1}(t)\} \longmapsto \sigma_i(t+1)\ , \end{aligned} \tag{12}$$

$$\begin{aligned} G(\mathscr{C}(t)) &: \mathbb{Z}_2^{\mathbb{Z}} \longrightarrow \mathbb{Z}_2^{\mathbb{Z}} \\ &: \mathscr{C}(t) \longmapsto \mathscr{C}(t+1)\ . \end{aligned} \tag{13}$$

Note that in Eq. (11), we assume that the *i*th cell's neighbourhood is represented by integer indices (i.e., the cells form a totally ordered set). This alleviates the need for an explicit representation of the cells themselves, as it is now sufficient to work with the cells' indices and states. The transition rule δ in Eq. (12) takes as its arguments a cell's index i and current time step t, but operates on the states of this cell's neighbourhood. The global map in Eq. (13) operates on the global configuration of the CA at time step t.

2.2. Basic variables and conventions

Conforming to the setup and notation discussed in the previous sections, we denote a TCAs discrete lattice by $\mathscr{L}$ (for the remainder of this section, we assume a *rectangular lattice*). This lattice physically represents the road on which vehicles will drive in a TCA model. It consists of $L_{\mathscr{L}}$ lanes, each of which has $K_{\mathscr{L}}$ cells, so in total there are $L_{\mathscr{L}} \times K_{\mathscr{L}}$ cells in the lattice ($L_{\mathscr{L}}, K_{\mathscr{L}} \in \mathbb{N}_0$). Each cell can either be empty, or occupied with a single vehicle that spans one or more consecutive cells. An example of a lattice containing several vehicles, can be seen in Fig. 5.

Based on the microscopic vehicle characteristics of a vehicle's space headway, space gap, length, time headway, time gap, and occupancy time, we propose to use the following set of definitions for *multi-lane* vehicular road traffic flows that are *heterogeneous* (in the sense of having different vehicle lengths) [50]:

$$g_{s_i}^{l,f} = x_i^{l,f} - x_i - l_i\ , \tag{14}$$

$$g_{s_i}^{r,f} = x_i^{r,f} - x_i - l_i\ , \tag{15}$$

$$g_{s_i}^{l,b} = x_i - x_i^{l,b} - l_i^{l,b}\ , \tag{16}$$

$$g_{s_i}^{r,b} = x_i - x_i^{r,b} - l_i^{r,b} \tag{17}$$

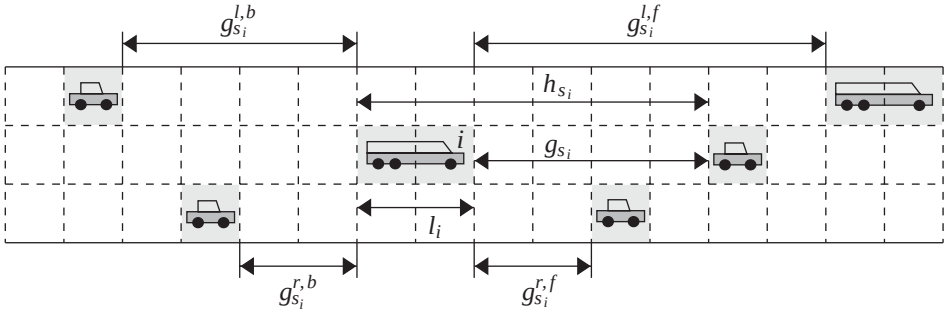

Fig. 5. A portion of the lattice $\mathscr{L}$ at a certain time step; it has $L_{\mathscr{L}} = 3$ lanes, containing six vehicles. The central vehicle i has a space headway $h_{s_i} = 6$ cells, consisting of a space gap $g_{s_i} = 4$ cells and its length $l_i = 2$ cells. There are four other space gaps to be considered when the neighbouring lanes are taken into account: $g_{s_i}^{l,f}$ (left-front), $g_{s_i}^{l,b}$ (left-back), $g_{s_i}^{r,f}$ (right-front), and $g_{s_i}^{r,b}$ (right-back), equalling 6, 4, 2 and 2 cells, respectively.

for which we assume that a vehicle's position is denoted by the cell that contains its rear bumper. For the example in Fig. 5, the left and right frontal and backward space gaps of the central vehicle i are 6, 4, 2 and 2 cells, respectively (all these space gaps thus represent effective distances, corresponding to the number of empty cells between vehicles). Similar definitions hold for the space headways $h_{s_i}^{l,f}$, $h_{s_i}^{r,f}$, $h_{s_i}^{l,b}$, and $h_{s_i}^{r,b}$, i.e., the vehicle lengths in the right-hand sides of Eqs. (14)–(17) are dropped. Derivations for the time gaps $g_{t_i}^{l,f}$, $g_{t_i}^{r,f}$, $g_{t_i}^{l,b}$, and $g_{t_i}^{r,b}$, and time headways $h_{t_i}^{l,f}$, $h_{t_i}^{r,f}$, $h_{t_i}^{l,b}$, and $h_{t_i}^{r,b}$ are analogous.

Discriminating between frontal an backward neighbours in the adjacent lanes to the ith vehicle, is done based on their positions, i.e.:

$$\{x_i^{l,b}, x_i^{r,b}\} < x_i \leqslant \{x_i^{l,f}, x_i^{r,f}\} \ . \tag{18}$$

According to Eq. (18), a vehicle that is driving alongside in an adjacent lane to the ith vehicle, will be considered as a backward neighbour as long as its rear bumper is located strictly behind the rear bumper of the ith vehicle (even if this neighbour has a large length that 'sticks out' in front of the ith vehicle).

Under the above set of assumptions, we can now write the conditions for a successful lane change (i.e., a possible gap acceptance) as the following constraints:

$$g_{s_i}^{l,f} \geqslant 0 \wedge g_{s_i}^{l,b} \geqslant 0 \quad \text{(left lane change)} \ , \tag{19}$$

$$g_{s_i}^{r,f} \geqslant 0 \wedge g_{s_i}^{r,b} \geqslant 0 \quad \text{(right lane change)} \ . \tag{20}$$

With respect to the domains of all variables, we note that all vehicle lengths, space gaps, and space headways are expressed as integers, or more specifically:

$$\begin{aligned} &l_i, h_{s_i}, h_{s_i}^{l,b}, h_{s_i}^{r,b} \in \mathbb{N}_0 \ , \\ &g_{s_i}, h_{s_i}^{l,f}, h_{s_i}^{r,f} \in \mathbb{N} \ , \\ &g_{s_i}^{l,b}, g_{s_i}^{r,b}, g_{s_i}^{l,f}, g_{s_i}^{r,f} \in \mathbb{Z} \ . \end{aligned}$$

In contrast to this, the occupancy times, time headways, and time gaps are not restricted to the domain of integers, i.e.:

$$\begin{aligned} &\rho_i, h_{t_i}, h_{t_i}^{l,b}, h_{t_i}^{r,b} \in \mathbb{R}_0^+ \ , \\ &g_{t_i}, h_{t_i}^{l,f}, h_{t_i}^{r,f} \in \mathbb{R}^+ \ , \\ &g_{t_i}^{l,b}, g_{t_i}^{r,b}, g_{t_i}^{l,f}, g_{t_i}^{r,f} \in \mathbb{R} \ . \end{aligned}$$

For example, the occupancy time ρ_i as defined by $\rho_i = l_i / v_i$ [50], corresponds to the time a vehicle 'spends' in its own cells.

To conclude, each vehicle i in the lattice has an associated speed $v_i \in \mathbb{N}$ (expressed in cells per time step ΔT), which is bounded by a maximum speed $v_{\max} \in \mathbb{N}_0$. For example, if we set $\Delta T = 1.2\,\text{s}$, $\Delta X = 7.5\,\text{m}$, and $v_{\max} = 5\,\text{cells/time}$

step, then $v_i \in \{0, \ldots, 5\}$ which corresponds to a maximum of $5 \times \Delta X/\Delta T = 5 \times 7.5\,\mathrm{m/s} \div 1.2\,\mathrm{s} = 31.25\,\mathrm{m/s} = 112.5\,\mathrm{km/h}$. As can be seen in this derivation, we only consider positive speeds in our models, i.e., vehicles always move forward.

2.3. Performing macroscopic measurements

The previously discussed quantities are all microscopic traffic stream characteristics. In this section, we reconsider the macroscopic quantities densities, flows, and mean speeds [50]. As we now have to measure these quantities on a TCAs lattice $\mathscr{L}$, we present three possibilities for obtaining the data points:

- by performing local measurements with an artificial loop detector of finite length (open and closed systems),
- by performing global measurements on the entire lattice (closed system),
- and by performing local measurements with an artificial loop detector of unit length (open and closed systems).

In the following three sections, we give detailed derivations of each of these measurement techniques. Locally measured quantities are indicated by a 'l' subscript, whereas globally measured ones are indicated by an 'g' subscript. A temporal and spatial discretisation of, respectively, ΔT (in seconds) and ΔX (in metres) is implicitly assumed.

For all following techniques, we assume an integer measurement period of T_{mp} time steps. Thus, aggregating data into intervals of 60 s with $\Delta T = 1.2\,\mathrm{s}$, requires a measurement period of:

$$T_{\mathrm{mp}} = \left\lceil \frac{60}{1.2} \right\rceil = 50 \text{ time steps} . \tag{21}$$

Furthermore, densities are expressed in vehicles per cell, flows in vehicles per time step, and space-mean speeds in cells per time step.

2.3.1. Local measurements with a detector of finite length

In this section, we deal with an artificial loop detector of finite length $K_{\mathrm{ld}} \in \mathbb{N}_0$, located in a single lane. Note that typically, $K_{\mathrm{ld}} \geqslant v_{\max}$, so as to ensure that no vehicles can 'skip' the detector between consecutive time steps. The first step in our approach for performing these measurements, is based on obtaining local measurements of the density and flow for such a spatial measurement region at a certain time step t [50]. Once these are known, the space-mean speed can be derived using the fundamental relation of traffic flow theory $q = k\overline{v}_s$ [50]:

$$k_l(t) = \frac{N(t)}{K_{\mathrm{ld}}} , \tag{22}$$

$$q_l(t) = \frac{1}{K_{\mathrm{ld}}} \sum_{i=1}^{N(t)} v_i(t) , \tag{23}$$

$$\Downarrow$$

$$\overline{v}_{s_l}(t) = \frac{q_l(t)}{k_l(t)} = \frac{1}{N(t)} \sum_{i=1}^{N(t)} v_i(t) , \tag{24}$$

where we assumed $N(t)$ vehicles are present at time t in the loop detector's segment. The density and flow measurements of consecutive time steps are now temporally averaged over subsequent spatial measurement regions. In similar fashion as before, the space-mean speed is derived using the previously mentioned fundamental

relation:

$$k_l = \frac{1}{T_{\text{mp}}} \sum_{t=1}^{T_{\text{mp}}} k_l(t) = \frac{1}{T_{\text{mp}} K_{\text{ld}}} \sum_{t=1}^{T_{\text{mp}}} N(t) \ , \tag{25}$$

$$q_l = \frac{1}{T_{\text{mp}}} \sum_{t=1}^{T_{\text{mp}}} q_l(t) = \frac{1}{T_{\text{mp}} K_{\text{ld}}} \sum_{t=1}^{T_{\text{mp}}} \sum_{i=1}^{N(t)} v_i(t) \ , \tag{26}$$

$$\Downarrow$$

$$\overline{v}_{s_l} = \frac{q_l}{k_l} = \sum_{t=1}^{T_{\text{mp}}} \sum_{i=1}^{N(t)} v_i(t) \Bigg/ \sum_{t=1}^{T_{\text{mp}}} N(t) \ , \tag{27}$$

$$= \sum_{t=1}^{T_{\text{mp}}} N(t) \frac{1}{N(t)} \sum_{i=1}^{N(t)} v_i(t) \Bigg/ \sum_{t=1}^{T_{\text{mp}}} N(t) \ ,$$

$$= \sum_{t=1}^{T_{\text{mp}}} N(t) \overline{v}_{s_l}(t) \Bigg/ \sum_{t=1}^{T_{\text{mp}}} N(t) \ . \tag{28}$$

Our derivations for k_l and q_l as outlined above, also correspond to the generalised definitions of density and flow, defined as the total time spent, respectively, the total distance travelled, divided by the area of the measurement region (which corresponds to $T_{\text{mp}} \times K_{\text{ld}}$). Furthermore, note that the last Eq. (28) essentially is a weighted mean of the local space-mean speeds $\overline{v}_{s_l}(t)$ at each time step t, with the number of vehicles $N(t)$ as weights.

2.3.2. Global measurements on the entire lattice

For the global measurements, we consider N vehicles that are driving in a closed single-lane system, i.e., with a length of $K_{\mathscr{L}}$ cells (the extension to multi-lane traffic is straightforward). As a consequence, the global density k_g remains constant during the entire measurement period. The derivations of the equations for k_g, q_g, and $\overline{v}_{s_g}$, are completely equivalent to those of the previous Section 2.3.1, but now with $K_{\text{ld}} = K_{\mathscr{L}}$:

$$k_g = \frac{N}{K_{\mathscr{L}}} \ , \tag{29}$$

$$q_g = \frac{1}{T_{\text{mp}} K_{\mathscr{L}}} \sum_{t=1}^{T_{\text{mp}}} \sum_{i=1}^{N} v_i(t) \ , \tag{30}$$

$$\Downarrow$$

$$\overline{v}_{s_g} = \frac{q_g}{k_g} = \frac{1}{T_{\text{mp}} N} \sum_{t=1}^{T_{\text{mp}}} \sum_{i=1}^{N} v_i(t) \ , \tag{31}$$

$$= \frac{1}{T_{\text{mp}} N} \sum_{t=1}^{T_{\text{mp}}} N \frac{1}{N} \sum_{i=1}^{N} v_i(t) \ ,$$

$$= \frac{1}{T_{\text{mp}}} \sum_{t=1}^{T_{\text{mp}}} \overline{v}_{s_g}(t) \ . \tag{32}$$

Note that, for single-cell TCA models, the global density computed with Eq. (29) actually corresponds to the macroscopic characteristic called occupancy ρ [50]. For multi-cell models, the number of vehicles is in general less than the number of occupied cells.

2.3.3. Local measurements with a detector of unit length

The third technique for measuring macroscopic traffic flow characteristics on a TCA's lattice, bears perhaps the closest resemblance to reality: it is based on an artificial loop detector with unit length, i.e., $K_{\text{ld}} = 1$ cell. The loop detector now explicitly counts all the vehicles that pass it at each time step ΔT during the measurement period T_{mp}.

This type of measurement corresponds to a point measurement in a temporal measurement region. Because of this, the appropriate method for computation is different from the one used in the previous two sections: we now first compute the local flow, and the local space-mean speed, both for single-lane traffic. The local density is then derived according to the previously mentioned fundamental relation, resulting in the following set of equations:

$$q_l = \frac{N}{T_{\text{mp}}} , \tag{33}$$

$$\overline{v}_{s_l} = \left(\frac{1}{N} \sum_{i=1}^{N} \frac{1}{v_i} \right)^{-1} , \tag{34}$$

$$\Downarrow$$

$$k_l = \frac{q_l}{\overline{v}_{s_l}} , \tag{35}$$

in which N now denotes the number of vehicles that have passed the detector during the measurement period T_{mp}. Because the detector physically occupies one cell and because a vehicle has to 'drive by' in order to get counted, this means that stopped vehicles are ignored: *only moving vehicles are counted*. Note that, as opposed to the previous two techniques, the above measurements no longer denote temporal averages. And because we are working with a temporal measurement region, we have to take the harmonic average of the vehicles' speeds v_i in order to obtain the local space-mean speed $\overline{v}_{s_l}$ [50].

2.4. Conversion to real-world units

Converting between TCA and real-world units seems straightforward, as we only need to suitably multiply with or divide by the temporal and spatial discretisations ΔT and ΔX, respectively. However, problems arise due to the discrete nature of a TCA model, involving some intricacies with respect to coordinate systems and their associated units. For example, as defined in Section 2.2, a vehicle i's space headway h_{s_i} is always an integer, expressing the number of cells. The same holds true for its space gap g_{s_i} and length l_i. The difficulty now lies in the fact that fractions of cells are not representable in our definition of a TCA model. Keeping in mind that $h_{s_i} = g_{s_i} + l_i$ [50], and noting that $h_{s_i} \in \mathbb{N}_0$, it follows that $g_{s_i} + l_i > 0$, which means that either $g_{s_i} \neq 0$ and/or $l_i \neq 0$.

As a solution, we therefore adopt throughout this report the convention that, without loss of generality, a vehicle's length $l_i \geqslant 1$ cell (which agrees perfectly with our earlier definitions in Section 2.2). Consequently, when a vehicle i is residing in a compact jam (i.e., 'bumper-to-bumper' traffic), its space headway $h_{s_i} = l$ cells and its space gap $g_{s_i} = 0$ cells. Our convention thus gives a rigorous justification to formulate the TCAs update rules more intuitively using space gaps, because as already stated in Section 1.4, the rules in a TCA rule set are typically not expressed in terms of space headways, but rather in terms of speeds and space gaps (i.e., the distance to the leading vehicle).

In a similar fashion, time headways, time gaps, and occupancy times represent multiples of the temporal discretisation ΔT. But note that, as explained before in Section 2.2, these are however no longer constrained to integer values.

In the following two sections, we explain how to convert between coordinate systems of TCA models and the real world. All common variables (e.g., h_{s_i}) are expressed in *TCA units*, except for their 'primed' counterparts (e.g., h'_{s_i}), which are expressed in *real-world units*. The conversions will be done with respect to the following conventions:

- **TCA model**
  - h_{s_i}, g_{s_i}, and l_i are dimensionless integers, denoting a number of cells,
  - h_{t_i}, g_{t_i}, and ρ_i are dimensionless real numbers, denoting a fractional multiple of a time step,
  - k_l and k_g are real numbers, expressed in vehicles/cell,
  - q_l and q_g are real numbers, expressed in vehicles/time step,
  - and v_i, $\overline{v}_{s_l}$, and $\overline{v}_{s_g}$ are real numbers, expressed in cells/time step.

- **Real world**
  - ΔX, h'_{s_i}, g'_{s_i}, and l'_i are real numbers, expressed in metres,
  - ΔT, h'_{t_i}, g'_{t_i}, and ρ'_i are real numbers, expressed in seconds,
  - k'_l and k'_g are real numbers, expressed in vehicles/kilometre,
  - q'_l and q'_g are real numbers, expressed in vehicles/hour,
  - and v'_i, $\overline{v}'_{s_l}$, and $\overline{v}'_{s_g}$ are real numbers, expressed in kilometres/hour.

2.4.1. From a TCA model to the real world

Under the previously mentioned convention that $l_i \in \mathbb{N}_0$, we can write the conversions of the microscopic characteristics related to the space and time headways and gaps, and the vehicle lengths and occupancy times, in a straightforward manner:

$$h'_{s_i} = h_{s_i} \cdot \Delta X, \quad g'_{s_i} = g_{s_i} \cdot \Delta X, \quad l'_i = l_i \cdot \Delta X \ ,$$

$$h'_{t_i} = h_{t_i} \cdot \Delta T, \quad g'_{t_i} = g_{t_i} \cdot \Delta T, \quad \rho'_i = \rho_i \cdot \Delta T \ . \tag{36}$$

Relative to Eqs. (36), there is a small but important detail that is easily overlooked: we cannot just convert between g_{s_i}, g'_{s_i}, l_i, and l'_i without making some assumptions. Because we adopted the convention that $l_i \geqslant 1$ cell, it follows that $l'_i \geqslant \Delta X$. So it is not possible to take the real length of a vehicle smaller than the spatial discretisation, because we assumed that the spatial units of a TCA model are all integer values.

The conversions for the macroscopic traffic stream characteristics densities, flows, and space-mean speeds, as well as the microscopic vehicle speed, are as follows:

$$k' = k \cdot \frac{1000}{\Delta X} \ ,$$

$$q' = q \cdot \frac{3600}{\Delta T} \ ,$$

$$\overline{v}'_s = \overline{v}_s \cdot 3.6 \cdot \frac{\Delta X}{\Delta T} \ . \tag{37}$$

To keep the previous equations clear, we have dropped the subscripts denoting global and local measurements.

It is interesting to see what happens at the jam density, i.e., the maximum density when all cells in the lattice are occupied. As all vehicles are standing still bumper-to-bumper, the associated space gap at this density, equals zero. Computing the space headway, results in $h_{s_i} = 0 + l_i$. By virtue of the fact that density is inversely proportional to the average space headway [50], we can cast this space headway into a density, e.g., for a single-cell TCA model: $k_j = \overline{h}_{s_j}^{-1} = \overline{l}^{-1} = l_i^{-1} = 1$. Applying the conversion by means of Eqs. (37) and assuming a spatial discretisation $\Delta X = 7.5\,\text{m}$, results in a real-world jam density $k'_j = 1000 \div 7.5\,\text{m} \approx 133\,\text{vehicles/km}$. Conversely, if we know k'_j, then we can derive k_j (see Section 2.4.2) and hence we have a method to pick a ΔX.

If we were to consider multi-cell traffic, e.g., vehicles with different lengths, then the jam density would be inversely proportional to the average vehicle length. A solution here is to assume a common unit for all vehicle lengths, e.g., passenger car units (PCU) [50]. Even though the jam density can be defined for each vehicle class separately, it would be more correct to speak of an *average jam density* at this point due to the temporal and spatial variations in traffic flows.

2.4.2. From the real world to a TCA model

Based on Eqs. (36), we can write the reverse conversion of the microscopic characteristics in the following manner:

$$h_{s_i} = \frac{h'_{s_i}}{\Delta X}, \quad g_{s_i} = \frac{g'_{s_i}}{\Delta X}, \quad l_i = \frac{l'_i}{\Delta X} \ ,$$

$$h_{t_i} = \frac{h'_{t_i}}{\Delta T}, \quad g_{t_i} = \frac{g'_{t_i}}{\Delta T}, \quad \rho_i = \frac{\rho'_i}{\Delta T} \ . \tag{38}$$

In order to agree with our previously stated convention, i.e., all spatial microscopic characteristics in a TCA model are integers, Eqs. (38) implicitly assume that the real-world spatial variables are multiples of the spatial discretisation (e.g., $h'_{s_i} = m \cdot \Delta X$ with $m \in \mathbb{N}_0$).

Another possible approach to the spatial conversion to TCA model units, is to *approximate* the real-world values as best as possible, whilst keeping our adopted convention. As $l_i \geqslant 1$ cell, this leads to the following scheme where we use upward rounding (i.e., ceiling):

$$h_{s_i} = \left\lceil \frac{h'_{s_i}}{\Delta X} \right\rceil, \quad l_i = \left\lceil \frac{l'_i}{\Delta X} \right\rceil ,$$

$$\Longrightarrow g_{s_i} = h_{s_i} - l_i \ . \tag{39}$$

For example, if $\Delta X = 7.5\,\text{m}$, $l'_i = 4.5\,\text{m}$, and $g'_{s_i} = 5\,\text{m}$, then $h'_{s_i} = 4.5 + 5 = 9.5\,\text{m}$, and from Eq. (39) it follows that $h_{s_i} = 2$ cells, $l_i = 1$ cell, and $g_{s_i} = 2 - 1 = 1$ cell. Because Eq. (39) is only an approximation, it more than often occurs that the computed space headway 'exceeds' the real-world space headway.

In similar spirit, the conversion for the macroscopic characteristics can be easily derived from Eqs. (37). However, as opposed to Eqs. (38) and (39), there is no need for an approximation by means of rounding, because these quantities are real numbers, as mentioned in the introduction of Section 2.4.

3. Single-cell models

Having discussed the mathematical and physical aspects of cellular automata and TCA models in particular, we now focus on single-cell models. As explained before in Section 1.3, each cell can either be empty, or is occupied by exactly one vehicle; all vehicles have the same length $l_i = 1$ cell. Traffic is also considered to be homogeneous, so all vehicles' characteristics are assumed to be the same. In the subsequent sections, we take a look at the following TCA models (accompanied by their suggested abbreviations):

- *Deterministic models*
  - Wolfram's rule 184 (CA-184)
  - Deterministic Fukui–Ishibashi TCA (DFI-TCA)
- *Stochastic models*
  - Nagel–Schreckenberg TCA (STCA)
  - STCA with cruise control (STCA-CC)
  - Stochastic Fukui–Ishibashi TCA (SFI-TCA)
  - Totally asymmetric simple exclusion process (TASEP)
  - Emmerich–Rank TCA (ER-TCA)
- *Slow-to-start models*
  - Takayasu–Takayasu TCA (T^2-TCA)
  - Benjamin, Johnson, and Hui TCA (BJH-TCA)
  - Velocity-dependent randomisation TCA (VDR-TCA)
  - Time-oriented TCA (TOCA)
  - TCA models incorporating anticipation
  - Ultra discretisation, slow-to-accelerate, and driver's perspective

For other excellent overviews of TCA models, we refer the reader to the works of Chowdhury et al. [3], Knospe et al. [19], Nagel [36], Nagel et al. [51], Schadschneider [52,53], and Schreckenberg et al. [54].

All following TCA models will be empirically studied using simulations that are performed on a *unidirectional*, *single-lane lattice* with periodic boundary conditions, i.e., a closed loop with $L_{\mathscr{L}} = 1$. The length of this lattice equals $K_{\mathscr{L}} = 10^3$ cells, which is taken large enough in order to reduce most unwanted *finite-size effects*. Our own

experiments indicate that larger lattice sizes do not render any significant advantage, aside from the burden of a larger computation time.

The importance of studying closed-loop, single-lane traffic: There is often a criticism expressed as to why it is important to study the behaviour of traffic flows in such a simplified system. After all, can such a basic system capture all the dynamics of real-life traffic flows, or be even representative of them? The answer to this question is that, in our opinion, the dynamics of these constrained systems play an important, non-negligible role. For example, when considering traffic flows on most unidirectional two-lane European motorways, drivers are by law obliged to drive on the right shoulder lane, unless when performing overtaking manoeuvres. A frequently observed phenomenon is then that under light traffic conditions (e.g., 10 vehicles/km/lane), a slower moving vehicle (e.g., a truck) is located on the right lane, and is acting as a *moving bottleneck*. As a result, all faster vehicles will line up on the left lane (overtaking on the right lane is prohibited by law), thereby causing a *density* or *lane inversion* [55,56,5,57]. It is under these circumstances that the stability of the car-following behaviour plays an important role. Similarly, in densely congested traffic, e.g., the synchronised-flow regime, the same stability may govern the fact whether or not a traffic breakdown is likely to be induced (see our work in [1] for a discussion on the nature of this breakdown). Even for multi-lane traffic, we believe its dynamics are essentially those of parallel single lanes when considering densely congested traffic flows. Another argument for the necessity of studying these simplified systems, is the one given by Nagel and Nelson. They state that this is the easiest way to determine whether or not internal effects of a traffic flow model play a role in e.g., the spontaneous breakdown of traffic, as all external effects (i.e., the boundary conditions) are eliminated [58]. Nevertheless, when applying these models to real-life traffic networks, closed-loop traffic is not very representative, as the behaviour near bottlenecks plays a far more important role [6].

All measurements on the TCA models' lattices are based on two possible initial conditions: depending on the nature of the study, we will either use *homogeneous initial conditions* (the default), or a *compact superjam* to start with. In the former case, all vehicles are uniformly distributed over the lattice, implying equal space headways. In the latter case, all vehicles are 'bunched up' behind each other, with zero space gaps. When going from one global density to another, an equivalent method would be to *adiabatically* add (or remove) vehicles to an already homogeneous or jammed state. In our experiments, however, we always reset the initial conditions, corresponding to the first method. The simulations ran each time for 10^4 time steps, after an initial period of 10^3 time steps was discarded in order to let transients from the initial conditions in the system die out. Global densities, flows, and space-mean speeds are computed by means of Eqs. (29)–(32), whereas, we use a point detector, i.e., Eqs. (33)–(35), to, compute their local variants. In this latter case, the data points were collected with a measurement period $T_{\text{mp}} = 60$ time steps. Based on these results, we can construct $(k_g, \overline{v}_{s_g})$, (k_g, q_g), $(k_l, \overline{v}_{s_l})$, and (k_l, q_l) diagrams. To keep a clear formulation, we will however from now on drop the subscripts denoting global and local measurements. All simulations were performed by means of our *Traffic Cellular Automata* + software (developed for the Java™ Virtual Machine); more information can be found in Appendix A.

For a deeper insight into the behaviour of the space-mean speed $\overline{v}_s$, the average space gap $\overline{g}_s$, and the median time gap $\overline{g}_t$, detailed histograms showing their *distributions* are provided. Note that with respect to the time gaps and time headways, we will work in the remainder of this report with the *median* instead of the arithmetic mean. The median gives more robust results when $h_{t_i}, g_{t_i} \to +\infty$, which occurs when a vehicle i stops. These histograms are interesting because in the existing literature (e.g., [59,52,6]) these distributions are only considered at several distinct global densities, whereas we show them for *all* densities. Each of our histograms is constructed by varying the global density k between 0 and 1, computing the space-mean speed, the average space gap and the median time gap for each simulation run. A simulation run consists of 5×10^4 time steps (with a transient period of 500 time steps) on systems of 300 cells, varying the density in 150 steps. Note that a larger size of the system's lattice, has no significant effects on the results, except for an increase of the variance [60].

Before giving an elaborate discussion of some of the classic TCA models, it is worthwhile to mention the first historical and practical implementations of traffic cellular automata. Cremer and Ludwig conceived an implementation of traffic flows based on *lattice gas automata* (LGA), which are a special case of cellular automata typically employed when simulating viscous fluids [61]. Their seminal work, using individual bits to represent vehicles, was extended by Schütt, who provided a simulation package for heterogeneous traffic, multi-lane motorways, and network and city traffic [62]. Unfortunately, the developed models were quite inefficient when they were used in setting that called for large scale Monte Carlo simulations [63].

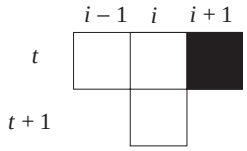

Fig. 6. An illustrative method for representing the evolution of a cell's state in time, based on its local neighbourhood. We can see the state $\sigma_i(t)$ of a central cell i at time step t, together with the states $\sigma_{i-1}(t)$ and $\sigma_{i+1}(t)$ of its two direct neighbours $i-1$ and $i+1$, respectively. This local neighbourhood is mapped onto a new state $\sigma_i(t+1)$. For binary states, we use a black square to represent a state of 1 (e.g., state $\sigma_{i+1}(t)$), and an empty (white) square for a state of 0. The depicted transition maps the triplet $(0\,0\,1)_2$ onto the state $\sigma_i(t+1)=0$.

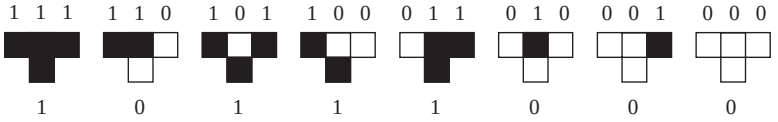

Fig. 7. A graphical representation of Wolfram's rule 184, which is written as $(1\,0\,1\,1\,1\,0\,0\,0)_2$ in base 2. All 8 possible configurations for the local neighbourhood are sorted in descending order, expressing the local transition rule $\delta(i,t)$ as explained by Fig. 6. For example, the local neighbourhood $(1\,0\,0)_2$ gets mapped onto a state of 1. This has the physical meaning that a particle (black square) moves to the right if its neighbouring cell is empty.

3.1. Deterministic models

In this section, we discuss Wolfram's original rule 184, and its generalisation to higher speeds as proposed by Fukui and Ishibashi's deterministic model. We abbreviate these two TCA models as CA-184 and DFI-TCA, respectively.

3.1.1. Wolfram's rule 184 (CA-184)

The first deterministic model we consider, is a one-dimensional TCA model with binary states. As $L_{\mathscr{L}}=1$, this model is called an elementary cellular automaton (ECA), according to the terminology introduced in Section 1.2. If we furthermore assume a local neighbourhood of three cells wide (i.e., a radius of 1), then there are $2^{2^3}=256$ different rules possible, according to Eq. (3). Around 1983, Stephen Wolfram classified all these 256 binary ECAs [21]. One of these is called *rule* 184, who's name is derived from Wolfram's naming scheme.

Wolfram's scheme is based on the representation of how a cell's state evolves in time, depending on its local neighbourhood. In Fig. 6, we have provided a convenient visualisation for the evolution of the states in a binary ECA. Here, we can see the state $\sigma_i(t)$ of a central cell i at time step t, together with the states $\sigma_{i-1}(t)$ and $\sigma_{i+1}(t)$ of its two direct neighbours $i-1$ and $i+1$, respectively. All three of them constitute the local neighbourhood $\mathscr{N}_i(t)$ of radius 1 (see also our example of a CA in Section 2.1.2). Because states are binary, we can indicate them with a colour, i.e., a black square represents a state of 1 (e.g., state $\sigma_{i+1}(t)$ in Fig. 6), whereas an empty (white) square represents a state of 0. According to the local transition rule $\delta(i,t)$, the local neighbourhood $\mathscr{N}_i(t)$ is then mapped from t to $t+1$ onto a new state $\sigma_i(t+1)$. The graphical representation in Fig. 6 thus provides us with an illustrative method to indicate the evolution of $\{\sigma_{i-1}(t),\sigma_i(t),\sigma_{i+1}(t)\}\longmapsto\sigma_i(t+1)$.

Considering the transition depicted in Fig. 6, we can see that a complete neighbourhood contains three cells, each of which can be in a 0 (white) or 1 (black) state. So in total, there are $2^3=8$ possible configurations for such a local neighbourhood. Wolfram's naming scheme for the binary ECAs is now based on an integer coding of this neighbourhood. Indeed, the local transition rule $\delta(i,t)$ is given by a table lookup containing eight entries, one for each of the possible local neighbourhoods. If we binary sort these eight configurations in the descending order $(1\,1\,1)$, $(1\,1\,0)$, $(1\,0\,1)$, $(1\,0\,0)$, $(0\,1\,1)$, …, then we obtain a graphic scheme such as the one in Fig. 7. As can be seen, for each of the local configurations, a resulting 0 or 1 state is returned for cell i at time step $t+1$. Collecting all resulting states, and writing them in base 2, results in the number $(1\,0\,1\,1\,1\,0\,0\,0)_2$. Converting this code to base 10, we obtain the number 184. Wolfram now coded all 256 possible binary ECAs by a unique number in the range from 0 to 255, resulting in 256 rules for these CAs.

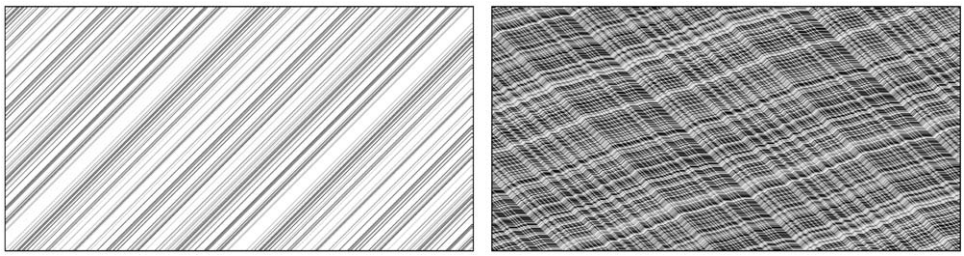

Fig. 8. Typical time–space diagrams of the CA-184 TCA model. The shown closed-loop lattices each contain 300 cells, with a visible period of 580 time steps (each vehicle is represented as a single coloured dot). *Left*: vehicles driving a free-flow regime with a global density $k = 0.2$ vehicles/cell. *Right*: vehicles driving in a congested regime with $k = 0.75$ vehicles/cell. The congestion waves can be seen as propagating in the opposite direction of traffic; they have an eternal life time in the system. Both time–space diagrams show a fully deterministic system that continuously repeats itself.

Rule 184 (which we abbreviate as CA-184) is an *asymmetrical* rule because $\delta((1\,1\,0)_2, t) = 0 \neq \delta((0\,1\,1)_2, t) = 1$. It is also called a *quiescent* rule because $\delta((0\,0\,0)_2, t) = 0$ (so all zero-initial conditions remain zero). As an example of the rule's evolution, Fig. 7 shows that the local neighbourhood $(100)_2$ gets mapped onto a state of 1. If we consider these 1 states as *particles* (i.e., vehicles), and the 0 states as *holes*, then rule 184 dictates that all particles move one cell to the right, on the condition that this right neighbour cell is empty. Equivalently, all holes have the tendency to move to the left for each particle that moves to the right, a phenomenon which is termed the *particle–hole symmetry*.

For a TCA model, we can rewrite the previous actions as a set of rules that are consecutively applied to all vehicles in the lattice, as explained in Section 1.4. For the CA-184, we have the following two rules:

(R1) *acceleration and braking*

$$v_i(t) \leftarrow \min\{g_{s_i}(t-1), 1\}\ , \tag{40}$$

(R2) *vehicle movement*

$$x_i(t) \leftarrow x_i(t-1) + v_i(t)\ . \tag{41}$$

Rule R1, Eq. (40), sets the speed of the ith vehicle, for the current updated configuration of the system; it states that a vehicle always strives to drive at a speed of 1 cell/time step, unless its impeded by its direct leader, in which case $g_{s_i}(t-1) = 0$ and the vehicle consequently stops in order to avoid a collision. The second rule R2, Eq. (41), is not actually a 'real' rule; it just allows the vehicles to advance in the system.

In Fig. 8, we have applied these rules to a lattice consisting of 300 cells (closed loop), showing the evolution over a period of 580 time steps. The time and space axes are oriented from left to right, and bottom to top, respectively. In the left part, we show a free-flow regime with a global density $k = 0.2$ vehicles/cell, in the right part we have a congested regime with $k = 0.75$ vehicles/cell. Each vehicle is represented as a single coloured dot; as time advances, vehicles move to the upper right corner, whereas congestion waves move to the lower right corner, i.e., backwards in space. From both parts of Fig. 8, we can see that the CA-184 TCA model constitutes a fully deterministic system that continuously repeats itself. A characteristic of the encountered congestion waves is that they have an eternal life time in the system.

In Fig. 9, we have plotted both the $(k, \overline{v}_s)$ and (k, q) diagrams. As can be seen from the left part, the global space-mean speed remains constant at $\overline{v}_s = 1$ cell/time step, until the critical density $k_c = 0.5$ is reached, at which point $\overline{v}_s$ will start to diminish towards zero where the critical density $k_j = 1$ is reached. Similarly, the global flow first increases and then decreases linearly with the density, below and respectively above, the critical density. Here, the capacity flow $q_{\text{cap}} = 0.5$ vehicles/time step is reached. The transition from the free-flowing to the congested regime is characterised by a first-order phase transition. As is evidenced by the *isosceles triangular shape* of the CA-184's resulting (k, q) fundamental diagram, there are only two possible kinematic wave speeds, i.e., $+1$ and -1 cell/time step. Both speeds are also clearly visible in the left, respectively right, time–space diagrams of Fig. 8. More analytical details on these values will be provided in the following Section 3.1.2.

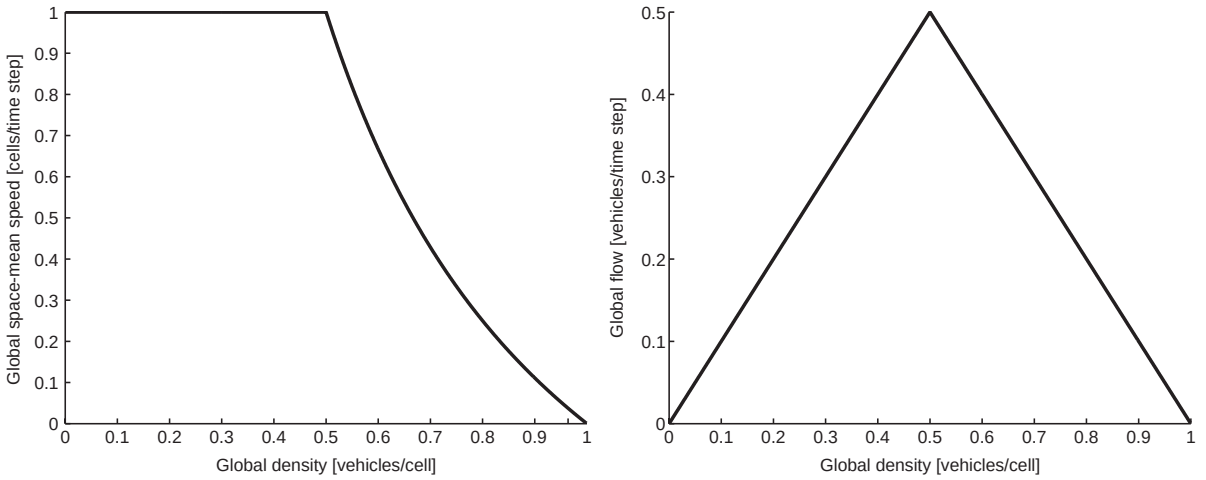

Fig. 9. *Left*: the $(k, \overline{v}_s)$ diagram for the CA-184, based on global measurements on the lattice. The global space-mean speed remains constant at $\overline{v}_s = 1$ cell/time step, until the critical density $k_c = 0.5$ is reached, at which point $\overline{v}_s$ will start to diminish towards zero. *Right*: the CA-184's (k, q) diagram, with its characteristic isosceles triangular shape. The transition between the free-flowing and the congested regime is of a first-order nature.

3.1.2. Deterministic Fukui–Ishibashi TCA (DFI-TCA)

In 1996, Fukui and Ishibashi constructed a generalisation of the prototypical CA-184 TCA model [64]. Although their model is essentially a stochastic one (see Section 3.2.3), we will first discuss its deterministic version. Fukui and Ishibashi's idea was two-fold: on the one hand, the maximum speed was increased from 1 to $v_{\max}$ cells/time step, and on the other hand, vehicles would accelerate *instantaneously* to the highest possible speed. Corresponding to the definitions of the rule set of a TCA model, the CA-184's rule R1, Eq. (40), changes as follows:

(R1) *acceleration and braking*

$$v_i(t) \leftarrow \min\{g_{s_i}(t-1), v_{\max}\} \ . \tag{42}$$

Just as before, a vehicle will now avoid a collision by taking into account the size of its space gap. To this end, it will apply an instantaneous deceleration: for example, a fast-moving vehicle might have to come to a complete stop when nearing the end of a jam, thereby *abruptly* dropping its speed from $v_{\max}$ to 0 in one time step.

Due to the strictly deterministic behaviour of the system, the time–space diagrams of the DFI-TCA do not differ much from those of the CA-184. The only difference is the speed of the vehicles in the free-flow regime, leading to steeper trajectories. It is however interesting to study the $(k, \overline{v}_s)$ and (k, q) diagrams in Fig. 10. Here we can see that increasing the maximum speed $v_{\max}$ creates—as expected—a steeper free-flow branch in the (k, q) diagram. Interestingly, the slope of the congested branch does not change, logically implying that the kinematic wave speed for jams remains constant, i.e., -1 cell/time step. This can be confirmed with an analytical kinematic wave analysis, as explained by Nagel [51].

Based on the behaviour of the vehicles near the critical density, we can analytically compute the capacity flow as follows: in the free-flow regime, all vehicles move with a constant speed of $v_{\max}$ cells/time step. When the critical density is reached, all vehicles drive collision-free at this maximum speed, which implies that $g_{s_i} = v_{\max}$ cells. The space headway $h_{s_i} = v_{\max} + 1$ (because $l_i = 1$ for single-cell models). Consequently, the value for the critical density as [50]:

$$k_c = \frac{1}{\overline{h}_{s_c}} = \frac{1}{v_{\max} + 1} \ . \tag{43}$$

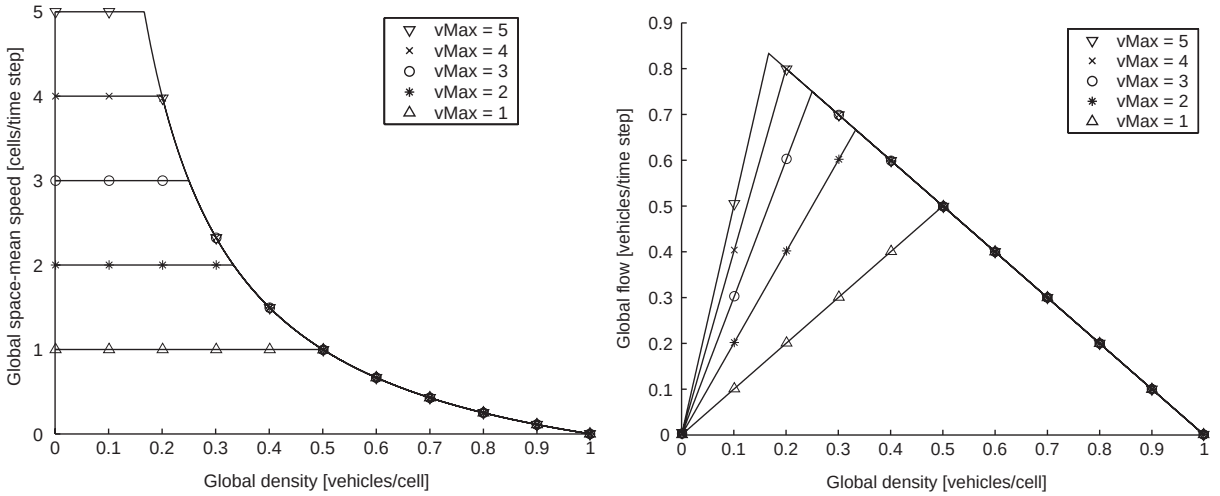

Fig. 10. *Left*: several $(k, \overline{v}_s)$ diagrams for the deterministic DFI-TCA, each for a different $v_{\max} \in \{1, \ldots, 5\}$. Similarly to the CA-184, the global space-mean speed remains constant, until the critical density is reached, at which point $\overline{v}_s$ will start to diminish towards zero. *Right*: several of the DFI-TCA's (k, q) diagrams, each having a triangular shape (with the slope of the congestion branch invariant for the different $v_{\max}$).

The capacity flow is now computed by means of the fundamental relation, i.e., $q_{\text{cap}} = k_c v_{\max}$:

$$q_{\text{cap}} = \frac{v_{\max}}{v_{\max} + 1} \ . \tag{44}$$

Applying Eqs. (43) and (44), for e.g., $v_{\max} = 5$ cells/time step, results in $k_c \approx 0.167$ vehicles/cell and $q_{\text{cap}} \approx 0.83$ vehicles/time step. If we furthermore assume $\Delta X = 7.5$ m and $\Delta T = 1$ s, then both values correspond to 22 vehicles/km and 3000 vehicles/h, respectively.

As opposed to the instantaneous acceleration in rule R1, Eq. (42), we can also assume a *gradual acceleration* of one cell per time step (the braking remains instantaneous):

(R1) *acceleration and braking*

$$v_i(t) \leftarrow \min\{v_i(t-1) + 1, g_{s_i}(t-1), v_{\max}\} \ . \tag{45}$$

However, our experimental observations have indicated that there is no difference in global system dynamics, with respect to either adopting gradual or instantaneous vehicle accelerations.

There exists a strong relation between the previously discussed deterministic TCA models, and the macroscopic first-order LWR model with a triangular $q_e(k)$ fundamental diagram [1]. Some of the finer results in this case, are the work of Nagel who extensively discusses some analytical results of both deterministic and stochastic TCA models [36], and the work of Daganzo who explicitly proves an equivalency between two TCA models and the kinematic wave model with a triangular $q_e(k)$ fundamental diagram [65]. More details with respect to such analytical relations, are given in Sections 3.2.4 and 5.3.

To conclude our discussion of deterministic models, we take a look at what happens in the limiting case where $v_{\max} \to +\infty$. As can be seen in Fig. 11, the congested branches in both $(k, \overline{v}_s)$ and (k, q) diagrams grow, at the cost of the free-flow branches which disappear. Interestingly, these diagrams correspond one-to-one with a triangular $q_e(k)$ fundamental diagram that is now expressed in a *moving coordinate system*, as explained by Newell [66]. In such a simplified system, the critical density $k_c = 0$, with a capacity flow $q_{\text{cap}} = 1$.

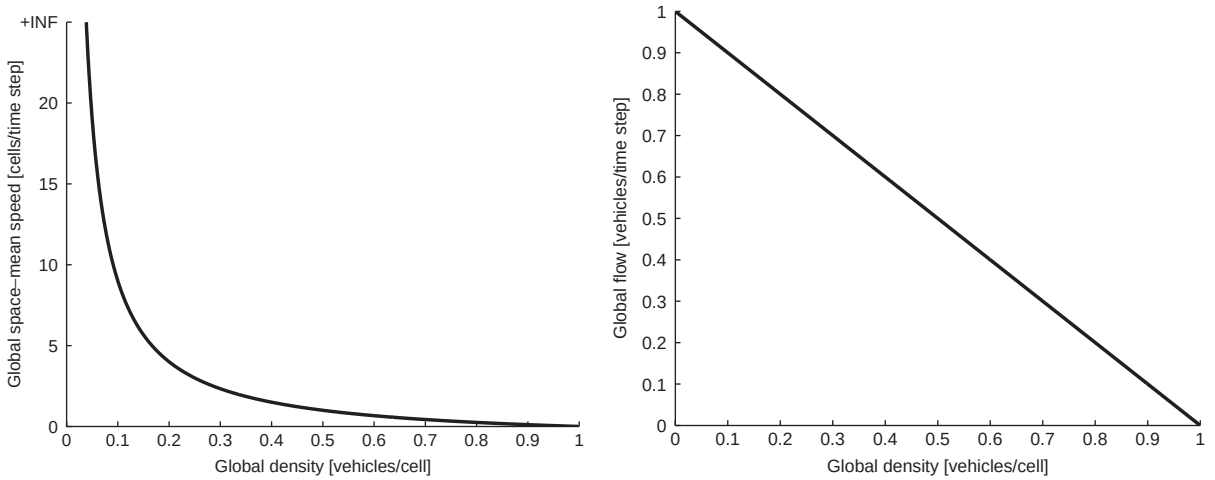

Fig. 11. *Left*: the $(k, \overline{v}_s)$ diagram for the deterministic CA-184, with now $v_{\max} \to +\infty$. *Right*: the (k, q) diagram for the same TCA model, resulting in a critical density $k_c = 0$, with a capacity flow $q_{\text{cap}} = 1$. This type of diagram corresponds to a simplified triangular $q_e(k)$ fundamental diagram that is expressed in a moving coordinate system.

3.2. Stochastic models

The encountered models in the previous section were all deterministic in nature, implying that there can be no spontaneous formation of jam structures. All congested conditions produced in those models, essentially stemmed from the assumed initial conditions. In contrast to this, we now discuss stochastic TCA models (i.e., these are probabilistic CAs) that allow for the spontaneous emergence of phantom jams. As will be shown, all these models explicitly incorporate a stochastic term in their equations, in order to accomplish this kind of real-life behaviour [67].

3.2.1. Nagel–Schreckenberg TCA (STCA)

In 1992, Nagel and Schreckenberg proposed a TCA model that was able to reproduce several characteristics of real-life traffic flows, e.g., the spontaneous emergence of traffic jams [37,63]. Their model is called the *NaSch TCA*, but is more commonly known as the *stochastic traffic cellular automaton* (STCA). It explicitly includes a stochastic noise term in one of its rules, which we present in the same fashion as those of the previously discussed deterministic TCA models. The STCA then comprises the following three rules (note that in Nagel and Schreckenberg's original formulation, they decoupled acceleration and braking, resulting in four rules):

(R1) *acceleration and braking*

$$v_i(t) \leftarrow \min\{v_i(t-1)+1, g_{s_i}(t-1), v_{\max}\} \,, \tag{46}$$

(R2) *randomisation*

$$\xi(t) < p \Longrightarrow v_i(t) \leftarrow \max\{0, v_i(t)-1\} \,, \tag{47}$$

(R3) *vehicle movement*

$$x_i(t) \leftarrow x_i(t-1) + v_i(t) \,. \tag{48}$$

Like in both CA-184 and DFI-TCA deterministic TCA models (see Sections 3.1.1 and 3.1.2), the STCA contains a rule for increasing the speed of a vehicle and braking to avoid collisions, i.e., rule R1, Eq. (46), as well as rule R3, Eq. (48), for the actual vehicle movement. However, the STCA also contains an additional rule R2, Eq. (47), which introduces stochasticity in the system. At each time step t, a random number $\xi(t) \in [0, 1[$ is drawn from a uniform distribution. This number is then compared with a stochastic noise parameter $p \in [0, 1]$ (called the *slowdown*

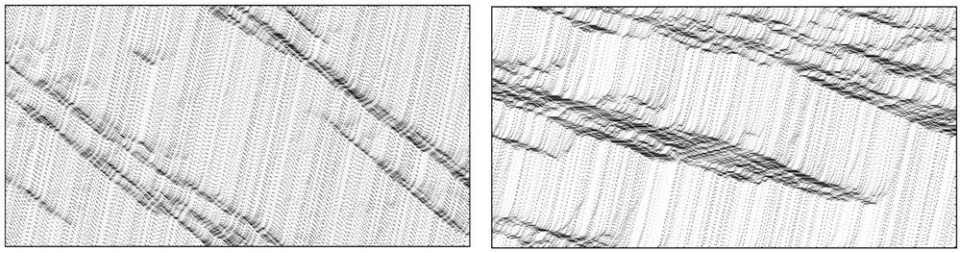

Fig. 12. Typical time–space diagrams of the STCA model (similar setup as for the CA-184 TCA model in Fig. 8). Both diagrams have a global density of $k = 0.2$ vehicles/cell. *Left*: the evolution of the system for $p = 0.1$. *Right*: the evolution of the system, but now for $p = 0.5$. The effects of the randomisation rule R2 are clearly visible in both diagrams, as there occur many unstable artificial phantom mini-jams. Furthermore, the speed w of the backward propagating kinematic waves decreases with an increasing p.

probability); as a result, there is a probability of p that a vehicle will slow down to $v_i(t) - 1$ cells/time step. The STCA model is called a *minimal model*, in the sense that all these rules are a necessity for mimicking the basic features of real-life traffic flows.

According to Nagel and Schreckenberg, the randomisation of rule R2 captures natural speed fluctuations due to human behaviour or varying external conditions. The rule introduces overreactions of drivers when braking, providing the key to the formation of spontaneously emerging jams.

Although the above rationale is widely agreed upon, much criticism was however expressed due to this second rule. For example, Brilon and Wu believe that this rule has no theoretical background and is in fact introduced quite heuristically [68].

To get an intuitive feeling for the STCA's system dynamics, we have provided two time–space diagrams in Fig. 12. Both diagrams show the evolution for a global density of $k = 0.2$ vehicles/cell, but with p set to 0.1 for the left diagram, and $p = 0.5$ for the right diagram. As can be seen in both diagrams, the randomisation in the model gives rise to many unstable artificial phantom mini-jams. The downstream fronts of these jams smear out, forming *unstable interfaces* [51]. This is a direct result of the fact that the intrinsic noise (as embodied by p) in the STCA model is too strong: a jam can always form at *any* density, meaning that breakdown can (and will) occur, even in the free-flow traffic regime. For low enough densities however, these jams can vanish as they are absorbed by vehicles with sufficient space headways, or by new jams in the system [69]. It has been experimentally shown that below the critical density, these jams have finite life times with a cut-off that is about 5×10^5 time steps and independent of the lattice size. When the critical density is crossed, these long-lived jams evolve into jams with an infinite life time, i.e., they will survive for an infinitely long time [70,63,71].

In free-flow traffic, a vehicle's speed will fluctuate between $v_{\max}$ and $v_{\max} - 1$, due to the randomisation rule R2. We can compute the space-mean speed in the free-flow regime by means of a weighted average. This average corresponds to the probability $1 - p$ for driving with the speed $v_{\max}$ and the probability p for slowing down to the speed $v_{\max} - 1$. As such, we get $\overline{v}_{s_{\text{ff}}} = \sum w_i v_i / \sum w_i = [(1-p)v_{\max} + p(v_{\max} - 1)]/[(1-p) + p] = v_{\max} - p$. In agreement with the space-mean speed observed in the left $(k, \overline{v}_s)$ diagram of Fig. 13, we can state that a vehicle will drive with an average free-flow speed of $\overline{v}_{\text{ff}} = v_{\max} - p$.

As mentioned in Section 3.1.2, the slope of the free-flow branch in a (k, q) diagram can be changed by adjusting $v_{\max}$. Similarly, the slope of the congested branch can be changed by tuning the slowdown probability p (note that this also affects the average free-flow speed). Looking at the (k, q) diagram in the right part of Fig. 13, we note that an increase of p will on the one hand result in a smaller $\overline{v}_{\text{ff}}$, and on the other hand the congested branch will lie lower, with a smaller critical density k_c. In this latter case, the speed w of the backward propagating kinematic waves will decrease, an effect that is also visible in the time–space diagrams of Fig. 12. Note that the presence of noise in the STCA model causes both free-flow and congested branches of the (k, q) diagram to be slightly curved, as opposed to the perfectly linear branches of the deterministic models.

If we set $p = 0$, then the STCA model becomes deterministic; additionally, setting $v_{\max}$ will recover the CA-184 TCA model. In the other deterministic case, when $p = 1$, the system behaves differently: in the congested state, all vehicles will come to a full stop, thereby reducing the global flow in the system to zero. As a result, the congested branch in the (k, q) regime will coincide with the horizontal axis. This implies that the behaviour of a system with $v_{\max}$ and $p = 1$ is totally different than that of a system with $v_{\max} - 1$ and $p = 0$.

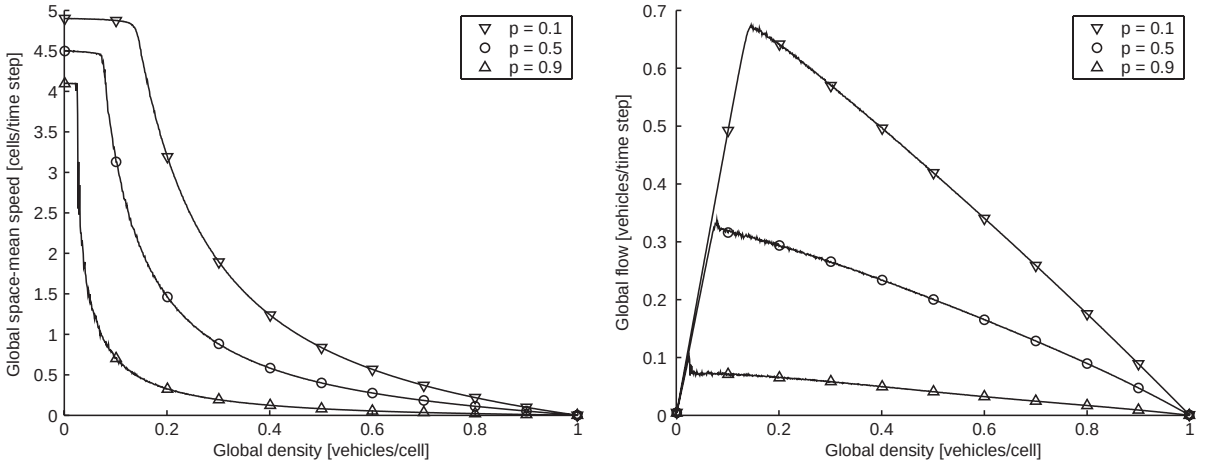

Fig. 13. *Left*: several $(k, \overline{v}_s)$ diagrams for the STCA, each for a different $p \in \{0.1, 0.5, 0.9\}$. It is clear from the diagram, that a vehicle will drive with an average free-flow speed of $\overline{v}_{\text{ff}} = v_{\max} - p$. *Right*: several (k, q) diagrams for the same STCA models as before. The slope of the congested branch tends toward zero for an increasing slowdown probability p. Note that the seemingly small capacity drops at the critical density in the right part, are actually finite-size effects [73,101].

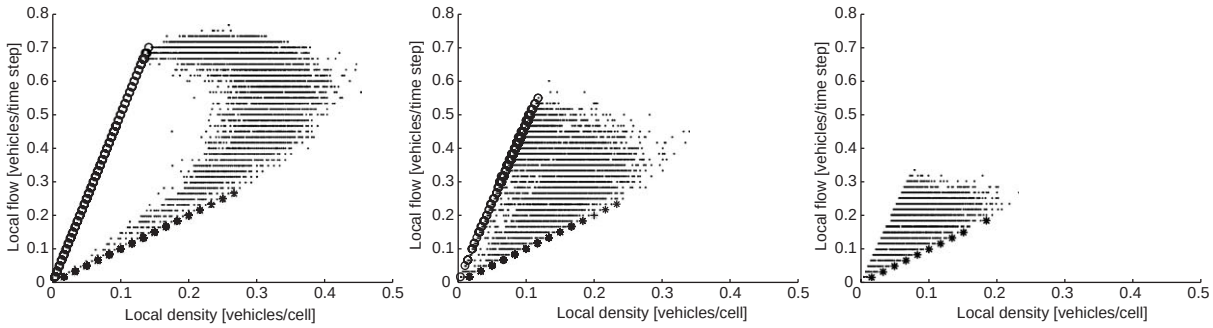

Fig. 14. Three (k, q) diagrams based on local measurements in the STCA model with $v_{\max} = 5$ cells/time step. *Left*: $p = 0$. *Middle*: $p = \frac{1}{3}$. *Right*: $p = \frac{2}{3}$. Points obtained in the free-flow regime (i.e., for $\overline{v}_s \approx v_{\max}$ cells/time step) are marked with a $\circ$, points obtained in the congested regime with a $\cdot$, and points that imply heavy congestion (i.e., for $\overline{v}_s < 1$ cell/time step) with a $\star$. Note that for these local diagrams, the slopes of the congested branches (indicated by the points marked as $\star$) are the negative of its corresponding slope in a global diagram.

Considering local measurements of the density, flow, and space-mean speed, the (k, q) diagrams in Fig. 14 reveal that an increasing slowdown probability p, results in (i) a lower value for the critical density, (ii) a lower capacity flow, and (iii) a more localised scatter of the data points.

In Fig. 15, we have plotted a histogram of the distributions of the STCA's vehicles' space gaps, for all global densities $k \in [0, 1]$. For very low densities, the distributions have a distinct maximum, indicating that all vehicles travel with very large space gaps. At higher densities, the maxima of the distributions shift toward smaller space gaps, as more and more vehicles encounter jams, even leading to a reduction of their space gap to zero. Around the critical density however, the distributions are smeared out across consecutive densities, but for each of those densities they exhibit a bimodal structure. Because the STCA contains many jams, the system now contains both vehicles in free-flow traffic, as well as vehicles that are in a congested state (i.e., driving closer to each other) [59,4,6,71].

In similar spirit, Fig. 16 shows the distribution of the vehicles' speeds and time gaps. Corresponding with our observations of the $(k, \overline{v}_s)$ diagrams in Fig. 13, the left part of Fig. 16 shows a distinct cluster of probability mass at the histogram class $v_{\max} - p$ for very low global densities. In this region, the standard deviation of the space-mean speed is more or less constant and equal to p. At higher global densities, the distributions become temporarily bimodal, after which they again tend to a unique maximum of 0 cells/time step, corresponding to severely congested traffic;

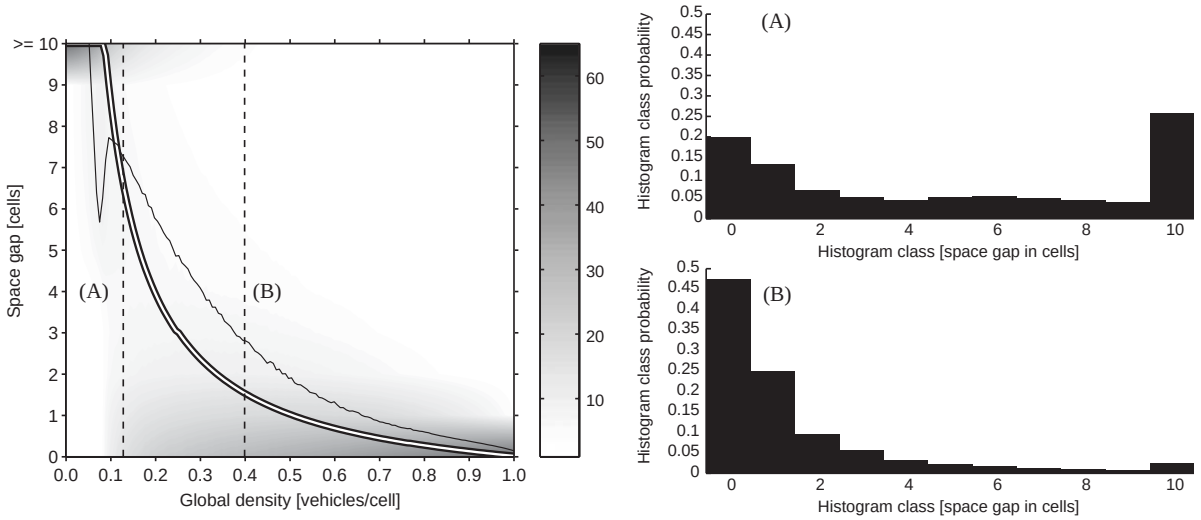

Fig. 15. A histogram of the distributions of the vehicles' space gaps g_s, as a function of the global density k in the STCA (with $v_{\max} = 5$ cells/time step and $p = 0.5$). In the contour plot to the left, the thick solid line denotes the average space gap, whereas the thin solid line shows its standard deviation. The grey regions denote the probability densities. The histograms (*A*) and (*B*) to the right, show two cross sections made in the left contour plot at $k = 0.1325$ and 0.4000, respectively: for example, in (*B*), the distribution exhibits a distinct unique maximum at the histogram class $g_s = 0$ cells, corresponding to the dark region in the lower right corner of the contour plot where high global densities occur.

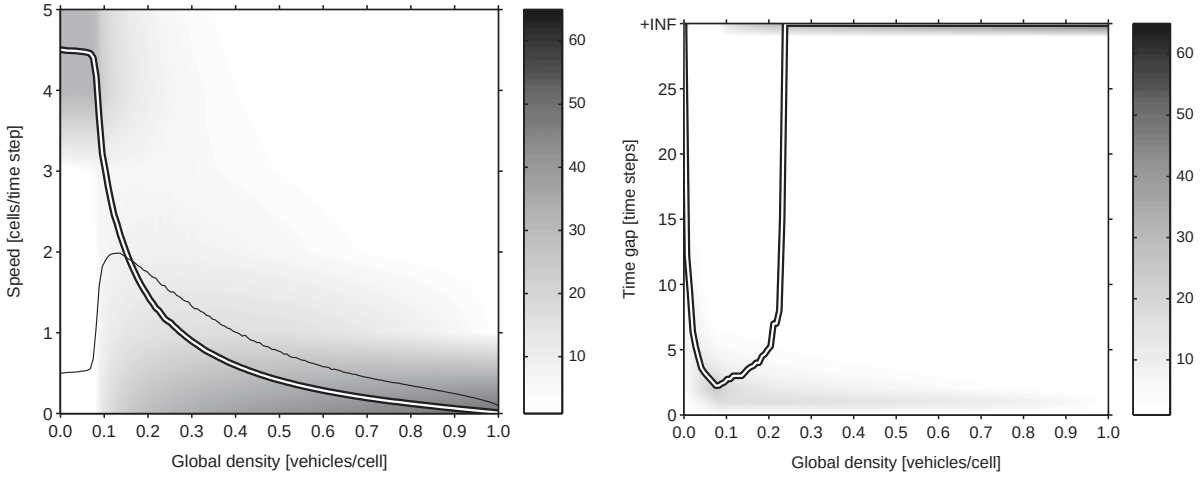

Fig. 16. Histograms of the distributions of the vehicles' speeds v (*left*) and time gaps g_t (*right*), as a function of the global density k in the STCA (with $v_{\max} = 5$ cells/time step and $p = 0.5$). The thick solid lines denote the space-mean speed and median time gap, whereas the thin solid line shows the former's standard deviation. The grey regions denote the probability densities.

the standard deviation drastically encounters a maximum at the critical density, after which it declines steadily. With respect to the distributions of the time gaps, the right part of Fig. 16 shows an rapidly decreasing median time gap as the critical density is approached. At this density, the time gaps settle around a local cluster at the minimum of 1 time step. Going to higher global densities, the number of stopped vehicles increases rapidly, frequently resulting in infinite time gaps. From the critical density on, all distributions exhibit a bimodal structure, corresponding to vehicles that are caught inside a jam, and other vehicles that are able to move freely (possibly at a lower speed) [59,72,71].

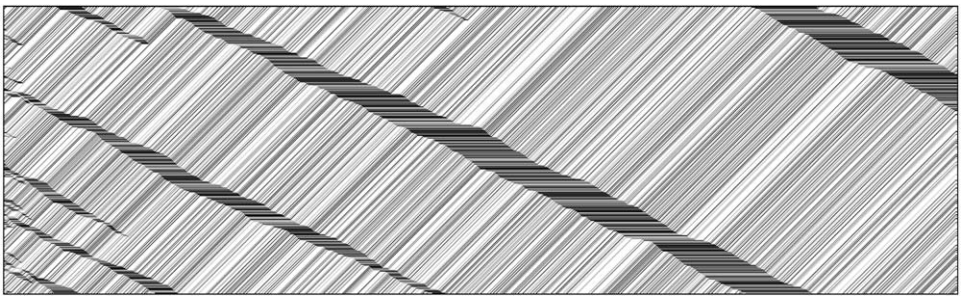

Fig. 17. A time–space diagram of the STCA-CC model for $v_{\max} = 1$ cell/time step and a global density of $k = 0.4$ vehicles/cell. The shown lattice contains 300 cells, with a visible period of 1000 time steps. We can see over ten initial jams evolving, coalescing over time into one superjam. The system exhibits two distinct phases, i.e., a free-flow and a congested regime with $\overline{v}_s = 1$ and 0 cells/time step, respectively.

3.2.2. STCA with cruise control (STCA-CC)

As mentioned in the previous Section 3.2.1, a typical artifact of the STCA model is that it gives rise to many unstable artificial jams. Due to the noise inherent in the model, a jam can always form at any density, even inducing a local breakdown of traffic in the free-flow traffic regime. One way to remedy this, is by stabilising the free-flow branch of the (k, q) diagram. This can be done by inhibiting the randomisation for high-speed vehicles. To this end, Nagel and Paczuski considered again rules R1–R3 of the STCA, i.e., Eqs. (46)–(48), but now complemented with a rule R0 [73]:

(R0) *determine stochastic noise*

$$\begin{aligned} v_i(t-1) = v_{\max} &\Longrightarrow p'(t) \leftarrow 0 \ , \\ v_i(t-1) < v_{\max} &\Longrightarrow p'(t) \leftarrow p \ , \end{aligned} \tag{49}$$

with now p replaced by $p'(t)$ in the STCA's randomisation rule R2, i.e., Eq. (47). This new rule effectively turns off the randomisation for high-speed vehicles, as only 'jammed' vehicles will now have stochastic behaviour. The resulting TCA model, is called the STCA in the *cruise-control limit*, or STCA-CC for short. If we set the maximum speed $v_{\max} = 1$ cell/time step, then all jams initially present in the system will coalesce with each other, giving rise to one superjam as depicted in Fig. 17. This superjam has been found to follow a *random walk* in the time–space diagram [73,36]. Note that $v_{\max} > 1$ cell/time step does not alter the critical behaviour of the model, even though jam clusters are now branching, having regions of free-flow traffic in between them [36].

In Fig. 18, we show the $(k, \overline{v}_s)$ and (k, q) diagram of the STCA-CC with $v_{\max} = 5$ cells/time step and $p = 0.2$. As can be seen in the right part, the (k, q) diagram has a typical inverted λ shape (see also our discussion in [1] about the hysteresis and capacity drop phenomena). The STCA-CC is said to be *bistable*, in that both the free-flow as well as the congested branches of the (k, q) diagram are stable (the former because it is noise-free). Vehicles going from the free-flow to the congested regime encounter at the critical density a phenomenon much like a capacity drop. The reverse transition to the free-flow branch proceeds via a lower density and, correspondingly, a lower flow (which is the outflow q_{out} of a jam). Comparing the right parts of Figs. 13 and 18, it is evident that a destabilisation of the free-flow branch forms the main reason for a lower capacity flow, reached at a lower critical density.

To conclude our discussion of the STCA-CC, we note that the use of cruise control as an ADAS can have unintended consequences. The traffic system can be perceived as having an underlying critical point, at which the life times of jams switch from finite to infinite (see our discussion at the beginning of Section 3.2.1). The existence of this point is closely tied to the *self-organised criticality* (SOC) of the STCA model: the outflow from an infinite jam automatically self-organises to a state of maximum attainable flow [74,67,63,75]. Stabilising the free-flow branch with cruise-control measures, results on the one hand in traffic higher achievable flows which is beneficial, but on the other hand the system is driven closer to its critical point which is more dangerous. At this stage, travel times will experience a high degree of variability, thereby reducing its predictability [76,73,63].

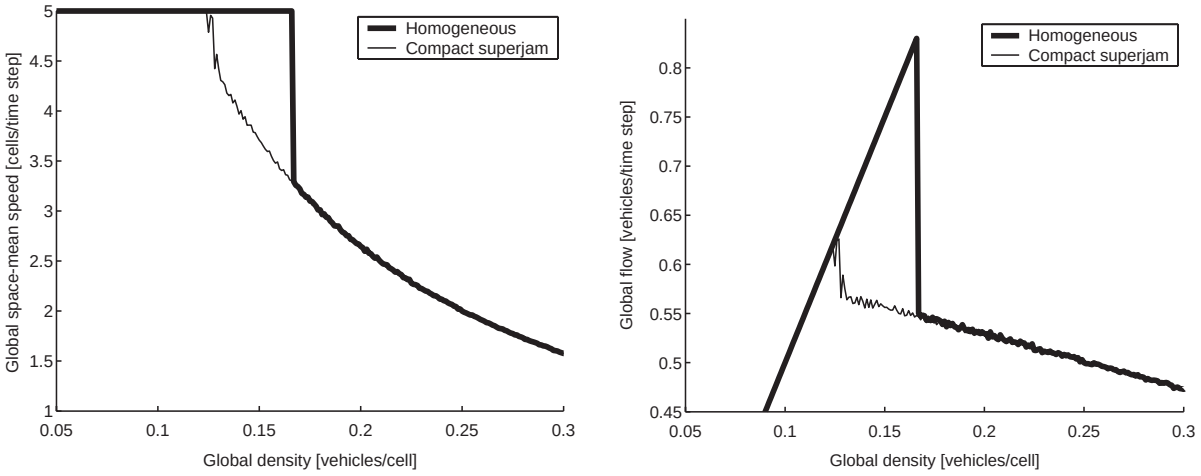

Fig. 18. Two $(k, \overline{v}_s)$ (*left*) and (k, q) (*right*) diagrams for the STCA-CC model, with $v_{\max} = 5$ cells/time step and $p = 0.2$. The thick solid line denotes global measurements that were obtained when starting from homogeneous initial conditions; the thin solid line is based on a compact superjam as the initial condition (see Section 3 for an explanation of these conditions). The right part clearly shows a typical reversed λ shape, which indicates a capacity drop. Note that the observed smaller drop in flow for the compact superjam, is actually a finite-size effect [73,101].

3.2.3. Stochastic Fukui–Ishibashi TCA (SFI-TCA)

In Section 3.1.2, we discussed the deterministic FI-TCA which is a generalisation of the CA-184 TCA model. In their original formulation, Fukui and Ishibashi also introduced stochasticity, but now only for vehicles driving at the highest possible speed of $v_{\max}$ cells/time step [64]. We can express the rules of this model, by considering the rules R2 and R3 of the STCA, i.e., Eqs. (47) and (48), but now complemented with the DFI-TCA's rule R1 for instantaneous accelerations, i.e., Eq. (42) of Section 3.1.2, and, as in the STCA-CC model, an extra rule R0:

(R0) *determine stochastic noise*

$$\begin{aligned} v_i(t-1) = v_{\max} &\Longrightarrow p'(t) \leftarrow p \ , \\ v_i(t-1) < v_{\max} &\Longrightarrow p'(t) \leftarrow 0 \ , \end{aligned} \tag{50}$$

with now p replaced by $p'(t)$ in the randomisation rule R2. It can be seen that for $v_{\max} = 1$, the SFI-TCA and STCA models are the same. Furthermore, for $p = 0$ the SFI-TCA becomes fully deterministic, and in contrast to the STCA's zero-flow behaviour (see Section 3.2.1), the SFI-TCA's $p = 1$ case corresponds to the STCA with $p = 0$ and $v_{\max} - 1$.

The rationale behind the specific randomisation in the SFI-TCA model, is that drivers who are moving at a high speed, are not able to focus their attention indefinitely. As a consequence, there will be fluctuations at these high speeds. As such, this corresponds to the opposite of a cruise-control limit, e.g., the STCA-CC model. There will be no capacity drop, but the effect on the $(k, \overline{v}_s)$ diagram is that its free-flow branch will become slightly downward curving, starting at $\overline{v}_s = v_{\max} - p$ for $k = 0$.

To conclude, we mention the related work of Wang et al. who studied the SFI-TCA both analytically and numerically, providing an exact result for $p = 0$, and a close approximation for the model with $p \neq 0$ [77]. Based on the SFI-TCA, Wang et al. developed a model that is subtly different. They assumed that drivers do not suffer from concentration lapses at high speeds, but are instead only subjected to the random deceleration when they are driving close enough to their direct frontal leaders [78]. And finally, we mention the work of Lee et al. who incorporate anticipation with respect to a vehicle's changing space gap g_s as its leader is driving away. This results in a higher capacity flow, as well as the appearance of a synchronised-traffic regime, in which vehicles have a lower speed, but are *all* moving [79].

3.2.4. Totally asymmetric simple exclusion process (TASEP)

The simple exclusion process is a simplified well-known particle transport model from non-equilibrium statistical mechanics, defined on a one-dimensional lattice. In the case of open boundary conditions (i.e., the bottleneck scenario), particles enter the system from the left side at an *entry rate* α, move through the lattice, and leave it at an *exit rate* β. The term 'simple exclusion' refers to the fact that a cell in the lattice can only be empty, or occupied by one particle. When moving through the lattice, particles move one cell to the left with probability γ, and one cell to the right with probability δ. When $\gamma = \delta$, the process is called the *symmetric simple exclusion process* (SSEP); if $\gamma \neq \delta$, then it is called the *asymmetric simple exclusion process* (ASEP) [80]. Finally, if we set $\gamma = 0$ and $\delta = 1$, the system is called the *totally asymmetric simple exclusion process* (TASEP). If we consider the TASEP as a TCA model, then all vehicles move with $v_{\max} = 1$ cell/time step to their direct right-neighbouring cell, on the condition that this cell is empty.

Updating the configuration of CA essentially amounts to updating the states of all its cells. In general, there are two methods for the update procedure:

Sequential update: This updating procedure considers each cell in the lattice one at a time. If all cells are considered consecutively, two updating directions are possible: *left-to-right* and *right-to-left*. There is also a third possibility, called *random sequential update*. Under this scheme and with N particles in the lattice, each time step is divided in N smaller substeps. At each of these substeps, a random cell (or vehicle) is chosen and the CA rules are applied to it. As a consequence of the updating procedure, each particle is on average updated after N smaller substeps, which introduces a certain amount of noise in the system. We have depicted several typical time–space diagrams for the ASEP with $\gamma = 1 - \delta$ in Fig. 19. Furthermore note that a hidden assumption here is that, after completing a substep, the local information is immediately available to the whole system, which can violate causality (as information is now transmitted through the lattice at an infinite speed).

Parallel update: This is the classic update procedure that is used for all TCA models discussed in this report. For a parallel update, all cells in the system are updated in one and the same time step. Compared to a sequential updating procedure, this one is computationally more efficient (note that it is equivalent to a left-to-right sequential update). There is however one peculiarity associated with this updating scheme: because all particles are considered simultaneously, certain lattice configurations cannot exist, i.e., the *Garden of Eden* (GoE) states mentioned in Section 1.2. An example of such a *paradisiacal state*, is two vehicles right behind each other, with the following having a non-zero speed. This state would imply that in single-lane traffic, the FIFO property was violated and consequently a collision occurred. Such GoE states do not exist when using a random sequential update.

In Fig. 20, we have depicted two time–space diagrams for the TASEP with a random sequential updating procedure, operating on a closed loop. As can be seen, the diagrams qualitatively look the same, and have some of the same characteristic features of the time–space diagrams in Fig. 19. For the TASEP, there is no free-flow regime, there are no large jams in the system, and, because of the random sequential update, all vehicles continuously have the tendency to collide with each other. As a consequence, the system is littered with mini-jams in both the low and high density regimes [63,36]. Note that the TASEP with open boundary conditions exhibits a very rich behaviour, depending on the values for the entry and exit rates α and β, respectively [81,18,53].

With respect to the relations between the TASEP with a random sequential update and other models, we mention the following two analogies: on the one hand, the LWR first-order macroscopic traffic flow model [1] corresponds to the TASEP in the hydrodynamic limit to a noisy and diffusive conservation law, which can be reduced to the LWR model [63,36]. On the other hand, the TASEP corresponds to the STCA (see Section 3.2.1), but now with $v_{\max} = 1$ cell/time step [3,6].

To gain more insight into the macroscopic behaviour of the TASEP with random sequential update, we provide its $(k, \overline{v}_s)$ and (k, q) diagrams in Fig. 21. Looking at the $(k, \overline{v}_s)$ diagram on the left part, we notice that the TASEP with $v_{\max} = 1$ cell/time step corresponds exactly to Greenshields' original linear relation between the density and the mean speed [82,50]. This in fact is a further testimony of the close link between the TASEP and the LWR model with a triangular $q_e(k)$ fundamental diagram. Increasing the TASEP's maximum speed, leads to a more curved relation, intersection the vertical axis at the point $(0, v_{\max})$. In any case, the $(k, \overline{v}_s)$ diagram also reveals the absence of a distinct free-flow branch, corresponding to the observations of the large amount of mini-jams for all global densities, as could be seen in the time–space diagrams of Fig. 20.

Studying the (k, q) diagram in the right part of Fig. 21, we can see that the TASEP corresponds with the STCA for $v_{\max} = 1$ and an arbitrary slowdown probability (e.g., $p = 0.1$). The diagram also shows how the CA-184 leads to a sharp transition between the free-flow and the congested regime, as opposed to the rounded peak of capacity

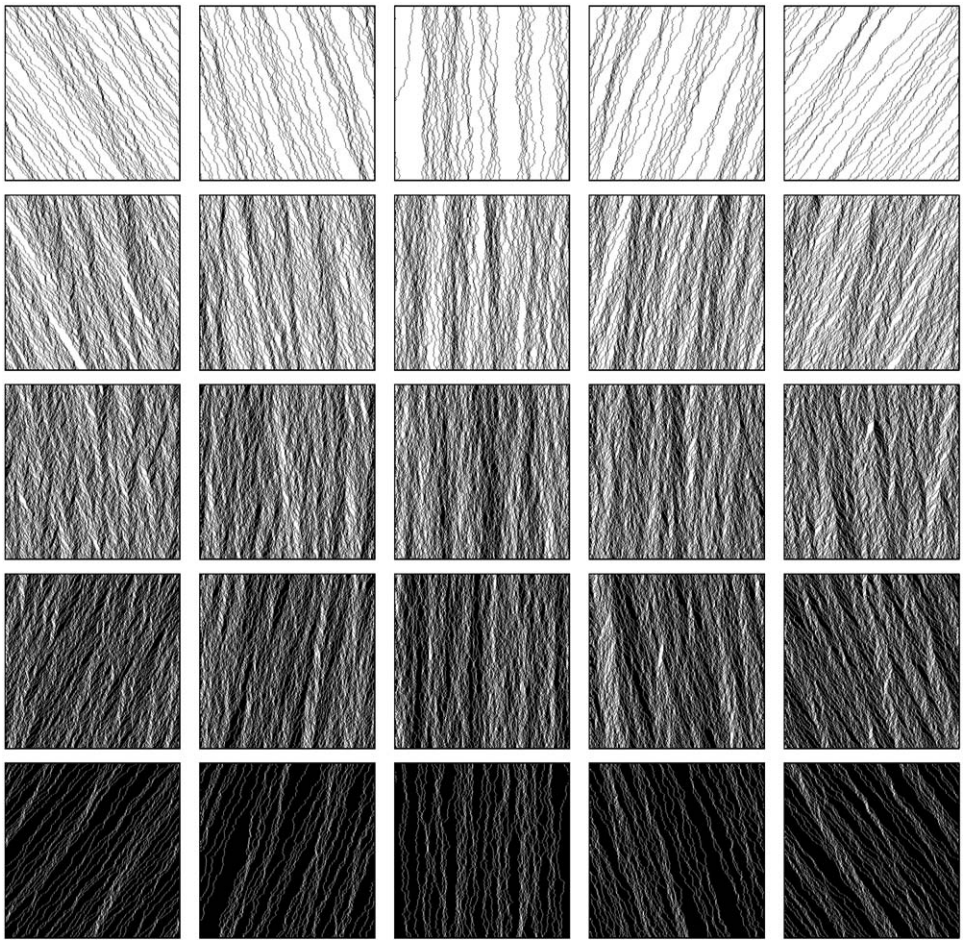

Fig. 19. Typical time–space diagrams of the asymmetric simple exclusion process (ASEP model) with a random sequential update and $\gamma = 1 - \delta$. The shown lattices each contain 400 cells, with a visible period of 400 time steps (note that for clarity, the space and time axes are located horizontally and vertically, respectively). The global densities in the systems were set for each row to $k \in \{0.1, 0.3, 0.5, 0.7, 0.9\}$ vehicles/cell. For each column, the ASEP's probability to move to the left was set to $\gamma \in \{0.1, 0.3, 0.5, 0.7, 0.9\}$.

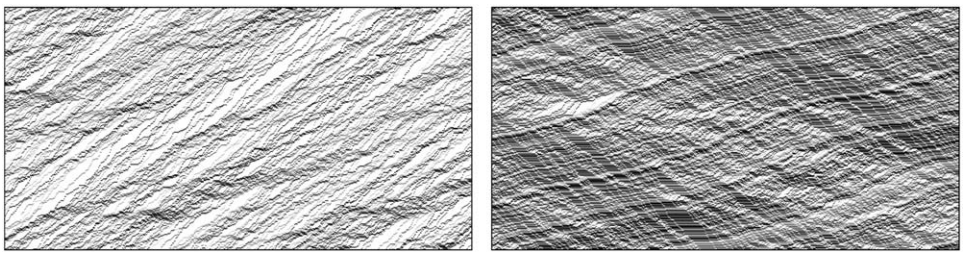

Fig. 20. Typical time–space diagrams of the TASEP model with a random sequential update. The shown lattices each contains 300 cells, with a visible period of 580 time steps. The global density in the system was set to $k = 0.3$ vehicles/cell (*left*), and $k = 0.7$ vehicles/cell (*right*). The evolution of the system dynamics qualitatively looks the same in both diagrams: the system is littered with mini-jams in both the low and high density regimes.

flow at $k = 0.5$ vehicles/cell for the STCA. However, whereas the TASEP also has its capacity flow at the same value, there does not occur such a phase transition as in the other models. Finally, we can see that increasing the maximum speed $v_{\max}$ for the TASEP introduces no significant qualitative changes, except for a skewing towards lower densities [63].

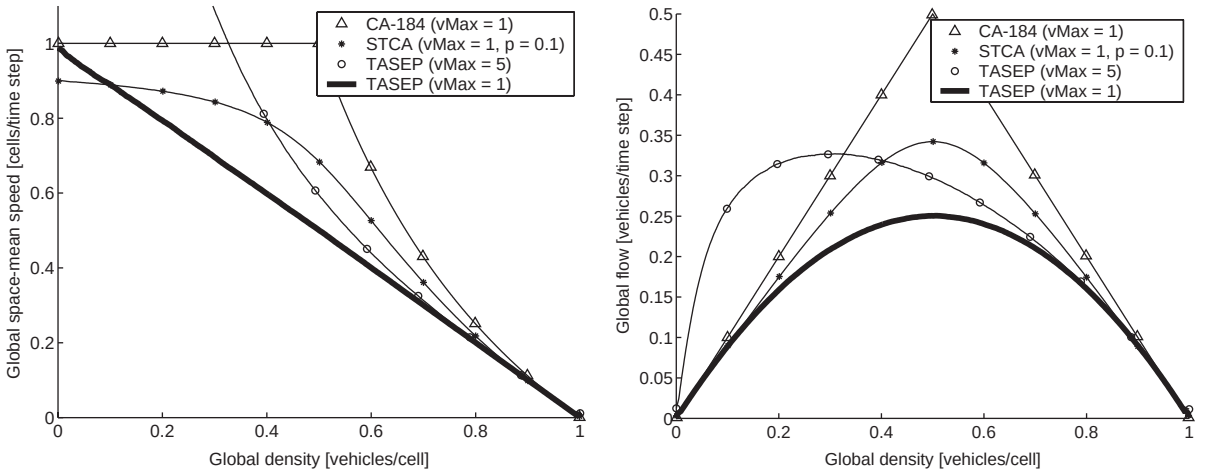

Fig. 21. A comparison of the $(k, \overline{v}_s)$ (*left*) and (k, q) (*right*) diagrams for the CA-184 with $v_{\max} = 1$ ($\triangle$), the STCA with $v_{\max} = 1$ and $p = 0.1$ ($\star$), the TASEP with random sequential update and $v_{\max} = 5$ ($\circ$), and the TASEP with random sequential update and $v_{\max} = 1$ (thick solid line). Some distinct characteristics of the TASEP are the absence of a free-flow regime, and for $v_{\max} = 1$ cells/time step, the exact correspondence with Greenshields linear relation between the density and the mean speed.

Note that with respect to the computational complexity of the implemented TCA models, most measurements in this report took a few hours to obtain, using an Intel P4 2.8 GHz with 512 MB RAM, running the Java^{TM} JDK 1.3.1 under Windows 2000. In sharp contrast to this, are the computations for the TASEP model, which took nearly 2 *weeks* to complete.

3.2.5. Emmerich–Rank TCA (ER-TCA)

Whereas the classical STCA model provided a reasonable qualitative agreement with real-world observations, Emmerich and Rank addressed the quantitative discrepancies between the model and real-world data. To this end, they proposed a variation on the STCA, extending the influence of the space gap on a vehicles updated speed [83].

In their work, Emmerich and Rank fundamentally modified the STCA in two steps: (i) they changed the parallel update procedure to a *right-to-left sequential update procedure* (see Section 3.2.4 for more details), and (ii) they changed the behaviour of vehicles that are slowing down. In a nutshell, (i) leads to the important result that vehicles are now able to drive directly behind each other (i.e., with a zero space gap) at high speeds, because the gaps in a traffic stream are used more efficiently. The reason is that due to the specific sequential update, a downstream vehicle is moved first (for a closed loop, the vehicle with the largest space gap is chosen first), after which the next vehicle upstream will see a larger space gap.

Just as the STCA can be seen as a special case of the optimal velocity model (OVM), based on a linear optimal velocity function (for a description of the OVM, we refer the reader to our overview in [1]), the ER-TCA model generalises this function by making a vehicle's speed dependent on a variable safe distance and its current speed [3]. This affects (ii), i.e., vehicles that are slowing down: when determining the new speed of a vehicle, the ER-TCA model first checks if the vehicle is within 10 cells of its direct frontal leader. If this is the case, then the vehicle will slow down according to a table lookup in a *gap-speed matrix* $M_{g_{s_i}, v_i}$. This matrix is constructed in such a way that collisions are avoided (i.e., $M_{i,j} \leqslant \min\{i, j\}$):

$$M^{\mathrm{T}} = \begin{pmatrix} 0 & 0 & 0 & 0 & 0 & 0 & 0 & 0 & 0 & 0 & 0 \\ 0 & 1 & 1 & 1 & 1 & 1 & 1 & 1 & 1 & 1 & 1 \\ 0 & 1 & 2 & 2 & 2 & 2 & 2 & 2 & 2 & 2 & 2 \\ 0 & 1 & 2 & 3 & 3 & 3 & 3 & 3 & 3 & 3 & 3 \\ 0 & 1 & 2 & 3 & 4 & 4 & 4 & 4 & 4 & 4 & 4 \\ 0 & 1 & 2 & 3 & 4 & 4 & 4 & 4 & 4 & 4 & 5 \end{pmatrix}. \tag{51}$$

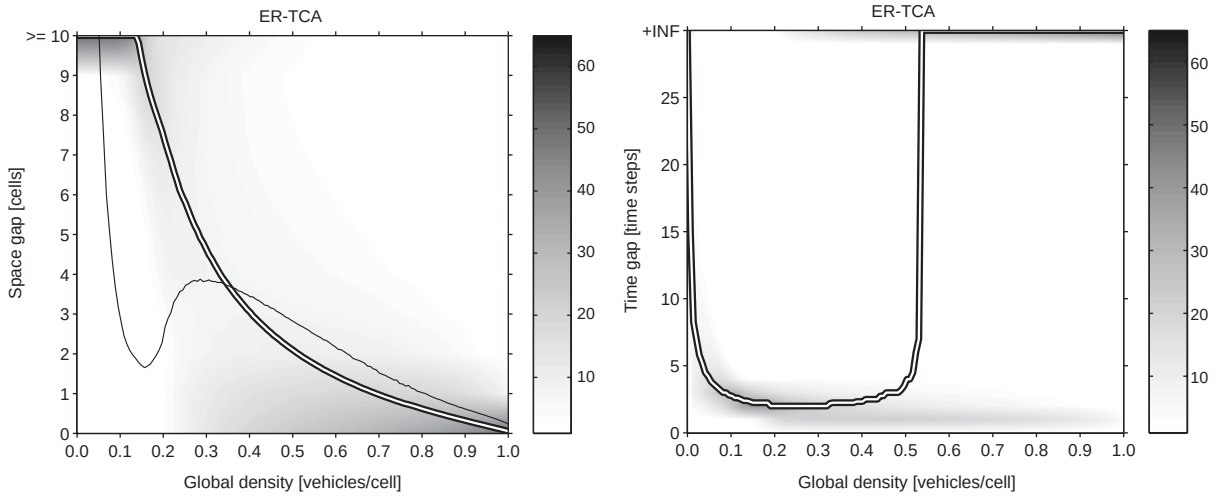

Fig. 22. Histograms of the distributions of the vehicles' space gaps g_s (*left*) and time gaps g_t (*right*), as a function of the global density k in the ER-STCA (with $v_{\max} = 5$ cells/time step and $p = 0.35$). The thick solid lines denote the mean space gap and median time gap, whereas the thin solid line shows the former's standard deviation. The grey regions denote the probability densities.

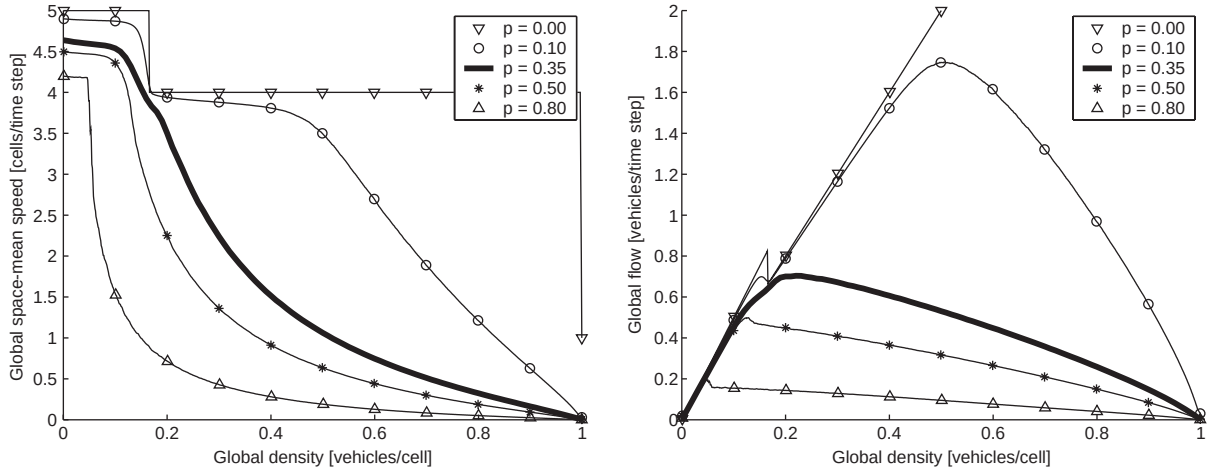

Fig. 23. *Left*: several $(k, \overline{v}_s)$ diagrams for the ER-TCA, each for a different slowdown probability p. It is clear from the diagram, that for low values of p, the resulting diagrams are unrealistic, including plateaus of constant space-mean speed in the congested regime. *Right*: several (k, q) diagrams for the same ER-TCA models as before. Due to the system dynamics in the ER-TCA, very high capacity flows are possible. To constrain these flows, the slowdown probability p has to be quite large in order to obtain realistic results. In both parts of the figure, the thick solid line denotes the original model of Emmerich and Rank, who used a value $p = 0.35$ as their best fit to experimental data.

The matrix in Eq. (51), conveys the idea that lower speeds require lower space gaps, and that vehicles tend to keep larger space gaps when travelling at higher speeds. This latter effect is also visible in the distribution of the vehicles' space gaps, as visualised in the histograms in the left part of Fig. 22, where, in contrast to the STCA's space gaps distribution of Fig. 15, large space gaps are observed for densities near the critical density. Furthermore, because of this mechanism, vehicles will have smoother decelerations, instead of the abrupt slowing down in the STCA model and some of its variations.

To understand some of the system dynamics of the ER-TCA model, we have provided several $(k, \overline{v}_s)$ and (k, q) diagrams in Fig. 23. For $p = 0.35$, we can see in the (k, q) diagram in right part, that the free-flow branch gets *curved*, implying that vehicles travel at a slightly lower speed when they approach the capacity-flow regime. Because vehicles

can travel at high speeds in dense platoons, the ER-TCA model can achieve very high capacity flows, even leading to $q > 1$ vehicle/time step. In order to constrain these flows to realistic values, the ER-TCA model needs a quite high slowdown probability, e.g., $p = 0.35$.

These two effects, i.e., a curving of the free-flow branch and an increased capacity flow, are basically what the ER-TCA model is all about, as there is no qualitative change in the congested branch of the (k, q) diagram. There are however some serious drawbacks to the ER-TCA model. First and foremost, the (k, q) diagram is no longer non-monotonic for low densities when the sequential update is replaced by a parallel one [3,19]. Secondly, the model exhibits too large time headways in the free-flow regime when compared with real-world data. This effect is also visible in the distribution of the vehicles' time gaps, as depicted in the histograms in the right part of Fig. 22, where, in contrast to the STCA's time gaps distribution of Fig. 16, a large amount of finite time gaps extends well into the region of medium densities. Third, due to the sequential update, the ER-TCA model's downstream jam dynamics are unstable, just as in the STCA model [19]. Fourth, as can be seen from the $(k, \overline{v}_s)$ diagram in the left part of Fig. 23, for small slowdown probabilities p, the resulting space-mean speed in the system is very unrealistic, even including plateaus of constant speed in the congested regime, e.g., the curve associated with $p = 0.1$ (we consider $p = 0$ as a degenerate case).

3.3. Slow-to-start models

In order to obtain a correct behavioural picture of traffic flow breakdown and stable jam, it is necessary that a vehicle's minimum time headway or reaction time should be smaller than its escape time from a jam, or equivalently, the outflow from a jam (i.e., the queue discharge rate) must be lower than its inflow [84,69,85–87,51]. If this is not the case, as in e.g., the STCA model where both times are exactly the same, then all jams will be unstable, as can be seen in the time–space diagram of Fig. 12. Because of their unstable jamming behaviour, the previously discussed stochastic models, experience neither a capacity drop nor a hysteresis loop, for which stable jams are a necessary prerequisite. Although the STCA-CC seems to be an exception to this rule, the downstream fronts of its jams are still too unstable, in the sense that new jams can emerge all too easily, which is unrealistic behaviour with respect to real-life traffic flows [5].

As just mentioned, one mechanism that deals with this, is by leaving free-flow traffic undisturbed, and by *significantly reducing the outflow from a jam* once a breakdown occurs, thereby stabilising the downstream front of a jam. Instead of just eliminating the noise in free-flow traffic in the STCA-CC, this reduced outflow can also be accomplished more intuitively, by making the vehicles wait a short while longer before accelerating again from stand still. As such, they are said to be "*slow to start*".

Note that there exists yet another mechanism that allows for the reproduction of the capacity drop and hysteresis phenomena (we will only briefly mention it here). The approach followed by Werth, is based on the premise that drivers take into account the *speed difference* with their direct frontal leader, instead of just the space gap as was previously assumed. This leads to *Galilei invariant* vehicle–vehicle interactions (i.e., the system dynamics remain the same if a new linear moving coordinate system is substituted in the equations). Interestingly, the metastability in this model is not due to cruise control or slow-to-start rules, but rather a result of the anticipation adopted. The model can exhibit stable dense platoons of fast vehicles, resulting in a stabilisation of the free-flow branch, and consequently leading to hysteretic behaviour [88,5,3].

With respect to real-world units, we give some typical values associated with the capacity drop and hysteresis phenomena (based on [5]): an outflow $q_{\text{out}} \approx 1800$ vehicles/h/lane at an associated density of $k_{\text{out}} \approx 20$ vehicles/km/lane, with q_{cap}, k_{crit}, and k_{jam} equal to 2700 vehicles/h/lane, 20 vehicles/km/lane, and 140 vehicles/km/lane, respectively.

3.3.1. Takayasu–Takayasu TCA (T^2-TCA)

In 1993, Takayasu and Takayasu proposed a deterministic TCA model, based on the CA-184 (see Section 3.1.1), that incorporated a *delay in acceleration for stopped vehicles* [89]. Their motivation stems from the fact that high-speed vehicles are in general able to decelerate very quickly, but conversely, it takes them a lot longer to attain this high speed when they start from a stopped condition. As such, Takayasu and Takayasu introduced a delay, based on the rationale that a vehicle will only start to move when it recognises movement of its direct frontal leader. Translating this into a rule set, we can write the T^2-TCA's rules based on those of the CA-184, but now with the following modifications

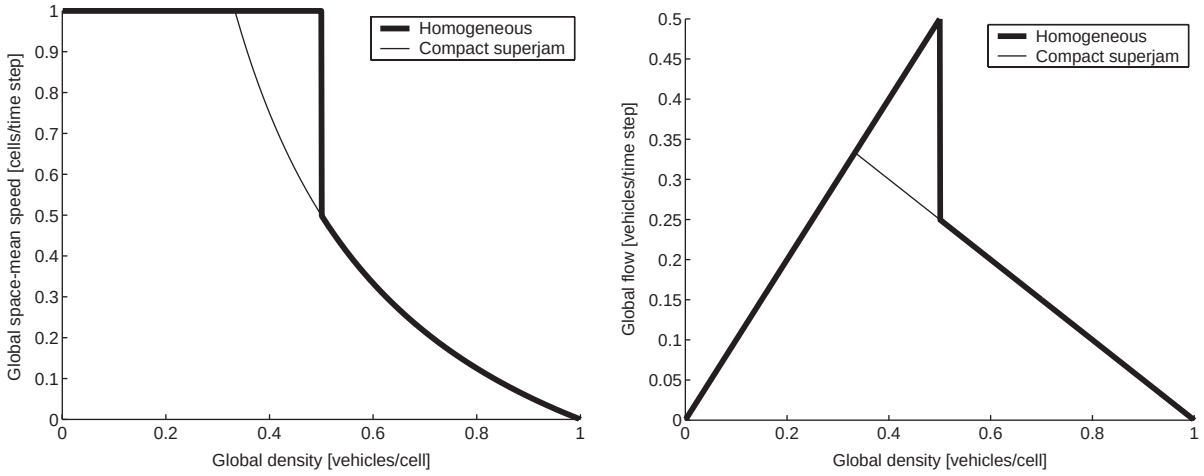

Fig. 24. Two $(k, \overline{v}_s)$ (*left*) and (k, q) (*right*) diagrams for the T^2-TCA model, with $v_{\max} = 1$ cells/time step. The thick solid line denotes global measurements that were obtained when starting from homogeneous initial conditions; the thin solid line is based on a compact superjam as the initial condition (see Section 3 for an explanation of these conditions). The right part clearly shows a typical reversed λ shape, which indicates a capacity drop.

(note that $v_{\max} = 1$ cell/time step):

(R1) *braking*

$$v_i(t-1) > g_{s_i}(t-1) \quad \Longrightarrow \quad v_i(t) \leftarrow g_{s_i}(t-1)\ , \tag{52}$$

(R2) *delayed acceleration*

$$v_i(t-1) = 0 \wedge g_{s_i}(t-1) \geqslant 2 \quad \Longrightarrow \quad v_i(t) \leftarrow 1\ , \tag{53}$$

(R3) *vehicle movement*

$$x_i(t) \leftarrow x_i(t-1) + v_i(t)\ . \tag{54}$$

From this rule set it follows that a vehicle will always drive at a speed of one cell/time step, unless it has to brake and stop according to rule R1, Eq. (52). Furthermore, the vehicle is only allowed to accelerate again to this speed of one cell/time step, on the condition that it has a sufficiently large space gap in front, as dictated by rule R2, Eq. (53). As a result, the introduced delay is *spatial in nature*, and it only affects stopped vehicles.

In Fig. 24, we have depicted the resulting $(k, \overline{v}_s)$ and (k, q) diagrams for the T^2-TCA model. The observed behaviour is similar to that of the STCA-CC model in Section 3.2.2, in that the T^2-TCA model also exhibits *bistability*. Starting from homogeneous initial conditions, the space-mean speed in the system undergoes a sharp drop once a vehicle has to stop. The reverse process, i.e., going from the congested to free-flow regime, is accompanied by a smooth continuous transition. Takayasu and Takayasu state that this corresponds to a second-order phase transition, because their order parameter (the sum of the jamming times) follows a power-law distribution, with jam times tending to infinity once the system goes beyond the critical density. With respect to the T^2-TCA's tempo-spatial behaviour, we note that the critical density for the former transition is located at $k_c = 0.5$ vehicles/cell, at which point all vehicles travel at a speed of one cell/time step with all space gaps equal to one cell. The density at which the recovery associated with latter transition occurs, is equal to $k = \frac{1}{3}$ vehicles/cell, at which point all vehicles travel at a speed of one cell/time step, but now with all space gaps equal to two cells. Fukui and Ishibashi later modified the delaying process, resulting in a system that always relaxes to a state in which the space-mean speed oscillates between two values, both smaller than one cell/time step [90].

The original background for Takayasu and Takayasu's work, was based on the presence of so-called $1/f$ noise (also known as *pink noise* or *flicker noise*) in the Fourier transformed density fluctuations of motorway traffic. The seemingly random stop-and-go motions of jammed vehicles, could indicate a chaotic behaviour (as opposed to just statistical noise), closely coupled with self-organised criticality (see also the end of Section 3.2.2) [67]. In the free-flow regime of the T^2-TCA model, jams have a finite life time leading to a flat spectrum, as opposed to the congested regime where jams have an infinite life time, leading to a $1/f$ spectrum [89].

Schadschneider and Schreckenberg later provided a generalisation of the T^2-TCA model: keeping $v_{\max} = 1$ cell/time step, they now modified the braking and acceleration behaviour of a vehicle. On the one hand, they kept Takayasu and Takayasu's original acceleration rule R2, Eq. (53), and on the other hand, they allowed a vehicle with a space gap of just one cell to accelerate with a *slow-to-start probability* $1 - p_t$ [91]. They furthermore also introduced a randomisation for moving vehicles, similar to the STCA (see Section 3.2.1), making vehicles stop with a slowdown probability p. Several interesting phenomena occur for certain values of both probabilities p and p_t. The modified spatial slow-to-start rule can lead to the appearance of an *inflection point* in the (k, q) diagram at very high densities. The effect gets strongly exaggerated when $p_t \to 1$, at which point a completely blocked state of zero flow appears for all global densities $k \geqslant 0.5$ vehicles/cell [91,18,3].

3.3.2. The model of Benjamin, Johnson, and Hui (BJH-TCA)

Around the same time that Takayasu and Takayasu proposed their T^2-TCA model, Benjamin, Johnson, and Hui (BJH) constructed another type of TCA model, using a slow-to-start rule that is of a *temporal nature* [92]. Their BJH-TCA model is based on the STCA (see Section 3.2.1), but extended it with a rule that adds a small delays to a stopped car that is pulling away from the downstream front of a queue. Benjamin et al. attribute this rule to the fact that it mimics the behaviour of a driver who momentarily looses attention, or when a vehicle's engine is slow to react. Their slow-to-start rule allows a stopped vehicle to move again with this *slow-to-start probability* $1 - p_s$. If the vehicle did not move, then it tries to move again but this time with probability p_s. Due to this peculiar acceleration procedure, all vehicles require a memory that, as mentioned before, makes the slow-start-rule temporal in nature [3]. As a result of this new systematic behaviour, jams will now become less ravelled (as opposed to the STCA), because the slow-to-start rule will have the tendency to merge queues.

The BJH-TCA model was also applied to the description of a motorway with an on-ramp, leading to the conclusions that (i) it actually is beneficial to have jams on the main motorway, due to the fact that these jams homogenise the traffic streams as they compete for stopped vehicles, and (ii) it is desirable to set a maximum speed limit on this main motorway which allows to maximise the performance of the on-ramp. Note that in their discussion, Benjamin et al. used the queue length at the on-ramp as a performance measure. In our opinion, this is not a very good choice as it ignores e.g., the total time spent in the system, which we believe is a more important measure (see also the work of Bellemans [93] and Hegyi [94] in this respect).

To conclude, we note that the (k, q) diagrams of the BJH-TCA and T^2-TCA models qualitatively look the same, with the exception the former does not have the possibility of an inflection point, or a density region with zero flow, as was the case for the latter model (see Section 3.3.1) [91,18].

3.3.3. Velocity-dependent randomisation TCA (VDR-TCA)

As already explained in the introduction of this section, reducing the outflow from a jam is responsible for the capacity drop and hysteresis phenomenon. To this end, Barlović et al. proposed a TCA model that generalises the STCA model (see Section 3.2.1) by employing an intuitive slow-to-start rule for stopped vehicles [95,96]. Similar to the STCA-CC (see Section 3.2.2), the complete rule set for the VDR-TCA is as follows:

(R0) *determine stochastic noise*

$$\begin{aligned} v_i(t-1) = 0 &\Longrightarrow p'(t) \leftarrow p_0 \ , \\ v_i(t-1) > 0 &\Longrightarrow p'(t) \leftarrow p, \end{aligned} \tag{55}$$

(R1) *acceleration and braking*

$$v_i(t) \leftarrow \min\{v_i(t-1) + 1, g_{s_i}(t-1), v_{\max}\} \ , \tag{56}$$

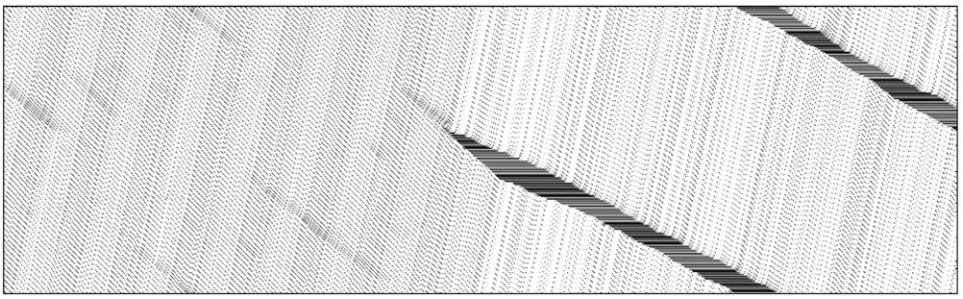

Fig. 25. A time–space diagram of the VDR-TCA model for $v_{\max} = 5$ cells/time step, $p_0 = 0.5$, $p = 0.01$, and a global density of $k = \frac{1}{6}$ vehicles/cell. The shown lattice contains 300 cells, with a visible period of 1000 time steps. We can see the breakdown of an initially homogeneous traffic pattern. As the phase separation takes place, a persistent compact jam is formed, surrounded by free-flow traffic. The significant decrease of the density in the regions outside the jam results from the jam's reduced outflow.

(R2) *randomisation*

$$\xi(t) < p'(t) \Longrightarrow v_i(t) \leftarrow \max\{0, v_i(t) - 1\} \,, \tag{57}$$

(R3) *vehicle movement*

$$x_i(t) \leftarrow x_i(t-1) + v_i(t) \,. \tag{58}$$

As before, in rule R2, Eq. (57), $\xi(t) \in [0, 1[$ denotes a uniform random number (specifically drawn for vehicle i at time t) and $p'(t)$ is the stochastic noise parameter, *dependent on the vehicle's speed* (hence the name 'velocity-dependent randomisation'). The probabilities p_0 and p are called the *slow-to-start probability* and the *slowdown probability*, respectively, with $p_0, p \in [0, 1]$. Note that Barlović et al. only considered the case with two different noise parameters (i.e., p_0 and p), ignoring the more general case where we can have a noise parameter for each possible speed (i.e., $p_0, \ldots, p_{v_{\max}}$). Their model was also considered for systems with open boundary conditions [97].

Depending on their speed, vehicles are subject to different randomisations: typical metastable behaviour results when $p_0 \gg p$, meaning that stopped vehicles have to wait longer before they can continue their journey. This has the effect of a reduced outflow from a jam, so that, in a closed system, this leads to an equilibrium and the formation of a *compact jam*. For such a typical situation, e.g., $p_0 = 0.5$ and $p = 0.01$, the tempo-spatial evolution is depicted in Fig. 25. We can see an initially homogeneous traffic pattern (one *metastable* phase) breaking down and kicking the system into a *phase-separated state*, consisting of a compact jam surrounded by free-flow traffic. In such a state, traffic jams in the system will absorb as many vehicles as is necessary, in order to have a free-flow phase in the rest of the system [6]. Note that the VDR-TCA can also be equipped with a cruise control, by turning of fluctuations for vehicles driving at the maximum speed $v_{\max}$.

In the left part of Fig. 26, we have plotted a histogram of the distributions of the vehicles' speeds, for all global densities $k \in [0, 1]$. Here we can clearly see the distinction between the free-flow and the congested regime: the space-mean speed remains more or less constant at a high value, then encounters a sharp transition (i.e., the capacity drop), resulting in a steady declination as the global density increases. Note that as the critical density is encountered, the standard deviation jumps steeply; this means that vehicles' speeds fluctuate wildly at the transition point (because they are entering and exiting the congestion waves). Once the compact jam is formed, the dominating speed quickly becomes zero (because vehicles are standing still inside the jam). Although most of the weight is attributed to this zero-speed, there is a non-negligible maximum speed present for intermediate densities. If the global density is increased further towards the jam density, this maximum speed disappears and the system settles into a state in which all vehicles either have speed zero or one (i.e., systemwide stop-and-go traffic).

Studying the (k, q) diagram in the right part of Fig. 26, gives us another view of this phase transition. We can see a capacity drop taking place at the critical density, where traffic in its vicinity behaves in a metastable manner. This metastability is characterised by the fact that sufficiently large disturbances of the fragile equilibrium can cause the flow to undergo a sudden decrease, corresponding to a first-order phase transition. The state of very high flow is then

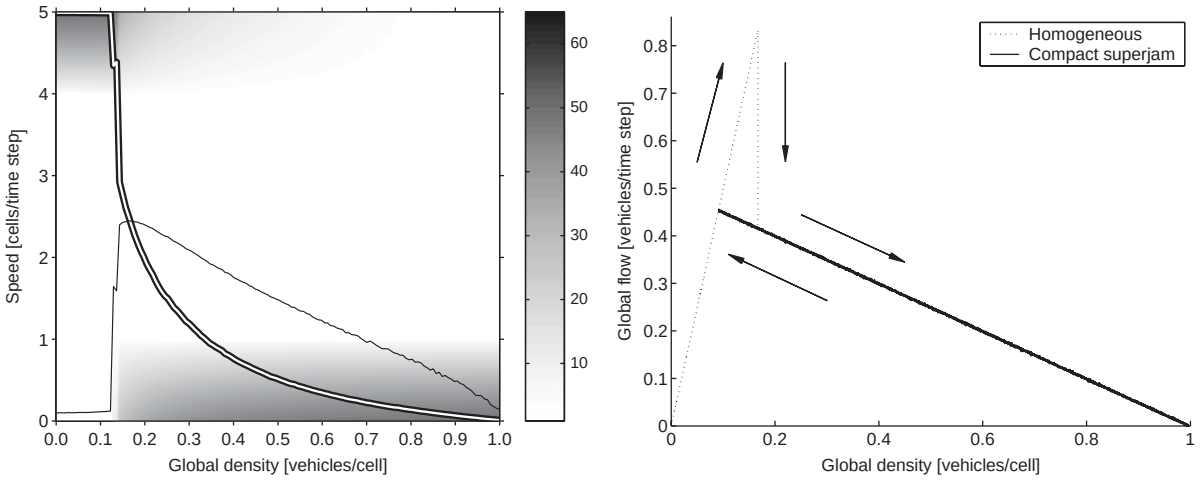

Fig. 26. *Left*: a contour plot containing the histograms of the distributions of the vehicles' speeds v as a function of the global density k in the VDR-TCA (with $v_{\max} = 5$ cells/time step, $p_0 = 0.5$ and $p = 0.01$). The thick solid line denotes the space-mean speed, whereas the thin solid line shows its standard deviation. The grey regions denote the probability densities. *Right*: a (k, q) diagrams for the same TCA model. The dotted line denotes global measurements that were obtained when starting from homogeneous initial conditions; the solid line is based on a compact superjam as the initial condition. The right part clearly shows a typical reversed λ shape, which indicates a capacity drop.

destroyed and the system settles into a phase separated state with a large megajam and a free-flow zone. The large jam will persist as long as the density is not significantly lowered, thus implying that recovery of traffic from congestion follows a hysteresis loop. In contrast to the STCA-CC's bistability, the VDR-TCA model is truly *metastable*, because now the free-flow branch in the (k, q) diagram becomes unstable for large enough perturbations. Furthermore, the spontaneous formation of jams in the downstream front that troubled the STCA, is suppressed in the VDR-TCA model.

Note that if $p_0 \ll p$, then the behaviour of the system will be drastically different. Four distinct traffic regimes emerge in the limiting case where $p_0 = 0$ and $p = 1$; in this case, the model is called *fast-to-start* [98]. In these four regimes, moving vehicles can never increase their speed once the system has settled into an equilibrium. Furthermore, there exists a regime which experiences forward propagating density waves, corresponding to a non-concave region in the system's flow–density relation. For more information, we refer to our work in [99,100].

3.3.4. Time-oriented TCA (TOCA)

Considering the STCA model (see Section 3.2.1), Brilon and Wu acknowledged the fact that it is quite capable of reproducing traffic dynamics in urban street networks. However, they also recognised the fact that the model performed rather inadequate when it comes to correctly describing the characteristics of traffic flows on motorways, e.g., compared to field data of a German motorway. Brilon and Wu blamed the unrealistic car-following behaviour of the STCA model for its inferior capabilities. At the core of their argument, they attributed this to the fact that the STCA model is exclusively based on spatial variables (e.g., space headways). In order to alleviate these problems, they proposed to use a model that was based on temporal variables (e.g., time headways), leading to more realistic vehicle–vehicle interactions [68]. The rule set for this time-oriented TCA model (TOCA) is as follows:

(R1) *acceleration*

$$\begin{aligned} g_{s_i}(t-1) &> (v_i(t-1) \cdot \overline{g}_{t_s}) \\ &\wedge \xi_1(t) < p_{\text{acc}} \\ &\Longrightarrow v_i(t) \leftarrow \min\{v_i(t-1)+1, v_{\max}\} \ , \end{aligned} \tag{59}$$

(R2) *braking*

$$v_i(t) \leftarrow \min\{v_i(t), g_{s_i}(t-1)\} \ , \tag{60}$$

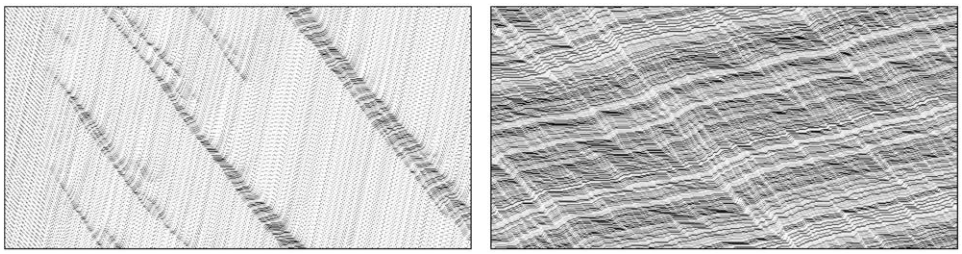

Fig. 27. Typical time–space diagrams of the TOCA model for $v_{\max} = 5$ cells/time step, $\overline{g}_{t_s} = 1.2$ time steps, and $p_{\text{acc}} = p_{\text{dec}} = 0.9$. The global density was set to $k = \frac{1}{6}$ vehicles/cell (*left*) and $k = 0.5$ vehicles/cell (*right*). The shown lattices each contain 300 cells, with a visible period of 580 time steps. In the left part, we can see the breakdown of an initially homogeneous traffic pattern, resulting in dilute jam that is surrounded by free-flow traffic. In the right part, we see a fully developed jam, dominating the entire system. As can be seen, for moderately light densities, the jams in the TOCA model contain moving vehicles.

(R3) *randomisation*

$$\begin{aligned} g_{s_i}(t-1) < (v_i(t-1) \cdot \overline{g}_{t_s}) \\ \wedge\, \xi_2(t) < p_{\text{dec}} \\ \Longrightarrow v_i(t) \leftarrow \max\{v_i(t) - 1, 0\}\ , \end{aligned} \tag{61}$$

(R4) *vehicle movement*

$$x_i(t) \leftarrow x_i(t-1) + v_i(t)\ . \tag{62}$$

In the above rules, $\xi_1(t), \xi_2(t) \in [0, 1[$ are random numbers drawn from a uniform distribution, $\overline{g}_{t_s \geqslant \Delta T}$ is the *safe time gap*, p_{acc} is the *acceleration probability*, and p_{dec} is the *deceleration probability*. Because all interactions between vehicles in the STCA are bounded by the update time step, their speeds will never oscillate, leading to a rigid and stable system. As a consequence of the TOCA's temporal rules however, vehicles will now behave more *elastically*, taking a safe time gap into account that allows them to adapt their speeds with a relaxation. In this case, a vehicle will resort to emergency braking (i.e., an instantaneous deceleration) only if it gets too close to its direct frontal leader [51]. Typical parameter values for the TOCA are $\overline{g}_{t_s} = 1.2$ time steps and $p_{\text{acc}} = p_{\text{dec}} = 0.9$. Brilon and Wu also extended their model with rudimentary rules that allowed for lane changes on unidirectional multi-lane roads.

In the left part of Fig. 27, we can see a similar tempo-spatial behaviour as with the VDR-TCA (see Section 3.3.3), in that an initially homogeneous traffic pattern breaks down, resulting in *dilute jam* that is surrounded by free-flow traffic. The major difference between jamming in the VDR-TCA and TOCA models however, is that in the former model, vehicles come to a complete stop when entering a jam (see Fig. 25). They remain stationary until they can leave the downstream front of the queue. In contrast to this, the jams in the TOCA model contain moving vehicles. Pushing the global density even further to $k = 0.5$ vehicles/cell as was done in the right part of Fig. 27, results in a fully developed jam that dominates the entire system and contains temporarily stopped vehicles.

Fig. 28 depicts two groups of (k, q) diagrams for the TOCA model, with $v_{\max} = 5$ cells/time step. The left part shows four diagrams for different combinations of p_{acc} and $p_{\text{dec}} \in \{(0.9, 0.1), (0.9, 0.9), (0.1, 0.1), (0.1, 0.9)\}$, each time with $\overline{g}_{t_s} = 1.2$ time steps. As can be seen, the default case with $p_{\text{acc}} = p_{\text{dec}} = 0.9$ leads to an inflection point at a moderately high density of $k = 0.5$ vehicles/cell, resulting in two different slopes for the congested branch of the TOCA's (k, q) diagram. At this point, vehicles will have average space gaps less than one cell, and because p_{dec} is rather high, vehicles will have the tendency to slow down (and p_{acc} is smaller then one, so their acceleration is somewhat inhibited). As a result, a large jam, comparable to the system's size, will dominate tempo-spatial evolution. Furthermore, the acceleration probability p_{acc} should take on rather high values, otherwise the global flow in the system is too low because vehicles are not accelerating anymore. In the right part of Fig. 28, we have shown a large amount of diagrams for different g_{t_s} with $p_{\text{acc}} = p_{\text{dec}} = 0.9$. Here we can see that, for $\overline{g}_{t_s} < \Delta T$, the resulting density–flow curves are non-monotonic. Higher values for $\overline{g}_{t_s}$ in more vehicles that drive more cautiously, apparently leading to higher values for the critical density and the capacity flow. Note that the seemingly small capacity drops at the end of each free-flow branch are in fact finite-size effects [73,101].

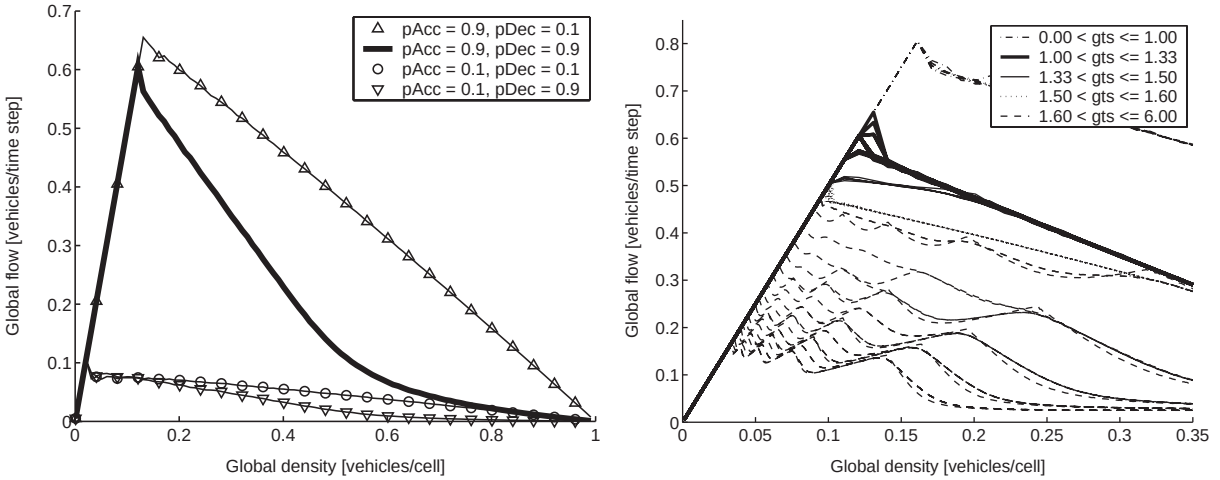

Fig. 28. Two groups of (k, q) diagrams for the TOCA model, with $v_{\max} = 5$ cells/time step. *Left*: four diagrams for different combinations of p_{acc} and p_{dec}, with $\overline{g}_{t_s} = 1.2$ time steps. *Right*: a large amount of diagrams for different g_{t_s} with $p_{\text{acc}} = p_{\text{dec}} = 0.9$. For $\overline{g}_{t_s} < \Delta T$, the resulting density–flow curves are non-monotonic. Note that the seemingly small capacity drops at the end of each free-flow branch are in fact finite-size effects [73,101].

In their original paper, Brilon and Wu claim that their TOCA model results in a better agreement with empirical data, a fact which is based on a qualitative comparison of the $(q, \overline{v}_s)$ diagrams [68]. Note that, after personal communication with the authors, it seems they performed a minimisation of the square errors in the $(k, \overline{v}_s)$ diagram. However, in order to get the correct values for calibrating the TOCA's parameters, they just manually guessed, without performing a thorough numerical optimisation. Despite this optimistic view, Knospe et al. later investigated the TOCA model's capabilities more thoroughly. Their conclusions state that a quite large value for the deceleration probability p_{dec} is necessary in order to obtain realistic capacity flows. Although the time headway distribution of a jam's downstream front in the TOCA model is correct with respect to real-life observations, its downstream front moves too fast due to the large deceleration probability. As a result, the jams in the TOCA model are more dilute, as could be seen in Fig. 27 [19].

3.3.5. TCA models incorporating anticipation

One of the models related to anticipative driving (i.e., only taking a leaders' reactions into account, without predicting them), can be found in the work of Krauß et al. who derived a collision-free model based on the STCA (see Section 3.2.1), but which uses *continuous* vehicle speeds. Their model can be considered as a simplified version of the Gipps model [1]. Although the model restricts vehicles' deceleration capabilities, it is still able to correctly reproduce the capacity drop and hysteresis phenomena [101].

Another model with anticipation was proposed by Eissfeldt and Wagner [40]. Their model is based on Krauß's work [1], and employs a next-nearest-neighbour interaction, which stabilises dense flows and results in a non-unique flow–density relation.

Recently, Lárraga et al. introduced a TCA model that includes a driver's *anticipation* of the leading vehicle's speed [41]. In contrast to the STCA model (see Section 3.2.1), the acceleration and braking rules are decoupled. As a first rule, the standard acceleration towards the maximum speed is applied, after which the randomisation is performed by means of a second rule. Only then, the model considers braking in its third rule; however, the deceleration is not only based on the space gap between both vehicles, but also on an anticipation of the leading vehicle's speed:

(R3) *anticipation and braking*

$$v_i(t) \leftarrow \min \left\{ v_i(t), \underbrace{g_{s_i}(t-1) + \left[(1-\alpha_i) \cdot v_{i+1}(t-1) + \frac{1}{2} \right]}_{\text{safe distance}} \right\} , \tag{63}$$

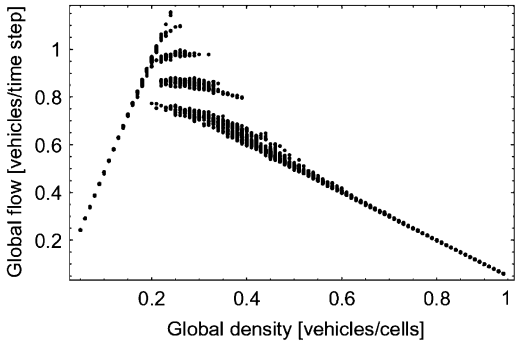

Fig. 29. A (k, q) diagram of Nishinari et al.'s extended BCA model, with $v_{\max} = 5$ cells/time step, $\Delta T = 1.3$ s, $\Delta X = 7.5$ m, and a driver's perspective of two vehicles ahead. The resulting diagram exhibits multiple metastable branches. Vehicles inside jams come to a complete stop only for the lowest metastable branch; for the higher branches, vehicles inside jams are still able to move forward. Depending on the strength of a local perturbation, traffic will shift from the highest branch to one of the lower branches (image reproduced after [109]).

with $v_i(t)$ on the right-hand side corresponding to the computed speed after applying rule R2, $[x]$ denoting x rounded to the nearest integer, $v_{i+1}(t-1)$ the speed of the leading vehicle at the current time step, and $\alpha_i \in [0, 1]$ an anticipatory driving parameter for the ith vehicle. In their work, Lárraga et al. considered all α_i to be equal.

The interesting aspect of this anticipatory TCA model, is that for certain values of α, it can result in *dense platoons of vehicles*, travelling coherently and thereby leading to forward propagating density structures. In the free-flow regime, the (k, q) diagram also exhibits a slight curvature near the capacity flow, similar to the ER-TCA model (see Section 3.2.5). Del Rió and Lárraga later also extended the model to accommodate for multi-lane traffic flows [102].

3.3.6. Ultra discretisation, slow-to-accelerate, and driver's perspective

It is also possible to derive a cellular automaton model, based on the discretisation of a partial differential equation. Starting from a PDE (e.g., the Burgers equation [1]), we can obtain an finite difference equation by discretising the spatial and temporal dimensions, resulting in a model that still has continuous state variables. As a further step, we can now also discretise these state variables, using a process called the *ultra-discretisation method* (UDM) [103]. The result of the UDM can be interpreted as a cellular automaton in the *Euler representation*. The latter means that for a TCA model, a road is considered to be a field, whereby the individual cars are not distinguished [104]. The interesting part of this type of CA is that its cells are allowed to hold multiple vehicles, which makes it possible to implicitly model multi-lane traffic in a simplified sense (because the effects of lane changes are neglected) [3]. As a next step, this obtained CA can be cast in its *Lagrangian representation*, by means of an *Euler–Lagrange transformation* [104,105]. The resulting Lagrange representation treats the positions of all vehicles individually, thus leading to the well-known position-based rule sets of the TCA models discussed in this report.

Nishinari proposed an interesting TCA model, based on the above UDM scheme. Their discretisation leads to the so-called *Burgers cellular automaton* (BCA), which is for single-lane traffic equivalent to the CA-184 TCA model (see Section 3.1.1) [106,107]. Emmerich et al. also provided a TCA model, by applying the UDM scheme to a Korteweg–de Vries equation. In contrast to the BCA model, their work resulted in a second-order TCA model because the CA's global map not only needs the configuration at the previous time step $t - 1$, but also the configuration at time step $t - 2$ [108,3].

Nishinari et al. recently extended the BCA model, thereby allowing for slow-to-start effects with $v_{\max} > 1$ cell/time step [109]. Their model contains a rule similar to the classic notion of slow-to-start rules, but now generalised for moving vehicles, leading to the terminology of a *slow-to-accelerate* rule. Taking the idea of anticipation one step further, they also incorporated a *driver's perspective*, meaning that a vehicle will base its acceleration and braking decisions not only on the basis of its space gap and the anticipated speed of the vehicle ahead, but also on the space gap with the *next* leading vehicle (or even a vehicle located more downstream). As a result, the model exhibits *multiple metastable branches* in the (k, q) diagram, as can be seen in Fig. 29. For the lowest metastable branch, vehicles inside jams will come to a complete stop. In contrast to this, vehicles will still be able to move forward inside jams for the

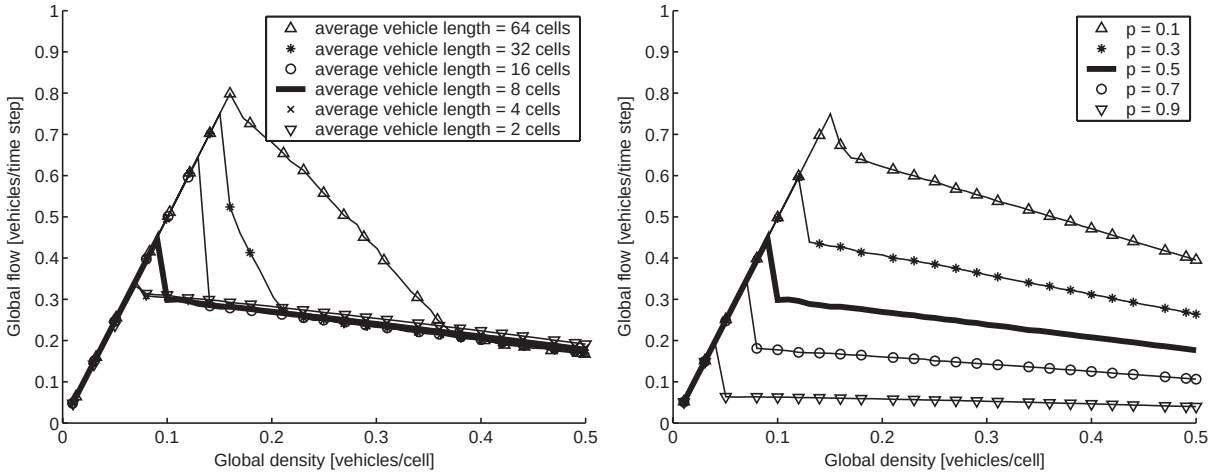

Fig. 30. *Left*: several (k, q) diagrams of the MC-STCA, for $\bar{l} \in \{2, 4, 8, 16, 32, 64\}$ cells and $p = 0.5$. As can be seen, an increase of the average vehicle length apparently results in a higher critical density, with an associated higher capacity flow (followed by a capacity drop). *Right*: the same setup for the MC-STCA, but now with a fixed $\bar{l} = 8$ cells and $v_{\max} = 5 \times 8 = 40$ cells/time step. The (k, q) diagrams depict the results of changing the slowdown probability $p \in \{0.1, 0.3, 0.5, 0.7, 0.9\}$: an increase of p, leads to decrease of both the critical density and the capacity flow.

higher branches. Note that depending on the strength of a local perturbation, traffic will shift from the highest branch to one of the lower branches. Finally, Nishinari et al. also combined the model with the classic STCA (see Section 3.2.1), thereby allowing for stochasticity in both the acceleration and braking rules.

4. Multi-cell models

Whereas all the previously discussed TCA models were based on a single-cell setup, this section introduces some of the existing multi-cell TCA models (still for single-lane traffic). In a multi-cell model, a vehicle is allowed to span a number of consecutive cells in the longitudinal direction, i.e., $l_i \geqslant 1$ cell.

In the subsequent sections, we discuss several multi-cell TCA models encountered in literature. We first start with an overview of the artifacts that can be introduced when switching to a multi-cell setup. Subsequently, we describe three multi-cell TCA models, which have more intricate rule sets than the simple models of Section 3:

- Helbing–Schreckenberg TCA (HS-TCA)
- Brake-light TCA (BL-TCA)
- The model of Kerner, Klenov, and Wolf (KKW-TCA)

Note that with respect to the measurements performed on the TCA models' lattices, we assume homogeneous traffic flows, i.e., all vehicles have the same length. This allows us, after suitable adjustment with the average vehicle length $\bar{l} = l_i$, to express the global density as $k_g \in [0, 1]$.

4.1. Artifacts of a multi-cell setup

It might seem that a translation of the classic STCA model (see Section 3.2.1) into a multi-cell version would be straightforward. However, using a finer discretisation introduces a very specific artifact, i.e, *hysteresis*. In order to investigate this phenomenon, we have performed several experiments based on a multi-cell translation of the STCA model (now called the MC-STCA). In what follows, we assume a closed-loop lattice consisting of 10^5 cells. The simulations ran each for 5×10^5 time steps, with $\Delta T = 1$ s.

Setting the slowdown probability to $p = 0.5$, the left part of Fig. 30 shows the resulting (k, q) diagrams for different spatial discretisations, each time for homogeneous initial conditions. The average vehicle length was set to

$\bar{l} \in \{2, 4, 8, 16, 32, 64\}$ cells. In these experiments, we also scaled the maximum speed $v_{\max}$ correspondingly (e.g., if $\bar{l} = 4$ cells, then $v_{\max}$ would become $5 \times 4 = 20$ cells/time step), as can be seen from the coinciding free-flow branches in the left part in Fig. 30. We also notice that an increase of the average vehicle length apparently results in a higher critical density, with an associated higher capacity flow. Furthermore, the flow seems to encounter a *capacity drop* at this critical dense.

What causes this capacity drop? To answer this question, we must first consider what happens in the deterministic case where $p = 0$. Here, our experiments have shown that there is no difference between a single- and a multi-cell setup. Setting $p > 0$, the randomisation rule R2, Eq. (47), introduces fluctuations in the high speeds of vehicles in free-flow traffic. However, these speed fluctuations are actually small compared to the vehicles' speeds themselves. Because of this limited influence, the free-flow branch of the (k, q) diagrams remains *very stable*. The smaller the discretisation, i.e., the larger the average vehicle length, the more stable the free-flow branch becomes for larger densities (note however that the capacity drop gets less pronounced for increasing average vehicle lengths). This capacity drop behaviour due to a stabilisation effect, is akin to the observations in the STCA's cruise-control limit (see Section 3.2.2), and thus different from the VDR-TCA (see Section 3.3.3), where a reduced outflow from a jam causes the drop in flow [19]. In contrast to this, random initial conditions or a superjam to start the simulations with, will always lead to the congested branch, thereby indicating a hysteretic phase transition. As the left part of Fig. 30 indicates, changing the discretisation level of the STCA, by adjusting the average vehicle length and relatively keeping the same maximum speed, has only an effect on the length of the free-flow branch; the traffic dynamics in the congested regime remain the same.

Holding $\bar{l}$ fixed at 8 cells and $v_{\max} = 5 \times 8 = 40$ cells/time step, the right part of Fig. 30 shows the resulting (k, q) diagrams for different values of the slowdown probability $p \in \{0.1, 0.3, 0.5, 0.7, 0.9\}$. It is clear that an increase of p, leads to a decrease of both the critical density and the capacity flow. Note that the size of the capacity drop remains approximately the same for the different p.

To conclude, we mention the work of Grabolus who performed extensive numerical studies on the STCA. He also noted that it is possible to translate any multi-cell STCA variant into an *equivalent* single-cell STCA model, by suitably adjusting the values of the density and the maximum speed [98].

Interestingly, the use of a smaller discretisation was already considered by Barrett et al. in the early course of the TRANSIMS project [110,1]. In their work, they introduce the terminology of *multi-resolution* TCA models, corresponding to our multi-cell setup. Although they discuss several methods for integral refinements of the TCA's lattice, they do not make any mention of the observed hysteresis phenomenon introduced by a finer discretisation.

4.2. Advanced multi-cell models

Having discussed the repercussions of switching to a multi-cell setup, we now illustrate three TCA models that have more complex rule sets. We discuss their properties by means of time–space diagrams, fundamental diagrams of global and local measurements, and histograms of the distributions of the space and time gaps.

4.2.1. The model of Helbing and Schreckenberg (HS-TCA)

Similar in spirit as the STCA (see Section 3.2.1) and the ER-TCA (see Section 3.2.5), Helbing and Schreckenberg proposed their HS-TCA model in analogy with the optimal velocity model [111]. In fact, their model can be seen as a direct discretisation of the OVM, with the following rule set:

(R1) *acceleration and braking*

$$v_i(t) \leftarrow v_i(t-1) + \lfloor \alpha(V(g_{s_i}(t-1)) - v_i(t-1)) \rfloor \ , \tag{64}$$

(R2) *randomisation*

$$\xi(t) < p \Longrightarrow v_i(t) \leftarrow \max\{0, v_i(t) - 1\} \ , \tag{65}$$

(R3) *vehicle movement*

$$x_i(t) \leftarrow x_i(t-1) + v_i(t) \ . \tag{66}$$

Table 1
A possible optimal velocity function (OVF) for the TCA model of Helbing and Schreckenberg (HS-TCA)

g_{s_i}	$V(g_{s_i})$	g_{s_i}	$V(g_{s_i})$
0, 1	0	11	8
2, 3	1	12	9
4, 5	2	13	10
6	3	14, 15	11
7	4	16–18	12
8	5	19–23	13
9	6	24–36	14
10	7	$\geqslant 37$	15

The OVF is represented as a table, giving the optimal speed $V(g_{s_i})$ (expressed as cells/time step) associated with each possible space gap g_{s_i} (expressed as a number of cells).

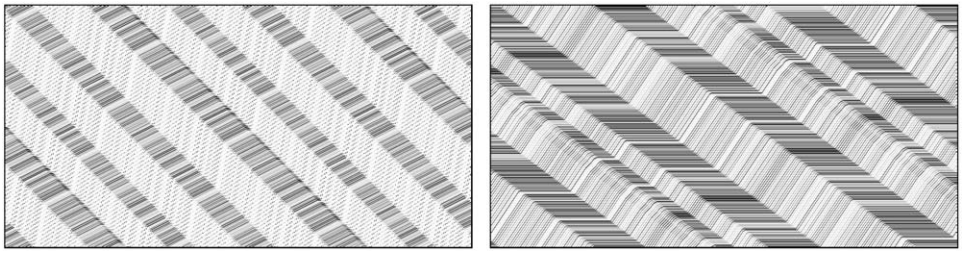

Fig. 31. Typical time–space diagrams of the HS-TCA model, with $l = 2$ cells, $p = 0.001$ $\alpha = 1 \div 1.3$, and $v_{\max} = 15$ cells/time step. The shown closed-loop lattices each contain $300 \times 2 = 600$ cells, with a visible period of 580 time steps. The global density k was set to 0.25 vehicles/cell (*left*) and 0.40 vehicles/cell (*right*). The formation of congestion waves leads to dense, compact jams containing stopped vehicles. Vehicles strive to decelerate smoothly, but are allowed to accelerate instantaneously when exiting jams fronts.

The function $V(g_{s_i})$ in rule R1, Eq. (64), is the discrete version of the optimal velocity function; it is specified in the form of a lookup table, containing speed entries for each space gap (see Table 1) and has the following meaning: higher values for the parameter α indicate an almost instantaneous adaptation of the vehicle's speed to the OVF, whereas lower values denote an increasing inertia and longer adaptation times [111]. However, as stated by Chowdhury et al. and Knospe et al., the role of α is a bit unclear as it does not exactly correspond to the timescale of the adaptation to the OVF (which is the case for the original optimal velocity model) [3,19]. Furthermore, certain values for α can, in combination with the OVF, lead to collisions between vehicles (because α reduces a vehicle's braking capability). Knospe et al. later provided the necessary conditions that guarantee collision-free driving, and avoid the possible backward moving of vehicles [19]. Note that, similar to the Fukui–Ishibashi models (see Sections 3.1.2 and 3.2.3), vehicles are allowed to accelerate instantaneously in the HS-TCA model. The model is stochastic, in that it introduces randomisation by means of rule R2, Eq. (65), with $\xi(t) \in [0, 1[$ a random number drawn from a uniform distribution.

In Fig. 31, we have given two time–space diagrams of the HS-TCA for global densities $k = 0.25$ and 0.40 vehicles/cell. The length of a vehicle was $l = 2$ cells, $p = 0.001$, $\alpha = 1$–1.3, $v_{\max} = 15$ cells/time step, $\Delta T = 1$ s, and $\Delta X = 2.5$ m. Due the small slowdown probability, the system dynamics are strongly deterministic, totally dependent on the initial (homogeneous) conditions. In the left diagram we can observe how vehicles can accelerate instantaneously when exiting a jam. Note that for higher densities, all jams become dense and compact, always containing stopped vehicles, as is depicted in the right diagram. Because of the non-linearity introduced by the discretised optimal velocity function, all tempo-spatial patterns in the system are of a chaotic nature (i.e., nonlinear with stochastic noise) [19].

The $(k, \overline{v}_s)$ and (k, q) diagrams in Fig. 32 are based on local and global measurements. A feature of these diagrams is that the local measurements tend to form clusters around certain space-mean speeds (see the left part of Fig. 32): these clusters correspond to the speeds dictated by the discretised optimal velocity function of Table 1, each time associated with an average space gap corresponding to the inverse of the locally measured density. As a result, the (k, q) diagram in the right part of Fig. 32 shows several branches, each one with a different OVF speed. The lowest branch corresponds to the speed of the backward propagating waves, i.e., the jam speed. Even more striking, is that from

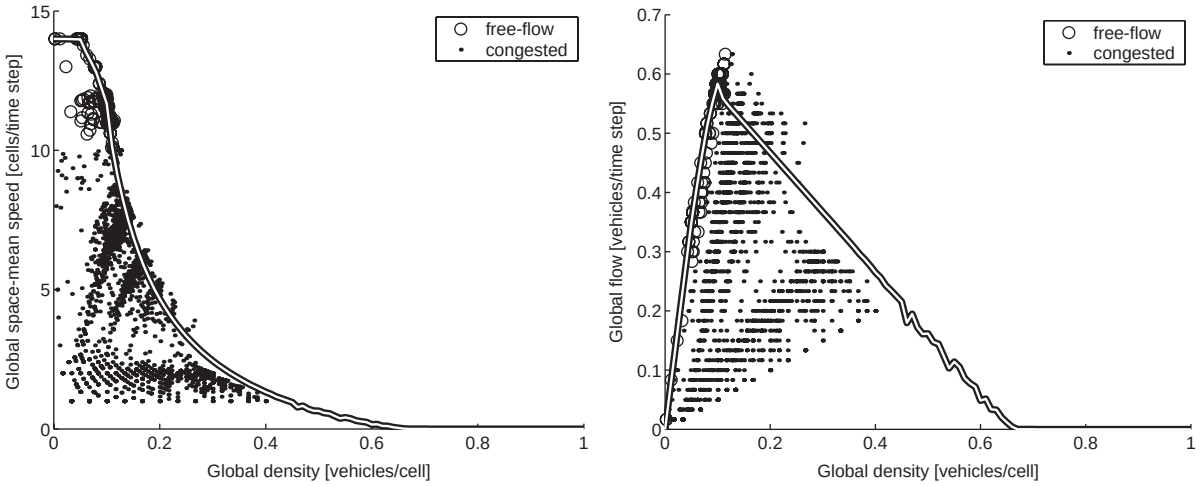

Fig. 32. The $(k, \overline{v}_s)$ (*left*) and (k, q) (*right*) diagrams for the HS-TCA, obtained by local and global measurements. The local measurements tend to form clusters around certain space-mean speeds, corresponding to the speeds dictated by the discretised optimal velocity function of Table 1. These clusters are visible in the right diagram as branches with different slopes. Remarkably, from a certain finite density $k \ll 1$ vehicle/cell on, all vehicles always come to a full stop and the flow in the system becomes zero.

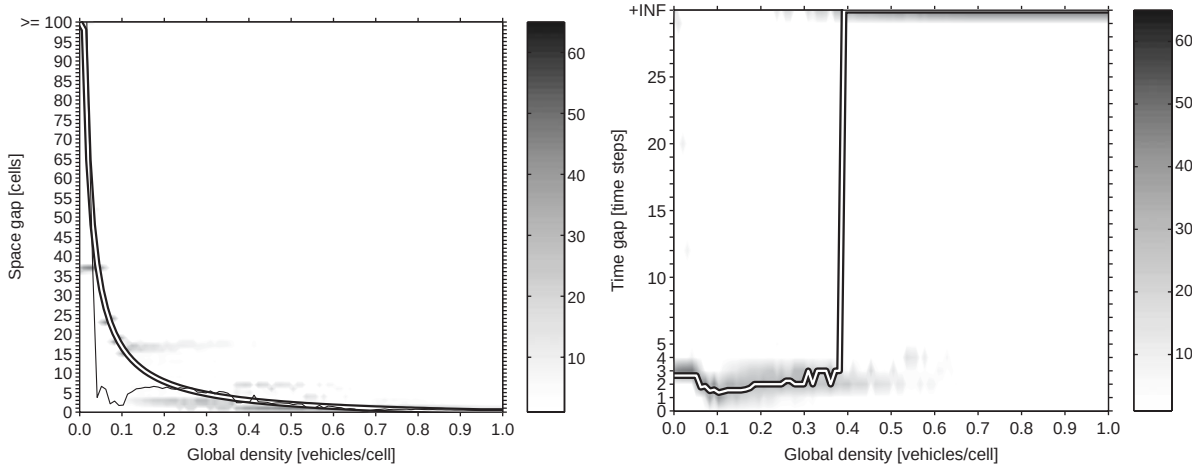

Fig. 33. Histograms of the distributions of the vehicles' space gaps g_s (*left*) and time gaps g_t (*right*), as a function of the global density k in the HS-TCA. The thick solid lines denote the mean space gap and median time gap, whereas the thin solid line shows the former's standard deviation. The grey regions denote the probability densities.

a certain finite density $k \ll 1$ vehicle/cell on, all vehicles always come to a full stop and the flow in the system becomes zero [111].

To conclude our discussion of the HS-TCA, we give the histograms of the distributions of the space and time gaps in the left and right parts, respectively, of Fig. 33. The most prominent features of these histograms, are that (i) there exist small clusters of probability mass between certain space gaps (i.e., 15–20, 25–25, and 35–40 cells), corresponding to groups of vehicles, (ii) for higher densities, we can observe a spread-out cluster of probability mass, corresponding to the lowest local measurements in the left part of Fig. 32, and (iii) in contrast to the previous TCA models, the median of the time gap for the HS-TCA is already very small for densities $k < 0.1$.

The HS-TCA might seem an interesting improvement, as its being based on a discretisation of the optimal velocity model. But although its authors state that it "*reproduces many of empirically observed features*" [111], Knospe et al. showed several shortcomings in the model [19]: care must be taken to avoid collisions, and the model fails to reproduce

the synchronised-flow regime entirely. This latter can be understood by looking at the dense, compact structure of jams in the time–space diagrams of Fig. 31, and the occurrence of branches with distinct speeds as in the right part of Fig. 32.

4.2.2. Brake-light TCA (BL-TCA)

Recently, an interesting idea was pursued by Knospe et al.; their TCA model includes *anticipation* effects, introduced by equipping the vehicles with *brake lights* [112]. The focus of this (and the following) TCA model lies in a correct reproduction of the three phases of traffic as introduced by Kerner et al. [57,1]. In a sense, the BL-TCA incorporates many of the features encountered in previously discussed single-cell TCA models. First of all, the BL-TCA has randomisation for spontaneous braking. Secondly, it has slow-to-start behaviour for the capacity drop and hysteresis phenomena. Moreover, it incorporates anticipation which can lead to a stabilisation of the free-flow branch. Finally, it includes elements for reproducing synchronised traffic. These latter two aspects clearly go beyond the standard incentive if drivers to avoid collisions. As such, it is the desire for smooth and comfortable driving (which resembles *human behaviour*), is responsible for the occurrence of traffic states like e.g., synchronised traffic [39]. To achieve all this, the rule set of the BL-TCA becomes quite complex, in comparison with some of the more standard single-cell TCA models of Section 3:

(R0) *determine stochastic noise*

$$\begin{aligned} b_{i+1}(t-1) = 1 \wedge t_{h_i}(t-1) < t_{s_i}(t-1) \\ \Longrightarrow p(t) \leftarrow p_b \ , \\ v_i(t-1) = 0 \\ \Longrightarrow p(t) \leftarrow p_0 \ , \\ \text{else} \\ \Longrightarrow p(t) \leftarrow p_d \ , \\ b_i(t) \leftarrow 0, \end{aligned} \tag{67}$$

(R1) *acceleration*

$$\begin{aligned} (b_i(t-1) = 0 \wedge b_{i+1}(t-1) = 0) \\ \vee\, t_{h_i}(t) \geqslant t_{s_i}(t) \\ \Longrightarrow v_i(t) \leftarrow \min\{v_i(t+1), v_{\max}\} \ , \end{aligned} \tag{68}$$

(R2a) *determine effective space gap*

$$g^*_{s_i}(t) \leftarrow g_{s_i}(t-1) + \max\left\{ \underbrace{\min\{v_{i+1}(t-1), g_{s_{i+1}}(t-1)\}}_{\text{anticipated speed of leading vehicle}} - g_{s_{\text{security}}}, 0 \right\} \ , \tag{69}$$

(R2b) *braking*

$$\begin{aligned} v_i(t) \leftarrow \min\{v_i(t), g^*_{s_i}(t)\} \ , \\ v_i(t) < v_i(t-1) \\ \Longrightarrow b_i(t) \leftarrow 1 \ , \end{aligned} \tag{70}$$

(R3) *randomisation*

$$\begin{aligned} \xi(t) < p(t) \Longrightarrow p(t) = p_b \wedge v_i(t) = v_i(t-1) + 1 \\ \Longrightarrow b_i(t) \leftarrow 1, \quad v_i(t) \leftarrow \max\{0, v_i(t) - 1\} \ , \end{aligned} \tag{71}$$

(R4) *vehicle movement*

$$x_i(t) \leftarrow x_i(t-1) + v_i(t) \ , \tag{72}$$

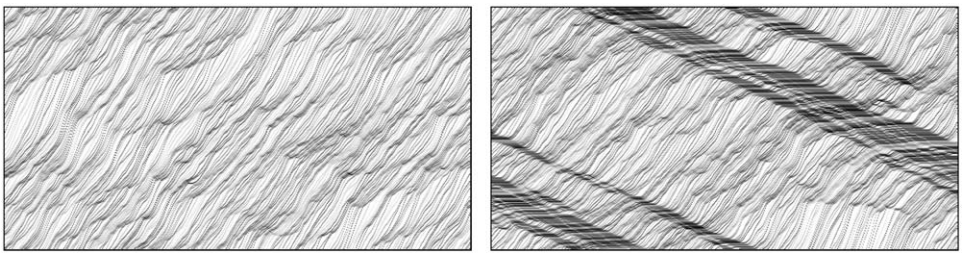

Fig. 34. Typical time–space diagrams of the BL-TCA model (refer to the text for the used parameter values). The shown closed-loop lattices each contain $300 \times 5 = 1500$ cells, with a visible period of 580 time steps. The global density k was set to 0.25 vehicles/cell (*left*) and 0.40 vehicles/cell (*right*). The visible forward propagating density waves are a result of the anticipation and synchronisation phenomena. At higher densities, stable jams occur, indicative of the wide-moving jam phase.

where $b_i(t)$ denotes the state (0 or 1) of the brake light of the ith vehicle at time step t, $t_{h_i} = g_{s_i}/v_i$ and $t_{s_i} = \min\{v_i, h\}$ with h the interaction range of the brake light. As such, t_{h_i} is the time to reach the leading vehicle, which gets compared with an *interaction horizon* t_{s_i} that depends on the speed v_i and is constrained by h. If the leading vehicle is far away, its brake light should not influence the following vehicle. Furthermore, rule R0 also takes into account that drivers are more alert when they are travelling at high speeds. The slowdown probability p in rule R0, Eq. (67), corresponds to either the *braking probability* p_b, the slow-to-start probability p_0, or the classic slowdown probability p_d for decelerations. Finally, $g^*_{s_i}(t)$ in rules R2a and R2b, Eqs. (69) and (70), respectively, denotes the *effective space gap*, based on the *anticipated speed* of the leading vehicle and taking into account a *security constraint* $g_{s_{\text{security}}}$. Just as the previous TCA models, the BL-TCA is stochastic, in that it introduces randomisation by means of rule R3, Eq. (71), with $\xi(t) \in [0, 1[$ a random number drawn from a uniform distribution. If a vehicle was in the process of braking due to the previous rules, then its brake light b_i is turned on. Note that Knospe also extended the BL-TCA with rules that allow asymmetric lane changing on a two-lane road (unidirectional), incorporating a right-lane preference as well as an overtaking prohibition on the right lane. As such, the model correctly reflects the density inversion phenomenon (see also Section 5.1) [39,113].

In the remainder of this discussion, we set $p_b = 0.94$, $p_0 = 0.5$, $p_d = 0.1$, $h = 6$ time steps, $g_{s_{\text{security}}} = 7$ cells, $v_{\max} = 20$ cells/time step, with a vehicle length of $l = 5$ cells, $\Delta T = 1$ s, and $\Delta X = 1.5$ m [112,19]. With respect to the calibration of the BL-TCA model's parameters, Knospe et al. provide a nice overview, giving intuitive analogies for each of these parameters (e.g., p_0 is associated with the speed of the backward propagating waves) [19].

In Fig. 34, we have given two time–space diagrams of the BL-TCA for global densities $k = 0.25$ and 0.40 vehicles/cell. As can be seen in the time–space diagram in the left part, the anticipation and synchronisation phenomena lead to forward propagating density waves, where vehicles carry the density downstream. Going to higher densities, we can see stable jams, indicative of the wide-moving jam phase (see also Kerner's three-phase traffic theory [57,1]).

Looking at the $(k, \overline{v}_s)$ and (k, q) diagrams in Fig. 35, we can use the local measurements to discriminate between the free-flow ($\circ$), synchronised-flow ($\cdot$), and jammed regimes ($\star$). The synchronised regime is visible as a wide scatter in the data points, having various speeds but relatively high flows. The data points in the wide-moving jam correspond to Kerner's so-called line J [57,1]. The use of a finer discretisation can lead to metastable states (see Section 4.1), but as Knospe et al. note, the slow-to-start behaviour in rule R0, Eq. (67), is necessary in order to produce the correct speed of the backward propagating wave, as a result of a reduced outflow from a jam [19].

Finally, Fig. 36 depicts the histograms of the distributions of the space and time gaps in the left and right parts, respectively. In contrast to the HS-TCA, there are no more clusters for the space gap (see left part of Fig. 33), but rather a smooth region of probability mass: as the global density of the system increases, the average space gap diminishes continuously and monotonically. The observations for the distributions of the time gaps correspond to those encountered in literature [112,19]: from the right part of Fig. 36, we can see a wide range of probability mass at low densities (free-flow traffic), corresponding to a wide distribution of time gaps. At intermediate densities (synchronised flow), the distribution tends to peak, leading to a small dense cluster at approximately $k = 0.15$ vehicles/cell, with a median time gap of 1 time step. Finally, at higher densities (jammed traffic), the distribution of the time gaps gets more peaked, as is illustrated by the narrowing of the grey region of probability mass.

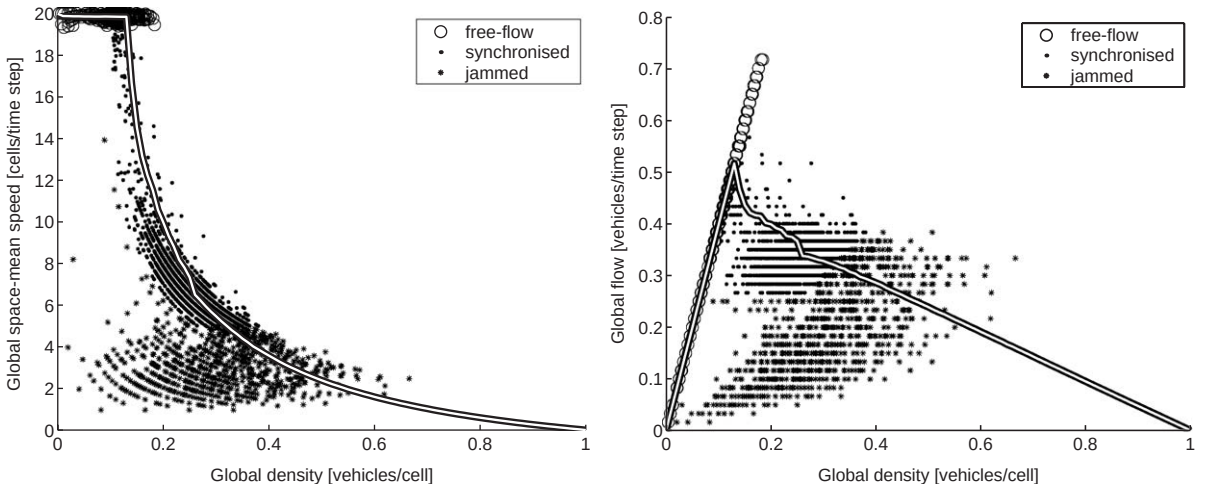

Fig. 35. The $(k, \overline{v}_s)$ (*left*) and (k, q) (*right*) diagrams for the BL-TCA model, obtained by local and global measurements. The local measurements discriminate between the free-flow ($\circ$), synchronised-flow ($\cdot$), and jammed regimes ($\star$). The synchronised regime is visible as a wide scatter in the data points, having various speeds but relatively high flows. The data points in the wide-moving jam correspond to Kerner's line *J*.

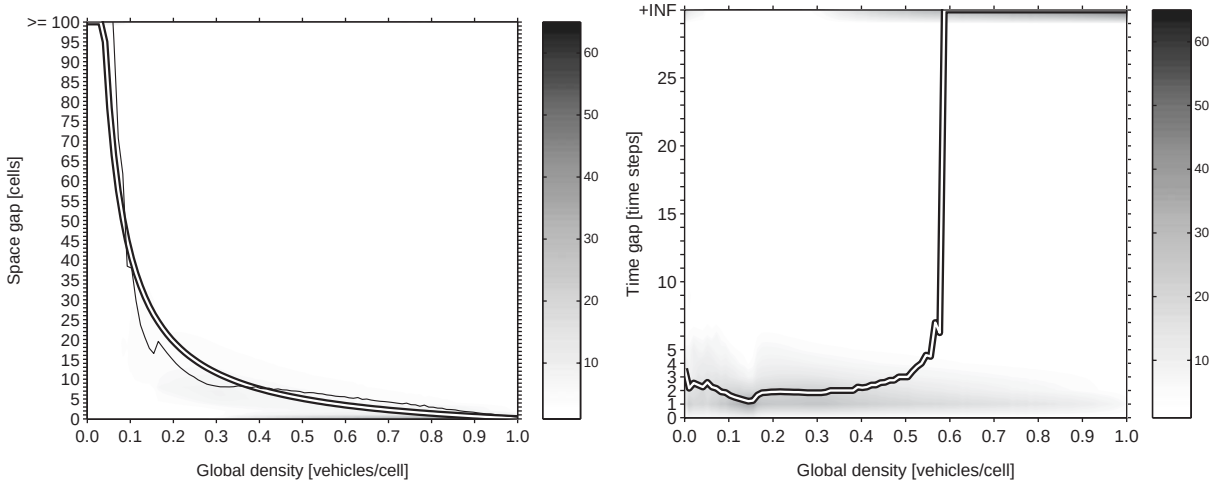

Fig. 36. Histograms of the distributions of the vehicles' space gaps g_s (*left*) and time gaps g_t (*right*), as a function of the global density k in the BL-TCA model. The thick solid lines denote the mean space gap and median time gap, whereas the thin solid line shows the former's standard deviation. The grey regions denote the probability densities.

4.2.3. The model of Kerner, Klenov, and Wolf (KKW-TCA)

Based upon the BL-TCA of Knospe et al., Kerner, Klenov, and Wolf (KKW) refined this approach by extending it. Their work resulted in a family of models that incorporate the notion of a *synchronisation distance* for individual vehicles [114]. Derived from this model class, Kerner et al. proposed discretised versions in the form of traffic cellular automata models. In this report, we consider the KKW-1 TCA model, of which the complex rule set is as follows [115]:

(R1a) *determine synchronisation distance*

$$D_i(t) \leftarrow D_0 + D_1 v_i(t-1) \ , \tag{73}$$

(R1b) *determine acceleration and deceleration*

$$\begin{aligned} &v_i(t-1) < v_{i+1}(t-1) \Longrightarrow \Delta_{\mathrm{acc}_i}(t) \leftarrow a \ , \\ &v_i(t-1) = v_{i+1}(t-1) \Longrightarrow \Delta_{\mathrm{acc}_i}(t) \leftarrow 0 \ , \\ &v_i(t-1) > v_{i+1}(t-1) \Longrightarrow \Delta_{\mathrm{acc}_i}(t) \leftarrow -b \ , \end{aligned} \tag{74}$$

(R1c) *determine desired speed*

$$\begin{aligned} &g_{s_i}(t-1) > (D_i(t) - l_i) \\ &\qquad \Longrightarrow v_{\mathrm{des}_i}(t) \leftarrow v_i(t-1) + a \ , \\ &g_{s_i}(t-1) \leqslant (D_i(t) - l_i) \\ &\qquad \Longrightarrow v_{\mathrm{des}_i}(t) \leftarrow v_i(t-1) + \Delta_{\mathrm{acc}_i}(t) \ , \end{aligned} \tag{75}$$

(R1d) *determine deterministic speed*

$$v_i(t) \leftarrow \max\{0, \min\{v_{\max}, g_{s_i}(t), v_{\mathrm{des}_i}(t)\}\} \ , \tag{76}$$

(R2a) *determine acceleration probability*

$$\begin{aligned} &v_i(t) < v_p \Longrightarrow p_a(t) \leftarrow p_{a_1} \ , \\ &v_i(t) \geqslant v_p \Longrightarrow p_a(t) \leftarrow p_{a_2} \ , \end{aligned} \tag{77}$$

(R2b) *determine braking probability*

$$\begin{aligned} &v_i(t) = 0 \Longrightarrow p_b(t) \leftarrow p_0 \ , \\ &v_i(t) > 0 \Longrightarrow p_b(t) \leftarrow p_d \ , \end{aligned} \tag{78}$$

(R2c) *determine stochastic noise*

$$\begin{aligned} &\xi(t) < p_a(t) \Longrightarrow \eta_i(t) \leftarrow a \ , \\ &p_a(t) \leqslant \xi(t) < p_a(t) + p_b(t) \Longrightarrow \eta_i(t) \leftarrow -b \ , \\ &\xi(t) \geqslant p_a(t) + p_b(t) \Longrightarrow \eta_i(t) \leftarrow 0 \ , \end{aligned} \tag{79}$$

(R2d) *determine stochastic speed*

$$v_i(t) \leftarrow \max\{0, \min\{v_{\max}, v_i(t) + \eta_i(t), v_i(t) + a\}\} \ , \tag{80}$$

(R3) *vehicle movement*

$$x_i(t) \leftarrow x_i(t-1) + v_i(t) \ . \tag{81}$$

As can be seen from this overview, the KKW-TCA model's rule set is mainly composed of a *deterministic* part (rules R1a–d) and a *stochastic* part (rules R2a–d). In the deterministic part, the synchronisation distance D_i is computed first with rule R1a, which uses a linear function (other forms, e.g., quadratic functions, are also possible). The parameters D_0 and D_1 need to be estimated. Rule R1c determines the desired speed v_{des_i}: the first part of the rule allows the vehicle to accelerate, whereas the second part of the rule uses an acceleration Δ_{acc_i} defined by rule R1b (a and b are parameters denoting the acceleration, and respectively braking, capabilities). As such, a vehicle will tend to adapt its speed to that of its direct frontal leader, whenever the vehicle is within a zone of interaction (i.e., the synchronisation distance). The deterministic speed is then computed by means of rule R1d, which takes into account the maximum speed $v_{\max}$, the space gap g_{s_i} to avoid a collision, and the previously computed desired speed of rule R1c.

In the stochastic part for computing the speed, a randomisation is introduced in rule R2d by means of a stochastic acceleration η_i. The values of η_i are obtained in rule R2c with probability p_a for accelerating, and probability p_b for braking. The former is dependent on the vehicles computed deterministic speed and the parameters v_p, p_{a_1}, and p_{a_2} with $p_{a_1} > p_{a_2}$ and $p_{a_1} + p_{a_2} \leqslant 1$. The latter, p_b is dependent on the vehicles computed deterministic speed and the slowdown probability p_d and the slow-to-start probability p_0 with $p_0 > p_d$.

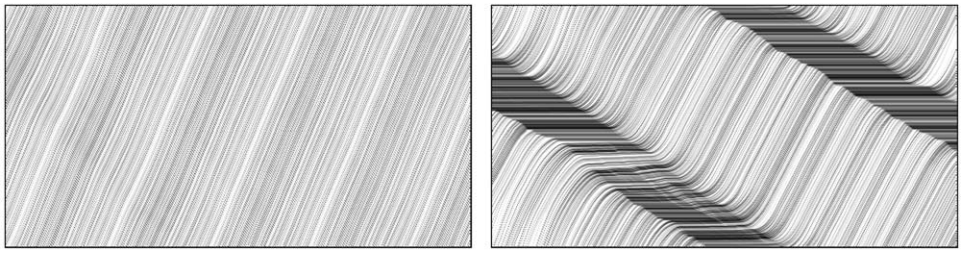

Fig. 37. Typical time–space diagrams of the KKW-TCA model (refer to the text for the used parameter values). The shown closed-loop lattices each contain $300 \times 15 = 4500$ cells, with a visible period of 580 time steps. The global density k was set to 0.25 vehicles/cell (*left*) and 0.40 vehicles/cell (*right*). Note the stable flow of vehicles surrounding the dense and compact superjams.

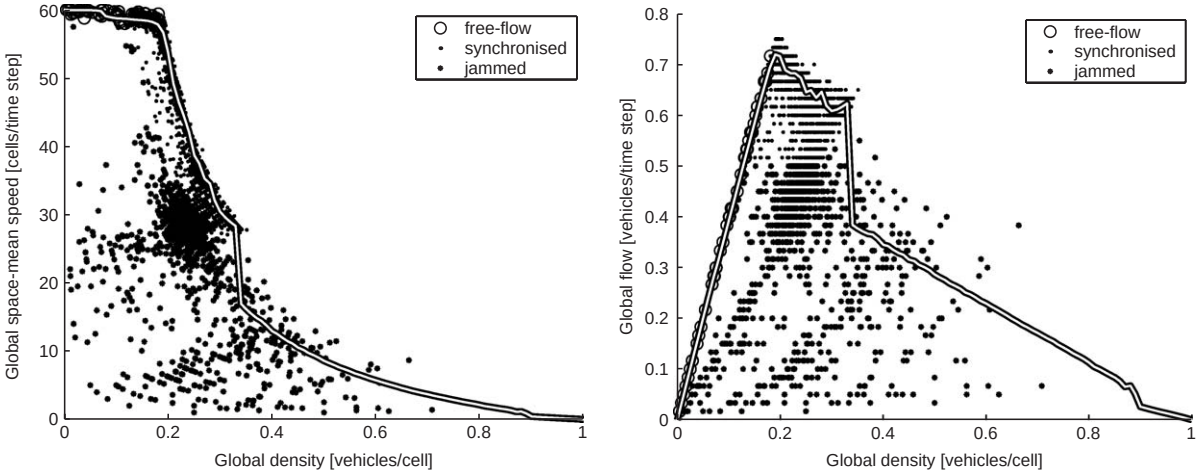

Fig. 38. The $(k, \overline{v}_s)$ (*left*) and (k, q) (*right*) diagrams for the KKW-TCA model, obtained by local and global measurements. The local measurements discriminate between the free-flow (○), synchronised-flow (·), and jammed regimes (⋆). The synchronised regime is visible as a wide scatter in the data points, having various speeds but flows comparable to the capacity flow.

In the remainder of this discussion, we set $D_0 = 60$, $D_1 = 2.55$, $a = b = 1$, $v_p = 28$, $p_{a_1} = 0.2$, $p_{a_2} = 0.052$, $p_0 = 0.425$, $p_d = 0.04$, $v_{\max} = 60$ cells/time step, with a vehicle length of $l = 15$ cells, $\Delta T = 1$ s, and $\Delta X = 0.5$ m [19].

Considering the KKW-TCA models' time–space diagrams in Fig. 37, we can see that, in contrast to the BL-TCA (see Section 4.2.2), there are less spontaneous formations of small traffic jams. The forward propagating density waves in Fig. 34 are absent in the KKW-TCA model. However, the two models show good correspondence with respect to the speed of the backward propagating waves.

Similar as in the BL-TCA model's effective space gap $g^*_{s_i}(t)$, the synchronisation distance D is responsible for producing the typical two-dimensional scatter in the $(k, \overline{v}_s)$ and (k, q) diagrams in Fig. 38. When a driver who is within the synchronisation distance adapts the vehicle's speed, the only factors taken into account are the current speed of the direct frontal leader and a safety criterion (in the form of the current space gap); it is this effect that produces the scatter in the data, because the exact specification of this speed is absent. In both diagrams of Fig. 38, the local measurements discriminate between the free-flow (○), synchronised-flow (·), and jammed regimes (⋆). One of the major differences between these two models, is that the flow in the synchronised regime is almost a factor two larger for the KKW-TCA than the BL-TCA. The KKW-TCA also experiences a capacity drop similar as in the BL-TCA, but also undergoes an abrupt transition when going from the synchronised-flow to the wide-moving jam regime around a global density of some 0.4 vehicles/cell (see the left part of Fig. 38). Because the model is built around the assumption that vehicles tend to approximate the behaviour of their direct leader within a certain synchronisation distance, the resulting traffic regimes correspond well to Kerner's empirical observations [57,1].

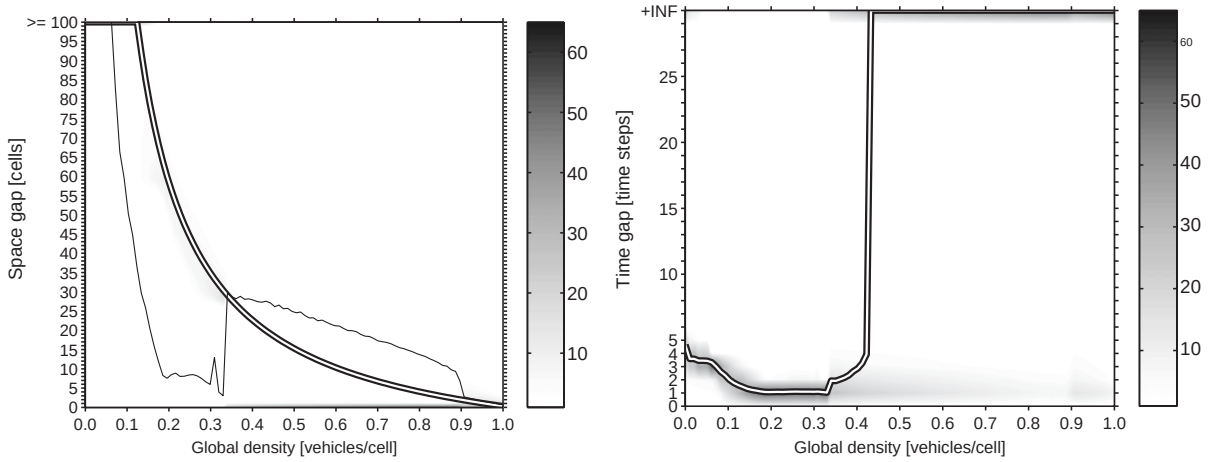

Fig. 39. Histograms of the distributions of the vehicles' space gaps g_s (*left*) and time gaps g_t (*right*), as a function of the global density k in the KKW-TCA model. The thick solid lines denote the mean space gap and median time gap, whereas the thin solid line shows the former's standard deviation. The grey regions denote the probability densities.

In Fig. 39, we have depicted the histograms of the distributions of the space and time gaps in the left and right parts, respectively. The distributions are similar to those of the BL-TCA, but there are some important differences. With respect to the space gaps in the left part of Fig. 39, there is a high variance in the jammed regime, due to the fact that there are vehicles in free-flow traffic, as well as inside the wide-moving jams (although most of the probability mass is assigned to the zero space gap inside the dense jams). Considering the time gaps in the right part of Fig. 39, we can see that they always form a tight cluster around the median of the distribution, indicating very narrow distributions with an pronounced peak. This is completely different behaviour than in the BL-TCA model (see the right part of Fig. 39). The main reason is probably due to the lack of an anticipation effect in the KKW-TCA model. Even more severe, is the fact that the KKW-TCA model, despite its elaborate construction based on a synchronisation distance, completely fails to describe the microscopic structure of motorway traffic. The BL-TCA model however succeeds in having a good fit on both macroscopic and macroscopic scales, as stated according to Knospe et al. [113,19].

5. Multi-lane traffic, city traffic, and analytical results

In this final section on traffic cellular automata models, we take a look at some other aspects related to TCA models. We first discuss some properties and methodologies for modelling multi-lane traffic in the context of a cellular automaton, after which we briefly consider several approaches for dealing with city traffic. The final part of the section concludes with an overview of different analytical treatments of TCA models.

5.1. Multi-lane traffic

In this section, we briefly discuss some properties and methodologies for modelling multi-lane traffic in the context of a cellular automaton. To this end, we illustrate the types of lane changes that are possible, then discuss the general setup for a lane-changing model. We conclude with a short overview on the implementation of lane-change rules and explain the phenomenon of ping-pong traffic, an artifact introduced by an inferior implementation.

5.1.1. Types of lane changes

In general, there are two types of lane changes identified: *mandatory lane changes* (MLC) and *discretionary lane changes* (DLC) [1]. In the former case, a vehicle is obliged to execute a lane change, e.g., because it needs to exit the motorway at an off-ramp, or because the vehicle is by law obliged to drive in the right shoulder lane. In the latter case, a vehicle changes a lane at its own discretion, e.g., when approaching and overtaking a slow-moving leading vehicle.

With respect to the rules for lane changing, there are also two approaches: *symmetric* and *asymmetric*. In the US, the symmetric approach is more applicable: this is embodied by the fact that motorways have a large number of lanes (i.e., more than three), with vehicles driving at lower speeds (e.g., 60 miles/h, corresponding to some 100 km/h), effectively using all lanes more homogeneously. Such a system is typically called "*keep-your-lane*", as frequent lane changes are discouraged. In contrast to this, people in most European countries are obliged by law to drive on the outer right shoulder lane whenever possible. Motorways have fewer lanes (typically either two or three, unidirectional), operating at higher speeds of e.g., 120 km/h. In addition, most of these countries have instituted an overtaking prohibition on the right lane, with large trucks restricted to the two most right lanes.

With respect to this latter system of asymmetric lane changes, the phenomenon of *density* or *lane inversion* plays an important role, especially on the numerous 2×2 motorways in Europe (see also the beginning of Section 3 for a discussion of this phenomenon). Another aspect that has a significant influence, is the change of driver behaviour, e.g., near on-ramps. Here, drivers might avoid the shoulder lane to allow traffic to enter, or because of their increased attention, they might induce a more subtle effect such as the capacity funnel (see also our discussion in [50] for more details on this phenomenon).

5.1.2. General setup for lane changing

Deciding on whether or not to perform a lane change, is typically split in two separate steps: first, a vehicle checks if it is *desirable* to change lanes, i.e., making the distinction between a mandatory or discretionary lane change. If a lane change is indeed desirable, then the second step proceeds to check whether or not such a lane change can be performed at all with respect to safety and collision avoidance. Thus, there is a check for *gap acceptance*.

One of the first approaches to model such lane-changing behaviour an a two-lane road in a TCA model, is due to Nagatani. His work was based on the deterministic CA-184 model (see Section 3.1.1) [116]. One of the artifacts of his lane-changing rules, was the existence of states in which blocks of vehicles alternated from one lane to another, without moving at all. To circumvent this problem, Nagatani randomised the lane-changing behaviour [117]. Rickert et al. later applied this lane-changing methodology, by extending the STCA model (see Section 3.2.1) to handle two-lane unidirectional traffic [118]. Wagner et al. later assessed the previous work of Rickert et al. concluding that it did not capture certain aspects (e.g., density inversion) of traffic flows very well [119]. To this end, they built upon the previous work, adding a more specialised security constraint that takes into account the fact that vehicles should also consider the following vehicles in the target lane, thereby avoiding severe disruptions. As a final comment, they state that the lane-changing rules in a TCA model typically do not provide a realistic microscopic model, but they rather lead to a good correspondence with respect to observed macroscopic features (e.g., the frequency of lane changes).

In order to address the correct reproduction of the density inversion phenomenon, Nagel et al. artificially introduced a *slack parameter*, capturing the inclination of a driver to change back to the right lane. They furthermore also provided an extensive classification of some 10 lane-changing rules and criteria encountered in literature [55]. Another excellent overview of multi-lane traffic is given by Chowdhury et al. [3].

As all the previous work dealt with unidirectional roads, it seems logical to consider *bidirectional traffic*, i.e., traffic with adjacent but opposing lanes. Simon and Gutowitz were among the first to consider a TCA model of such traffic, with vehicles driving on two lanes [120]. Central to their approach, is the notion of a *local density* that each driver must assess before attempting to complete an overtaking manoeuvre. When a driver encounters a slower moving vehicle, a check is made whether or not there is enough space *in front* of this leading vehicle (this is the local density). If the check is positive, then a lane change can be performed (under the condition of course that there is a safe gap in the opposing lane). With this scheme in mind, high density traffic thus excludes such overtaking manoeuvres, due to the fact that the local density is too low to complete them.

Note that some authors, e.g., Gundaliya et al. [121], Mallikarjuna and Ramachandra Rao [122], use a peculiar variant of a multi-lane setup. Their models have essentially a multi-cell structure, but now the multi-cell concept is extended in the lateral direction. So cells not only get smaller, but also 'thinner', allowing *variable-width vehicles*, e.g., motor cycles that can more easily pass other vehicles in the same lane. In our opinion, this leads to unnecessary complexity, giving little benefits. In fact, we believe that such a scheme directly opposes the idea behind a CA model, as explained at the introduction of this report. We strongly feel that heterogeneity in a TCA model should *only* be incorporated by means of different lengths, maximum speeds, acceleration characteristics, anticipation levels, and stochastic noise for distinct classes of vehicles and/or drivers. Any other approach would be better off with a continuous microscopic model.

5.1.3. Implementation of lane-changing rules and the phenomenon of ping-pong traffic

The basic implementation of a lane-changing model in a TCA setting, leads to two substeps that are consecutively executed at each time step of the CA:

- first, the lane-changing model is executed, exchanging vehicles between *laterally* adjacent lanes,
- then, all vehicles are moved forward (i.e., *longitudinal*) by applying the car-following part of the TCA model's rules.

One immediate result from this approach, is that a lane change in a TCA model is completed within one time step (i.e., ΔT). This is in contrast to real-life traffic, where lane changes have a duration of several seconds [55].

For more than two lanes, care must be taken to avoid so-called *scheduling conflicts* during the first substep. Consider for example three lanes, with two vehicles driving in the outer left, respectively outer right, lane at the same longitudinal position. If the cell in the middle lane is empty, then the vehicles may decide to move to this location, resulting in a lateral collision. In order to compensate this, one possibility is to choose a vehicle at random (or by preference), thereby allowing it to perform its requested lane change. Another possibility is to perform left-to-right lane changes in even time steps, and right-to-left lane changes in odd time steps.

As hinted earlier, the 'correctness' of a lane-change model should be judged on the basis of certain macroscopic observations. Examples of these are the frequency of lane changes with respect to different densities, the capacity flows for all lanes separately and combined, the critical density at which a breakdown occurs in each of the lanes, ... Good indicators can be found in the many small fluctuations typically exhibited by multi-lane TCA models, instead of the large jams in single-lane traffic. Traffic flows get more fluid if vehicles are allowed to pass moving bottlenecks [119,55]. However, under certain conditions, Helbing and Huberman have shown the existence of coherent states, where vehicles' speeds are synchronised across adjacent lanes. For heterogeneous traffic flows, this can lead to a moving 'solid block' of vehicles [123].

When implementing lane-change rules in a TCA model, care must however be taken that the implementation does not introduce any unrealistic artifacts. A prominent example of this, plaguing many TCA models, is a phenomenon called *ping-pong traffic*. Nagatani was among the first to observe this peculiar behaviour of vehicles in traffic flows (see Section 5.1.2). In ping-pong traffic, vehicles typically alternate between lanes during successive time steps. As explained earlier, one way to resolve this behaviour is by randomising the lane-change decision, thereby quickly destroying any such artificial patterns [117,118].

5.2. City traffic and intersection modelling

When modelling city traffic, essentially two approaches can be followed: either the entire road network is considered as a two-dimensional lattice (i.e., a *grid*), or each road in the network is a single longitudinal lattice (single- or multi-lane) with explicitly modelled intersections. The former was historically used in the context of phase transitions in a CA, whereas the latter is more applicable to describe real-life traffic flows in populated cities.

In this section, we illustrate both approaches, starting with a classic grid layout as embodied by the Biham–Middleton–Levin (BML) and Chowdhury–Schadschneider (ChSch) TCA models, after which we briefly comment on explicit descriptions of intersections in TCA models.

5.2.1. Grid traffic

The first model of 'city traffic' was proposed by Biham, Middleton, and Levine (BML). It was developed around the same time Nagel and Schreckenberg presented their STCA (see Section 3.2.1). The BML-TCA, is a two-dimensional model that describes traffic on a square grid in a toroidal setup (i.e., opposing sides are identified), with vehicles distributed randomly over the lattice [124]. The model is in fact a very simplistic model, in that it assumes that all vehicles either move from the south to the north direction, or from the west to the east. Each cell of the lattice is assumed to contain a traffic light, in the sense that all west–east vehicles try to move during even time steps, and all south–north vehicles during odd time steps (thus $v_{\max} = 1$ cell/time step for all vehicles). The BML-TCA constitutes a fully deterministic model, where the only randomness is introduced through the initial conditions. Note that its one-dimensional version corresponds to the CA-184 and the TASEP (see Sections 3.1.1 and 3.2.4).

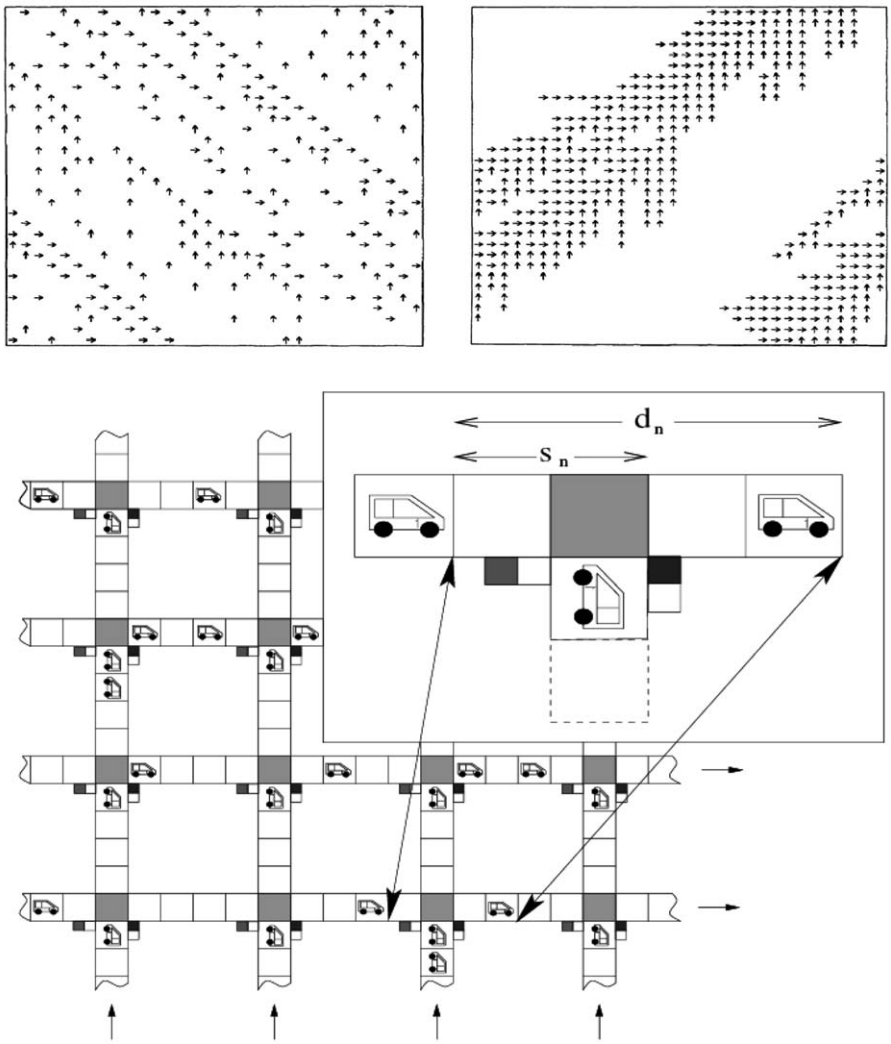

Fig. 40. *Left*: snapshot of the spatial structure in the BML-TCA for $k = 0.25$. In this free-flow regime, all vehicles move alternatingly, with the right-oriented arrows denoting west–east travelling vehicles, and the upward-oriented arrows denoting south–north travelling vehicles. *Right*: same setup as before, but now for $k \approx 0.4082$. In this congested regime, a global cluster emerges, completely composed of blocked vehicles. *Bottom*: an overview of the ChSch-TCA, showing the street segments of finite length between the BML-TCA's original intersections. The first two images are reproduced after [124], the third after [96].

Depending on the global density of vehicles in the lattice, the model results in two distinct traffic regimes, with a *sharp first-order phase transition* between them. The first regime, i.e., free-flow traffic, corresponds to a state with alternate moving vehicles (i.e., west–east and south–north moving); an example is depicted in the left part of Fig. 40. In the congested regime, a self-organised global cluster emerges, completely composed of blocked vehicles (see e.g., the right part of Fig. 40). When the phase transition between both regimes occur, the space-mean speed changes abruptly from one to zero cells/time step [124,125]. Fukui and Ishibashi studied the repercussions of a local disruption in the lattice (e.g., a crashed vehicle that remains stopped for an eternal period), and found that it provides the seed of a growing global cluster [126]. Biham et al. also considered a less restrictive version of the above model, in which now all vehicles try to move at each time step. In case of conflicts between a west–east and a south–north vehicle, one of them is chosen at random. Another variation considers also opposing traffic, which can lead to *grid-locked* situations where no vehicles are able to move at all. A generalisation of the BML-TCA, was provided by Freund and Poschel who consider a similar setup, but now with traffic moving in all four directions [127]. Finally, Shi

is able to obtain analytical expressions for the critical densities at which the previously mentioned phase transitions occur [128].

In the work of Chowdhury et al. a comprehensive overview is given, describing extensions to the BML-framework [3]. This overview includes asymmetric distributions of the west–east and south–north vehicles, unequal maximum speeds, two-level crossings (where two vehicles can share the same cell), faulty traffic lights (here, either a west–east or south–north vehicle is chosen at random to occupy a cell, irrespective of the current time step), road blocks, line- and point-defects (i.e., a crowded 'street' of the model, corresponding to a dense horizontal or vertical row of cells), random turning of vehicles, cut-off streets (similar to a row of two-level crossings), and so forth and so on.

Chowdhury and Schadschneider later extended the BML-TCA model to incorporate randomisation effects like in the STCA model, having the result that jamming can now occur spontaneously [129]. Their model furthermore contains street segments of finite length between the cells, with vehicles driving according to the STCA's rules on these streets. The original cells in the BML-TCA model form the signallised intersections of the Chowdhury–Schadschneider model (ChSch-TCA), as can be seen in the bottom part of Fig. 40. At sufficiently large densities, a transition can occur that leads to a self-organising state of completely gridlocked traffic. Barlović later provided a solution to this problem, making the model well-suited for assessing the results of different traffic light control policies in a city [96].

5.2.2. Explicit intersection modelling

In contrast to the previous section were all traffic operations were essentially defined on a two-dimensional lattice, it is also possible to consider a complete road network, consisting of *separate links* that are connected to each other by means of *intersections*. These intersections can either be signallised, or unsignallised, turning priorities can be defined, as well as different geometrical layouts (e.g., roundabouts).

Road networks based on the above assumptions, typically combine a set of basic building blocks. As such, the network is logically decomposed in a set of *nodes* and *links*. The former denote the intersections, whereas the latter can, depending on the implementation, refer to individual lanes, a group of adjacent lanes, or even a road with two-way traffic. In general, traffic operations on motorways are primarily influenced by the behaviour of vehicles on links, i.e., their car-following and lane-changing behaviour. Conversely, traffic operations in cities and denser street networks, are primarily defined by the behaviour of vehicles at intersections, i.e., queueing delays at traffic lights, priority turns, etc. In many cases, the intersection logic is simplified, such that all decisions (conflict resolving, etc.) are taken *before* a vehicle enters the intersection [14].

Several non-exhaustive examples include the work of Esser and Schreckenberg with applications to the city of Duisburg [130], the work of Simon and Nagel who primarily focussed on single-lane traffic in combination with several setups for controlling traffic lights, applying their work to the city of Dallas (different links have different slowdown probabilities associated with them, thus enabling to model different street capacities) [131], the work of Diedrich et al. who consider the effects of various implementations of on- and off-ramps in the classic STCA model [132], and all the references on TRANSIMS, the travel behaviour in Switzerland, the region of Dallas, the city of Portland, and the city of Geneva (where all intersections are replaced by generalised roundabouts), mentioned in our discussion in [1].

All these examples have in common that they are based on simple building blocks. Despite this elegance, most of them however, do not provide satisfactory information regarding the calibration and validation of their underlying models (this for example with respect to the correct observed queueing delays at intersections). A popular technique is to use *sources* and *sinks*, where vehicles are added and removed, allowing tuning of the simulator in order to agree with incoming on-line measurements. Clearly, we feel that besides a need for elaborate descriptions of the employed models, there is perhaps even a bigger need for correct information with respect to these models' fidelity and accuracy.

5.3. Analytical results

Because most studies based on TCA models heavily rely on numerical simulations, this creates the danger of introducing artifacts (e.g., finite-size effects) that obscure the true dynamics of the systems under consideration. Although most of these problems should resolve in the so-called *thermodynamic limit* where $K_{\mathscr{L}}, T_{\mathrm{mp}} \rightarrow +\infty$ (i.e., a lattice with infinite length considered over an infinite time period), resorting to this approach is computationally not feasible. As a result, researchers have focussed on analytical methods. Except for the most trivial cases with a deterministic (i.e., noiseless) TCA model, these analytical methods most of the time provide approximations at best.

In this section, we illustrate several of these analytical methods encountered in literature. Our discussion focusses on the concept of a mean-field theory, after which we elaborate on some of its improvements that lead to better agreement with numerical results.

Note that other avenues for analytical treatments of CA models, and TCA models in particular, are also explored. In this section, we will however not go into detail about them. For more information, we refer the reader to the interesting work of Fukś and Boccara [133–137].

5.3.1. Mean-field theory

As mentioned in the introduction of this section, for the case of arbitrary $v_{\max}$ and $p=0$ or 1, or for $v_{\max}=1$ cell/time step, the analytical solution of the resulting TCA model is exactly known. This solution, expressed as its (k,q) diagram, corresponds to the set of diagrams as depicted in Fig. 10 (see Section 3.1.2) for the DFI-TCA.

The problem is to find an analytical description of how the system evolves in time through the state space, i.e., what are the occurring configurations? The evolution of a system, can be described by what is called a *master equation*. For cellular automata, this equation is a first-order differential equation, describing the change in probability of a system's lattice to be in a certain configuration. The downside is that, in general, this master equation cannot be solved exactly.

For the TASEP model (see Section 3.2.4) with open boundary conditions and random sequential update, the master equation can be solved exactly [138,18]. In a first step, the master equation is elegantly written in vector form, comprising a *transfer matrix* that contains the time-evolution of the probabilities. By assuming the *matrix-product ansatz* (MPA) formalism, the transfer matrix can be rewritten as a product of local transfer matrices, operating on sets of cells. This provides a algebra that can be solved exactly, thereby solving the TASEP analytically. Note that for the TASEP with a parallel update however, obtaining the exact solution is difficult, because no simple MPA decomposition into local matrices is possible.

In contrast to this promising result, obtaining an analytical solution becomes harder to even intractable for the STCA model (see Section 3.2.1) with $v_{\max}>1$ cell/time step and $0<p<1$. In the master equation, probabilities of cluster of cells will occur, making its solution very hard [53]. One well-known method that is suitable for dealing with many-particle systems in statistical mechanics, is the construction of a *mean-field theory* (MFT) of the model. Such a MFT can provide an approximation of the master equation; in some cases, the MFT turns out to be an exact solution.

The idea behind a MFT, is that all correlations between neighbouring cells are neglected. For TCA models, such a *site-oriented mean-field theory* (SOMF) assumes that all cluster probabilities are replaced by single cell probabilities. The MFT now replaces the effects of these individual cells with an average effect (the 'mean field'), which simplifies computations considerably. When translating the STCA's rules R1–R3, i.e., Eqs. (46)–(48), R1 is decoupled into separate acceleration and braking rules R1a and R1b, after which their order is changed to R1b, R3, R4, R1a. The upshot of this is that there are no stopped vehicles in the system, thereby reducing the number of possible states for a cell by one. If $v_{\max}=1$ cell/time step, then the system can be fully described by cell occupancies. Applying this SOMF theory to the STCA model, results in considerably underestimation of the flow in the system (even for the restricted case of $v_{\max}=1$ cell/time step) [139,71,53].

5.3.2. Improving the SOMF theory

As mentioned in the previous section, setting $v_{\max}=1$ cell/time step leads to an underestimation of the flow. However, when switching from a parallel update procedure to a random sequential one, the resulting SOMF theory becomes exact! It turns out that the reason for the underestimation, can be traced back to its neglecting of all correlations between cells (which are a consequence of the parallel update procedure). As explained in the beginning of Section 3.2.4, using a parallel update excludes certain Garden of Eden states. However, the SOMF theory naively includes these paradisiacal states. As a solution, these GoE states can be eliminated, resulting in a *paradisiacal mean-field theory* (pMFT). In systems with higher maximum speeds, more GoE states occur, making it difficult to derive a pMFT. Even then, the theory still remains an approximation (albeit a better one) when using a parallel update procedure [140,71,53].

Taking into account short-range correlations, can be done by considering a *car-oriented mean-field theory* (COMF). Instead of dealing with cells and their occupancies, the COMF theory computes the probabilities $P_n(v)$ of finding

a space gap of n cells for a vehicle driving with speed v [141]. In a sense, the COMF theory approximates the problem by neglecting the correlations between space gaps of successive vehicles [3]. As such, it gives qualitatively good approximations for $p \to 0$; in all other cases, the COMF theory starts to fail, because there are also correlations between the space gaps [18,3]. Note that the COMF theory has also been applied to the BJH-TCA and VDR-TCA models (see Sections 3.3.2 and 3.3.3, respectively) [91].

Another approach to analytically solve the master equation, is to explicitly take into account the correlations between neighbouring cells, by considering *clusters* composed of n consecutive cells [71,53]. Such a *site-oriented cluster-theoretic approach* proves to perform better than the COMF theory from the previous section [139]. The improvement of the approximation is even better when considering larger clusters; it is exact for $n \to +\infty$ [142,18,3].

6. Summary and outlook

This report gave an elaborate and understandable review of traffic cellular automata (TCA) models, which are a class of computationally efficient microscopic traffic flow models. TCA models arise from the physics discipline of statistical mechanics, having the goal of reproducing the correct macroscopic behaviour based on a minimal description of microscopic interactions.

We began with an overview of cellular automata (CA) models, their background and physical setup. Applying this technique to the modelling of traffic flows, we discretise a road into a number of small cells (a procedure called coarse graining), having a width of e.g., $\Delta X = 7.5\,\mathrm{m}$. Time is also discretised into units of approximately $\Delta T = 1\,\mathrm{s}$. After introducing the mathematical notations, we showed how to perform measurements on a TCA model's lattice of cells, and how to convert these quantities into real-world units and vice versa.

Subsequently, we gave an extensive account of the behavioural aspects of several TCA models encountered in literature. Already, several reviews of TCA models exist, but none of them consider all the models exclusively from the behavioural point of view. In this respect, our overview fills this void, as it focusses on the behaviour of the TCA models, by means of time–space diagrams, (k, q) diagrams and the like, and histograms showing the distributions of vehicles' speeds, space, and time gaps. In the report, we have distinguished between single- and multi-cell models, whereby in the latter vehicles are allowed to span a number of consecutive cells. We concluded with a concise overview of TCA models in a multi-lane setting, and some of the TCA models used to describe city traffic as a two-dimensional grid of cells, or as a road network with explicitly modelled intersections. The final part of the report illustrated some of the more common analytical approximations to single-cell TCA models.

Considering the state-of-the-art in using TCA models, our analysis indicates that the field has evolved rapidly over the last decade. Starting from initial attempts based on rather crude models, the past few years have seen an increase in the computational complexity as well as the available computational power. More complex models are developed, of which we believe the brake-light TCA model of Section 4.2.2 is the most promising: it is able to faithfully reproduce the correct real-life empirical observations, and quite some work has been done at calibrating the model, see e.g., the recent work of Knospe et al. [19]. To conclude, we note an evolving trend of using these TCA models as the physical models underlying multi-agent systems, in part describing the behaviour of individual people in large-scale road networks [1].

Acknowledgements

Dr. Bart De Moor is a full professor at the Katholieke Universiteit Leuven, Belgium. Our research is supported by: Research Council KUL: GOA AMBioRICS, several PhD/postdoc & fellow grants, Flemish Government: FWO: PhD/postdoc grants, projects, G.0407.02 (support vector machines), G.0197.02 (power islands), G.0141.03 (identification and cryptography), G.0491.03 (control for intensive care glycemia), G.0120.03 (QIT), G.0452.04 (new quantum algorithms), G.0499.04 (statistics), G.0211.05 (Nonlinear), research communities (ICCoS, ANMMM, MLDM), IWT: PhD Grants, GBOU (McKnow), Belgian Federal Science Policy Office: IUAP P5/22 ('Dynamical Systems and Control: Computation, Identification and Modelling', 2002–2006), PODO-II (CP/40: TMS and Sustainability), EU: FP5-Quprodis, ERNSI, Contract Research/agreements: ISMC/IPCOS, Data4s,TML, Elia, LMS, Mastercard.

Appendix A. TCA + Java™ software

As already briefly mentioned in the paper, all simulations were performed by means of our *Traffic Cellular Automata+* software [100]. It was developed for the Java™ Virtual Machine (JVM), and can be downloaded[1] from:

`http://smtca.dyns.cx`

The software is also referenced on the *Traffic Forum*[2] (see section *Links*, subsection *Online Traffic Simulation or Visualization* (*Java Applets*), item *Java* (*Swing*) *application for several cellular automata models*).

In this appendix, we summarise our rudimentary TCA+ software. We start with an overview of its features, explain how to run the software, and conclude with some technical details with respect to the implementation of its code base.

A.1. Overview and features

The TCA+ software package's goal is two-fold: on the one hand, it provides an *intuitive didactical tool* for getting acquainted with the concept of single-lane traffic cellular automata models. On the other hand, it provides a rich enough code base to perform hand-tailored *simulation experiments*, as well as giving insight into the details of programming TCA models.

In a nutshell, our software considers one-dimensional traffic cellular automata with periodic boundary conditions, i.e., vehicles driving on a unidirectional circular road. Different sets of rules can be chosen, and for each set its parameters (e.g., stochastic noise) can be changed at run time. Both local and global measurements can be performed on the lattice by means of artificial loop detectors. A traffic light with cyclical red and green phases was also added, allowing to study elementary queueing behaviour. In the software, we have implemented the TCA models listed in Table A.1.

In Fig. 41, we show a screenshot of the main graphical user interface (GUI). As can be judged from the image, the TCA+'s GUI is rather huge, spanning approximately 1400×1200 pixels (scrollbars are automatically placed if it does not fit on the screen). It consists of several panels:

- a scrolling time–space diagram containing vehicle trajectories and an animation of the road situation,
- a panel containing some simulation statistics,
- several simulator controls,
- and scrolling loop detector plots and plots of the (k, q), $(k, \overline{v}_s)$, and $(q, \overline{v}_s)$ diagrams.

In the following paragraphs, we describe each of these features in more detail. Note that there currently are two versions of the GUI: a standard version for all the single-cell TCA models, and a modified multi-cell TCA version with limited functionality (mainly for creating coloured tempo-spatial diagrams).

A.1.1. Vehicle animation

Looking at the time–space diagram in the upper-left panel, we can discern the individual vehicle trajectories, as well as the typical backwards-travelling shock waves of congestion. In this scrolling diagram, the time axis goes from the left to the right, while the space axis goes from the bottom to the top (and is a one-to-one mapping of the consecutive cells on the ring road). Each pixel here corresponds to a unique cell of the simulator and each vehicle is coloured with a certain shade of yellow (in order to easily distinguish between different neighbouring vehicles). There is also a setting available that allows stopped vehicles to be coloured red. In the upper-middle panel, the actual geometrical configuration of the ring road is depicted. This allows us to view the current physical situation on the road, i.e., the positions of all the vehicles. Each vehicle can be coloured with a certain shade of yellow (the same as in the time–space diagram). The current phase of the traffic light is also shown, as well as the positions of all the loop detectors: their positions are indicated by the small purple boxes alongside the road. The small green box indicates the position of the traffic light, with vehicles travelling in clockwise fashion.

---

[1] From May 2002 until June 2005, the software has been downloaded some 800 times, of which we suspect one third to be traffic coming from search engines' indexing robots.

[2] `http://www.trafficforum.org`

Table A.1
All TCA models implemented in our TCA+ software, accompanied by references to the respective sections in the paper where they are extensively discussed

TCA model	Refer to section
CA-184	3.1.1
DFI-TCA	3.1.2
STCA	3.2.1
STCA-CC	3.2.2
SFI-TCA	3.2.3
TASEP	3.2.4
ER-TCA	3.2.5
Deterministic T^2-TCA	3.3.1
Stochastic T^2-TCA	3.3.1
VDR-TCA	3.3.3
VDR-CC-TCA	3.3.3
TOCA	3.3.4
MC-STCA	4.1
HS-TCA	4.2.1
BL-TCA	4.2.2
KKW-TCA	4.2.3

A.1.2. Simulation statistics

In the upper-right panel, we can find the length of the ring road (expressed in the number of cells), the number of vehicles currently in the simulator, the global vehicle density, and the current time step. There is also a small panel that allows to quickly set the status of the traffic light to either red or green.

A.1.3. Simulator controls and settings

The middle-left panel contains buttons for starting, stopping (i.e., pausing), resetting, and quitting the simulator. Several preferences can also be specified, i.e., whether or not to activate several panels containing the simulator's output. There is also the possibility to log the measurements from the loop detectors to a default file (called *detector-values.data*). And finally, the type of traffic cellular automaton (i.e., its rule set) can also be selected from a list, specified by radio control buttons.

Note that there are several initial conditions possible for each density level: it is possible to start with a homogeneous state (all vehicles are spaced evenly), with a compact superjam of vehicles that are all stopped, or with a random initialisation (see also the introduction of Section 3).

If the simulation goes (visually) too fast, the cycle hold time can be increased, thereby freezing the simulation for a while between two consecutive time steps. Besides this, the ring road's global density and the vehicles' maximum speed can be specified. The sampling time for the artificial loop detectors can be adjusted (to increase or smooth out fluctuations). And finally, all probabilities can be adjusted between 0% and 100% in incremental steps of 1%.

The red and green cycle times for the traffic light can be specified, such that the light can operate automatically, thereby inducing artificial queues at regular intervals. One can also control the traffic light manually (enabling the red or green phase) using the small upper-right panel; but if applied, the traffic-light controls override these manual settings.

A.1.4. Plots of macroscopic measurements

The software has the ability to extract both local and global macroscopic flow measurements from several uniformly road-side placed loop detectors which record flows, densities, and space-mean speeds.

The three large coloured regions in the middle panel represent the measured (and averaged) values of the local flows, local densities, and local space-mean speeds of the loop detectors. Pair-wise correlating these values, results in the plots of the (k, q), $(k, \overline{v}_s)$, and $(q, \overline{v}_s)$ diagrams in the lower-right panel. The coloured dots indicate locally obtained measurements, whereas the black dots represent globally obtained ones.

Note the small button that allows to construct these diagrams: when it is pressed, the global density is incrementally increased from 0% to 100%, each time adding a single vehicle to the ring road. The simulation is then ran for a

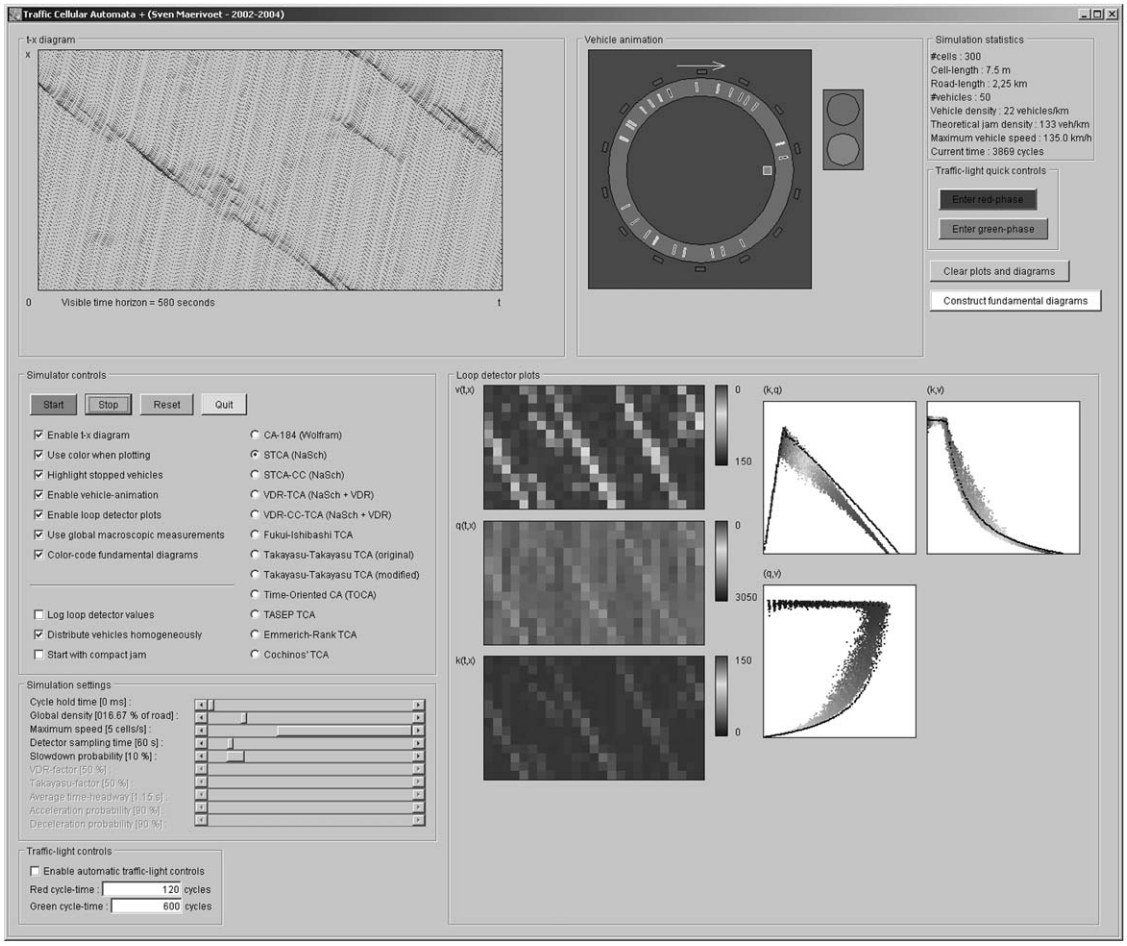

Fig. 41. A screenshot of the TCA+'s main graphical user interface (GUI) for single-cell TCA models. The GUI is rather huge, spanning approximately 1400×1200 pixels, consisting of several panels: a scrolling time–space diagram containing vehicle trajectories, an animation of the road situation, a panel containing some simulation statistics, several simulator controls, scrolling loop detector plots and plots of the (k, q), $(k, \overline{v}_s)$, and $(q, \overline{v}_s)$ diagrams.

certain amount of time and the measurements from all the loop detectors are recorded. When all densities are processed (an indicator of the total time left is shown), the diagrams should be clearly visible in the loop detector plots in the lower-right panel.

A.2. Running the software

When visiting the website mentioned in the introduction of this appendix, there are two options for downloading the software. One is by downloading the *compiled classes*, whereas the other is to download the programme's *source code*. Once the compiled software has been downloaded, it is relatively easy to start the graphical user interface. Considering the single-cell setup GUI, the software is ran by executing the following command:

Note that a Java™ Development Kit (JDK) (preferably Sun's[3]) should be installed. Furthermore, due to a change in the threading of the Java™ Swing™ API, it appears that only JDK/JRE 1.3.1 is suitable!

[3] http://java.sun.com

A.3. Technical implementation details

It should be noted that the software is not implemented as an applet, but instead as a full Java™ application because it uses Swing™ components that are not standard supported by most browsers (at least not without installing a necessary plugin). The source itself logically consists of three different parts:

- the TCA engine with different rule sets,
- the graphical user interface,
- and a whole range of predefined experiments.

The geometrical configuration used in the single-cell TCA engine is a unidirectional ring road with a single lane. Vehicles are located in cells of $\Delta X = 7.5$ m and can have speeds of 0 to 5 cells/time step (corresponding to a maximum speed of 135 km/h). One iteration in the simulation corresponds to a time step of $\Delta T = 1$ s.

A number of artificial loop detectors are uniformly placed alongside the road, aggregating various macroscopic traffic measurements (i.e., flows, densities and space-mean speeds). In the GUI, global measurements on the entire lattice are performed according to the methodology explained in Section 2.3.2, whereas local measurements are performed according to Section 2.3.1. Note that for the TCA software itself, it is also possible to perform local measurements using a detector of unit length, according to the methodology explained in Section 2.3.3.

Besides the standard single-cell GUI and the limited multi-cell GUI, there also exist some predefined experiments. These allow to create the (k, q), $(k, \overline{v}_s)$, and $(q, \overline{v}_s)$ diagrams, histograms of the vehicles' speeds, space gaps, and time gaps, as well as several order parameters (density correlations, nearest neighbours, and an inhomogeneity measure that compares the locally recorded densities to the current global density).

Inside the TCA+ software, several packages are available:

- `tca.base` containing the definitions of cells, global states, loop detectors, and the traffic cellular automaton's lattice,
- `tca.automata` containing implementations of all the TCA models mentioned in Section A.1,
- `tca.simulator` containing the classes related to the single-cell and multi-cell GUIs,
- `tca.experiments.fundamentaldiagrams`, `tca.experiments.histograms`, and `tca.experiments.orderparameters` containing setups for the previously mentioned experiments.

Appendix B. Glossary of terms

B.1. Acronyms and abbreviations

ASEP	asymmetric simple exclusion process
BCA	Burgers cellular automaton
BJH	Benjamin, Johnson, and Hui
BJH-TCA	Benjamin–Johnson–Hui traffic cellular automaton
BL-TCA	brake-light traffic cellular automaton
BML	Biham, Middleton, and Levine
BML-TCA	Biham–Middleton–Levine traffic cellular automaton
CA	cellular automaton
CA-184	Wolfram's cellular automaton rule 184
ChSch-TCA	Chowdhury–Schadschneider traffic cellular automaton
CML	coupled map lattice
COMF	car-oriented mean-field theory
DFI-TCA	deterministic Fukui–Ishibashi traffic cellular automaton
DLC	discretionary lane change
ECA	elementary cellular automaton
ER-TCA	Emmerich–Rank traffic cellular automaton

GoE	Garden of Eden state
HS-TCA	Helbing–Schreckenberg traffic cellular automaton
JDK	Java^{TM} Development Kit
KKW-TCA	Kerner–Klenov–Wolf traffic cellular automaton
LGA	lattice gas automaton
LWR	Lighthill, Whitham, and Richards
MC-STCA	multi-cell stochastic traffic cellular automaton
MFT	mean-field theory
MLC	mandatory lane change
MPA	matrix-product ansatz
NaSch	Nagel and Schreckenberg
NCCA	number conserving cellular automaton
OVF	optimal velocity function
OVM	optimal velocity model
PCE	passenger car equivalent
PCU	passenger car unit
pMFT	paradisiacal mean-field theory
SFI-TCA	stochastic Fukui–Ishibashi traffic cellular automaton
SMS	space-mean speed
SOC	self-organised criticality
SOMF	site-oriented mean-field theory
SSEP	symmetric simple exclusion process
STCA	stochastic traffic cellular automaton
STCA-CC	stochastic traffic cellular automaton with cruise control
T^2-TCA	Takayasu–Takayasu traffic cellular automaton
TASEP	totally asymmetric simple exclusion process
TCA	traffic cellular automaton
TMS	time-mean speed
TOCA	time-oriented traffic cellular automaton
TRANSIMS	TRansportation ANalysis and SIMulation System
UDM	ultra-discretisation method
VDR-TCA	velocity-dependent randomisation traffic cellular automaton

B.2. List of symbols

$\mathscr{C}(0)$	a CA's initial configuration
$\mathscr{C}(t)$	a CA's global configuration at time step t
δ	a CA's local transition rule
G	a CA's global map
G^{-1}	a reversible CA's inverse global map
$K_{\mathscr{L}}$	the number of cells in one lane of a TCA's lattice
$\mathscr{L}$	a CA's lattice (e.g., $\mathbb{Z}^2$)
$\mathscr{N}_i$	the (partially) ordered set of cells in the neighbourhood of the ith cell
$\lvert\mathscr{N}\rvert$	the number of cells in the neighbourhood of each cell
$\mathscr{O}^-_{\mathscr{C}(t)\lvert G^{-1}}$	the backward orbit of the configuration $\mathscr{C}(t)$ under G^{-1}
$\mathscr{O}^+_{\mathscr{C}(0)\lvert G}$	the forward orbit of the initial configuration $\mathscr{C}(0)$ under G
$\sigma_i(t)$	the state of the ith cell at time step t
Σ	the set of all possible states a CA's cells can be in (e.g., $\mathbb{Z}_2$)
$\Sigma^{\mathscr{L}}$	the set of all possible global configurations of a CA

$\Sigma^{\mathscr{N}}$	the set of all possible configurations of a cell's neighbourhood
$\lvert\Sigma^{\Sigma^{\mathscr{N}}}\rvert$	the number of all possible rules of a CA
$\mathscr{T}_{\mathscr{C}(0)\lvert G}$	the trajectory/orbit of the initial configuration $\mathscr{C}(0)$ under G
α	the entry rate of particles in the TASEP model
α_i	the anticipatory driving parameter of vehicle i
a	the acceleration capability of a vehicle in the KKW-TCA model
β	the exit rate of particles in the TASEP model
b	the deceleration capability of a vehicle in the KKW-TCA model
$b_i(t)$	the state of the brake light of vehicle i at time t in the BL-TCA model
δ	the probability for a particle to move to the right inthe TASEP model
Δ_{acc_i}	the deterministic acceleration of vehicle i in the KKW-TCA model
ΔT	a TCA's temporal discretisation
ΔV	a TCA's speed discretisation
ΔX	a TCA's spatial discretisation
D_0	a parameter for the synchronisation distance in the KKW-TCA model
D_1	a parameter for the synchronisation distance in the KKW-TCA model
D_i	the synchronisation distance of vehicle i in the KKW-TCA model
η_i	the stochastic acceleration of vehicle i in the KKW-TCA model
γ	the probability for a particle to move to the left in the TASEP model
$\overline{g}_s$	the average space gap
$g^*_{s_i}(t)$	the effective space gap of vehicle i at time t in the BL-TCA model
$g_{s_{\mathrm{security}}}$	a security constraint for the space gap in the BL-TCA model
$\overline{g}_t$	the median time gap
$\overline{g}_{t_s}$	the safe time gap in the TOCA model
h	the upper limit to the interaction horizon in the BL-TCA model
$\xi(t)$	a random number in [0, 1[drawn at time t from a uniform distribution
k_g	the global density of a TCA's lattice
k_l	the local density of a TCA's lattice
$K_{\mathscr{L}}$	the number of cells in one lane of a TCA's lattice
$\mathscr{L}$	a TCA's lattice
l_i	the length of vehicle i
$\overline{l}$	the average length of allvehicles on a TCA's lattice
$L_{\mathscr{L}}$	the number of lanes in a TCA's lattice
$M_{g_{s_i},v_i}$	the gap-speed matrix of the ER-TCA model
p	the slowdown probability in [0, 1]
p_0	the slow-to-start probability in [0, 1]
p_a	the acceleration probability in [0, 1] in the KKW-TCA model
p_{a_1}	a parameter for the acceleration probability in the KKW-TCA model
p_{a_2}	a parameter for the acceleration probability in the KKW-TCA model
p_{acc}	the acceleration probability in [0, 1] in the TOCA model
p_b	the braking probability in [0, 1] in the BL-TCA model the deceleration probability in [0, 1] in the KKW-TCA model
p_d	the slowdown probability in [0, 1] in the BL-TCA model
p_{dec}	the deceleration probability in [0, 1] in the TOCA model
p_s	the slow-to-start probability in [0, 1] in the BJH-TCA model
p_t	the slow-to-start probability in [0, 1] in the T^2-TCA model
$P_n(v)$	the probabilities of finding a space gap of n cells for a vehicle driving with speed v
q_g	the global flow of a TCA's lattice
q_l	the local flow of a TCA's lattice

t_{s_i}	the interaction horizon in the BL-TCA model
v_{des_i}	the desired speed of vehicle i in the KKW-TCA model
v_p	a parameter for the acceleration probability in the KKW-TCA model
$\overline{v}_{s_{\text{ff}}}$	the space-mean speed in the free-flow regime
$\overline{v}_{s_g}$	the global space-mean speed of a TCA's lattice
$\overline{v}_{s_l}$	the local space-mean speed of a TCA's lattice
$x_i^{l,b}$	the longitudinal position of vehicle i's left-back neighbour
$x_i^{l,f}$	the longitudinal position of vehicle i's left-front neighbour
$x_i^{r,b}$	the longitudinal position of vehicle i's right-back neighbour
$x_i^{r,f}$	the longitudinal position of vehicle i's right-front neighbour

References

[1] S. Maerivoet, B. De Moor, Transportation Planning and Traffic Flow Models, 05-155, Katholieke Universiteit Leuven, Department of Electrical Engineering ESAT-SCD (SISTA), July 2005.
[2] R. Barlović, J. Esser, K. Froese, W. Knospe, L. Neubat, M. Schreckenberg, J. Wahle, Online traffic simulation with cellular automata, Traffic and Mobility: Simulation-Economics-Environment, Institut für Kraftfahrwesen, RWTH Aachen, Duisburg, 1999, pp. 117–134.
[3] D. Chowdhury, L. Santen, A. Schadschneider, Statistical physics of vehicular traffic and some related systems, Phys. Rep. 329 (2000) 199–329.
[4] D. Chowdhury, L. Santen, A. Schadschneider, Vehicular traffic: a system of interacting particles driven far from equilibrium, Curr. Sci. 77 (411).
[5] D.E. Wolf, Cellular automata for traffic simulations, Physica A 263 (1999) 438–451.
[6] D. Helbing, Traffic and related self-driven many-particle systems, Rev. Mod. Phys. 73 (2001) 1067–1141.
[7] D. Helbing, T. Vicsek, Optimal self-organization, New J. Phys. 1 (13) (1999) 1–17.
[8] I. Karafyllidis, A. Thanailakis, A model for predicting forest fire spreading using cellular automata, Ecol. Model. 99 (1997) 87–97.
[9] K. Nagel, E. Raschke, Self-organizing criticality in cloud formation?, Physica A: Statist. Theor. Phys. 182 (4) (1992) 519–531.
[10] S. Gobron, N. Chiba, Crack pattern simulation based on 3D surface cellular automaton, Visual Comput.—Special Issue: Comput. Graph. Int. 2000 17 (5) (2001) 287–309.
[11] K. Nishinari, D. Chowdhury, A. Schadschneider, Cluster formation and anomalous fundamental diagram in an ant trail model, Phys. Rev. E 67 (2003) 036120-1–036120-11.
[12] B. Immers, M. Westerman, H. de Ruiter, Sturen zonder structuren, in: Proceedings Colloquium Vervoersplanologisch Speurwerk, Amsterdam, The Netherlands, 1998.
[13] H.J. van Zuylen, Het spel van de regels; Het richting geven aan chaotische maatschappelijke processen, Technische Universiteit Delft, 1999.
[14] D. Helbing, K. Nagel, The physics of traffic and regional development, Contemp. Phys. 45 (5) (2004) 405–426.
[15] K. Nagel, Distributed intelligence in large scale traffic simulations on parallel computers, in: Collective Cognition: Mathematical Foundations of Distributed Intelligence, Santa Fe Institute, 2002.
[16] K. Nagel, Traffic networks, in: S. Bornholdt, H. Schuster (Eds.), Handbook on Networks, 2002.
[17] D. Chowdhury, K. Nishinari, A. Schadschneider, Self-organized patterns and traffic flow in colonies of organisms, Phase Trans. 77 (2004) 601–624.
[18] L. Santen, Numerical investigations of discrete models for traffic flow, Ph.D. Thesis, Universität zu Köln, 1999.
[19] W. Knospe, L. Santen, A. Schadschneider, M. Schreckenberg, An empirical test for cellular automaton models of traffic flow, Phys. Rev. E 70 (016115).
[20] J. von Neumann, The general and logical theory of automata, in: L.A. Jeffress (Ed.), Cerebral Mechanisms in Behavior, Wiley, New York, 1948, pp. 1–41, paper presented at the Hixon Symposium.
[21] S. Wolfram, Statistical mechanics of cellular automata, Rev. Mod. Phys. 55 (1983) 601–644.
[22] M. Delorme, An introduction to cellular automata, in: M. Delorme, J. Mazoyer (Eds.), Cellular Automata—a Parallel Model, Kluwer Academic Publishers Group, 1998 (ISBN 0792354931).
[23] A.M. Turing, The chemical basis of morphogenesis, Philos. Trans. R. Soc. London 237 (641) (1952) 37–72.
[24] M. Gardner, Mathematical games—the fantastic combinations of John Conway's new solitaire game "Life", Sci. Am. (1970) 120–123.
[25] S. Wolfram, A New Kind of Science, Wolfram Media, Inc., 2002 (ISBN 1-579-955008-8).
[26] L. Gray, A mathematician looks at Wolfram's new kind of science, Notices Amer. Math. Soc. 50 (2) (2003) 200–211.
[27] L. Chua, A Nonlinear Dynamics Perspective of Wolfram's New Kind of Science, From Bernoulli Shift to Universal Computation, Inaugural Lecture of the International Francqui Chair, Katholieke Universiteit Leuven, June 2005.
[28] R. Gosper, Life is universal!, in: E. Berlekamp, J. Conway, R. Guy (Eds.), Winning Ways for your Mathematical Plays, vol. 2, 1982, Proceedings of the Winter Simulation Conference, Washington DC, 1974, Academic Press, New York, 1974 (Chapter 25).
[29] K. Zuse, Rechnender raum, Elektron. Datenverarb. 8 (1967) 336–344.
[30] K. Zuse, Rechnender raum, Schriften zur Datenverarbeitung 1, Friedrich Vieweg & Sohn, Braunschweig, Germany.
[31] E. Fredkin, Digital mechanics: an informational process based on reversible universal CA, Physica D 45 (1990) 254–270.

[32] H. Gutowitz, Cellular automata and the sciences of complexity (part I), Complexity 1 (5).
[33] P. Sarkar, A brief history of cellular automata, ACM Comput. Surveys 32 (1) (2000) 80–107 (ISSN 0360-0300).
[34] J.P. Crutchfield, K. Kaneko, Phenomenology of spatiotemporal chaos, in: B.L. Hao (Ed.), Directions in Chaos, World Scientific, Singapore, 1987, pp. 272–353.
[35] K. Kaneko, Simulating physics with coupled map lattices, in: K. Kawasaki, A. Onuki, M. Suzuki (Eds.), Formation, Dynamics, and Statistics of Patterns, World Scientific, Singapore, 1990, pp. 1–52.
[36] K. Nagel, Particle hopping models and traffic flow theory, Phys. Rev. E 53 (5) (1996) 4655–4672.
[37] K. Nagel, M. Schreckenberg, A cellular automaton model for freeway traffic, J. Phys. I France 2 (1992) 2221–2229.
[38] A. Moreira, Universality and decidability of number-conserving cellular automata, Theoret. Comput. Sci. 292 (2003) 711–721.
[39] W. Knospe, L. Santen, A. Schadschneider, M. Schreckenberg, Human behavior as origin of traffic phases, Phys. Rev. E 65.
[40] N. Eissfeldt, P. Wagner, Effects of anticipatory driving in a traffic flow model, Eur. Phys. J. B 23 (2003) 121–129.
[41] M. Lárraga, J. del Río, A. Schadschneider, New kind of phase separation in a CA traffic model with anticipation, J. Phys. A: Math. Gen. (37) (2004) 3769–3781.
[42] S. Wolfram, O. Martin, A. Odlyzko, Algebraic properties of cellular automata, Commun. Math. Phys. 93 (1984) 219–258.
[43] S. Wolfram, Universality and complexity in cellular automata, Physica D 10 (1984) 1–35.
[44] K. Čulik, S. Yu, Undecidability of CA classification schemes, Complex Systems 2 (2) (1988) 177–190.
[45] W. Li, N. Packard, The structure of the elementary cellular automata rule space, Complex Systems 4 (1990) 281–297.
[46] G. Braga, G. Cattaneo, P. Flocchini, C.Q. Vogliotti, Pattern growth in elementary cellular automata, Theoret. Comput. Sci. 45 (1995) 1–26.
[47] A. Wuensche, Classifying cellular automata automatically, Complexity 4 (3) (1999) 47–66.
[48] J.-C. Dubacq, B. Durand, E. Formenti, Kolmogorov complexity and cellular automata classification, Theoret. Comput. Sci. 259 (1–2) (2001) 271–285.
[49] N. Fatès, Experimental study of elementary cellular automata dynamics using the density parameter, in: M. Morvan, É. Rémila (Eds.), Discrete Models for Complex Systems—DMCS03, vol. AB, 2003, pp. 155–166, Discrete Mathematics Theoretical Computer Science.
[50] S. Maerivoet, B. De Moor, Traffic Flow Theory, 05-154, Katholieke Universiteit Leuven, Department of Electrical Engineering ESAT-SCD (SISTA), July 2005.
[51] K. Nagel, P. Wagner, R. Woesler, Still flowing: old and new approaches for traffic flow modeling, Oper. Res. 51 (5) (2003) 681–710.
[52] A. Schadschneider, Statistical physics of traffic flow, Physica A (285) (2000) 101.
[53] A. Schadschneider, Traffic flow: a statistical physics point of view, Physica A 313 (2002) 153–187.
[54] M. Schreckenberg, R. Barlović, W. Knospe, H. Klüpfel, Statistical physics of cellular automata models for traffic flow, in: K.H. Hoffmann, M. Schreiber (Eds.), Computational Statistical Physics, Springer, Berlin, 2001, pp. 113–126.
[55] K. Nagel, D.E. Wolf, P. Wagner, P. Simon, Two-lane traffic rules for cellular automata: A systematic approach, Phys. Rev. E 58 (2) (1998) 1425–1437.
[56] G.F. Newell, A moving bottleneck, Transport. Res. B 32B (8) (1998) 531–537.
[57] B.S. Kerner, The Physics of Traffic—Empirical Freeway Pattern Features, Engineering Applications, and Theory, Understanding Complex Systems, Springer, 2004 (ISBN 3-540-20716-3).
[58] K. Nagel, P. Nelson, A critical comparison of the kinematic-wave model with observational data, in: H.S. Mahmassani (Ed.), Proceedings of the 16th International Symposium on Transportation and Traffic Theory (ISTTT16), University of Maryland, 2005.
[59] D. Chowdhury, A. Pasupathy, S. Sinha, Distributions of time- and distance-headways in the Nagel–Schreckenberg model of vehicular traffic: effects of hindrances, Eur. Phys. J. B Condens. Matter 5 (3) (1998) 781–786.
[60] S. Maerivoet, B. De Moor, Non-concave fundamental diagrams and phase transitions in a stochastic traffic cellular automaton, Eur. Phys. J. B—Condens. Matter Phys. 42 (1) (2004) 131–140.
[61] M. Cremer, J. Ludwig, A fast simulation model for traffic flow on the basis of boolean operations, Math. Comput. Simul. 28 (4) (1986) 297–303.
[62] H. Schütt, Entwicklung und Erprobung eines sehr schnellen, bitorientierten Verkehrssimulationssystems für Straßennetze, Technical Report No. 6, Schriftenreihe der AG Automatisierungstechnik, T.U. Hamburg, Hamburg, 1991.
[63] K. Nagel, High-speed microsimulations of traffic flow, Ph.D. Thesis, Universität zu Köln, March 1995.
[64] M. Fukui, Y. Ishibashi, Traffic flow in 1D cellular automaton model including cars moving with high speed, J. Phys. Soc. Jpn. 65 (6) (1996) 1868–1870.
[65] C.F. Daganzo, In traffic flow, cellular automata = kinematic waves, UCB-ITS-RR-2004-05, Institute of Transportation Studies, University of California at Berkeley, October 2004.
[66] G.F. Newell, Delays caused by a queue at a freeway exit ramp, Transport. Res. B 33B (1999) 337–350.
[67] K. Nagel, H.J. Herrmann, Deterministic models for traffic jams, Physica A (199) (1993) 254.
[68] W. Brilon, N. Wu, Evaluation of cellular automata for traffic flow simulation on freeway and urban streets, in: Traffic and Mobility: Simulation-Economics-Environment, Institut für Kraftfahrwesen, RWTH Aachen, Duisburg, 1999, pp. 163–180.
[69] S. Krauß, K. Nagel, P. Wagner, The mechanism of flow breakdown in traffic flow models, in: Proceedings of the International Symposium on Traffic and Transportation Theory (ISTTT99), Jerusalem, 1999.
[70] K. Nagel, Life-times of simulated traffic jams, Int. J. Mod. Phys. C 5 (3) (1994) 567–580.
[71] A. Schadschneider, The Nagel–Schreckenberg model revisited, Eur. Phys. J. B 10 (3) (1999) 573–582.
[72] K. Ghosh, A. Majumdar, D. Chowdhury, Distribution of time-headways in a particle–hopping model of vehicular traffic, Phys. Rev. E 58 (3) (1998) 4012–4015.
[73] K. Nagel, M. Paczuski, Emergent traffic jams, Phys. Rev. E 51 (4) (1995) 2909–2918.
[74] P. Bak, C. Tang, K. Wiesenfeld, Self-organized criticality, Phys. Rev. A 38 (1988) 368.

[75] D.L. Turcotte, Self-organized criticality, Rep. Prog. Phys. 62 (1999) 1377–1429.
[76] K. Nagel, S. Rasmussen, Traffic at the edge of chaos, in: R.A. Brooks, P. Maes (Eds.), Artificial Life IV: Proceedings of the Fourth International Workshop on the Synthesis and Simulation of Living Systems, 1994, p. 222.
[77] B.-H. Wang, Y.-R. Kwong, P.-M. Hui, Statistical mechanical approach to Fukui–Ishibashi traffic flow models, Phys. Rev. E 57 (3) (1998) 2568–2573.
[78] L. Wang, B.-H. Wang, B. Hu, A cellular automaton traffic flow model between the Fukui–Ishibashi and Nagel–Schreckenberg models, Traffic Forum—Statistical Mechanics, February 2001.
[79] K. Lee, P. Hui, D. Mao, B.-H. Wang, Q.-S. Wu, Fukui–Ishibashi traffic flow models with anticipation of movement of the car ahead, J. Phys. Soc. Jpn. 71 (7) (2002) 1651–1654.
[80] B. Derrida, E. Domany, D. Mukamel, An exact solution of a one-dimensional asymmetric exclusion model with open boundaries, J. Statist. Phys. 69 (1992) 667–687.
[81] A.B. Kolomeisky, G.M. Schütz, E.B. Kolomeisky, J.P. Straley, Phase diagram of one-dimensional driven lattice gases with open boundaries, J. Phys. A: Math. Gen. 31 (1998) 6911–6919.
[82] B.D. Greenshields, A study of traffic capacity, Highway Research Board Proceedings, vol. 14, 1935, pp. 448–477.
[83] H. Emmerich, E. Rank, An improved cellular automaton model for traffic flow simulation, Physica A 234 (1997) 676–686.
[84] B. Eisenblätter, L. Santen, A. Schadschneider, M. Schreckenberg, Jamming transition in a cellular automaton model for traffic flow, Phys. Rev. E 57 (1998) 1309–1314.
[85] C. Kayatz, Stability analysis of traffic flow models, Master's Thesis, Eidgenössische Technische Hochschule in Zürich, August 2001.
[86] D. Jost, Breakdown and recovery in traffic flow models, Master's Thesis, Department of Computer Science, ETH Zürich, August 2002.
[87] D. Jost, K. Nagel, Probabilistic traffic flow breakdown in stochastic car following models, in: Transportation Research Board Annual Meeting, Washington DC, 2003, paper 03-4266.
[88] J. Werth, Galilei-invariante Fahrzeugwechselwirkungen im Straßenverkehr, Master's Thesis, Duisburg University, Duisburg, Germany, 1998.
[89] M. Takayasu, H. Takayasu, $1/f$ noise in a traffic model, Fractals 1 (4) (1993) 860–866.
[90] M. Fukui, Y. Ishibashi, Effect of delay in restarting of stopped cars in a one-dimensional traffic model, J. Phys. Soc. Jpn. 66 (2) (1997) 385–387.
[91] A. Schadschneider, M. Schreckenberg, Traffic flow models with 'slow-to-start' rules, Ann. Phys. 6 (7) (1997) 541–551.
[92] S.C. Benjamin, N.F. Johnson, P. Hui, Cellular automata models of traffic flow along a highway containing a junction, J. Phys. A: Math. Gen. 29 (1996) 3119–3127.
[93] T. Bellemans, Traffic control on motorways, Ph.D. Thesis, Katholieke Universiteit Leuven, Department of Electrical Engineering ESAT-SCD (SISTA), May 2003.
[94] A. Hegyi, B.D. Schutter, J. Hellendoorn, S. Hoogendoorn, C. Tampère, Gelijke behandeling voor verkeersstroommodellen, Verkeerskunde 52 (4) (2001) 32–36.
[95] R. Barlović, L. Santen, A. Schadschneider, M. Schreckenberg, Metastable states in cellular automata for traffic flow, Eur. Phys. J. B5 (793).
[96] R. Barlović, Traffic jams—cluster formation in low-dimensional cellular automata models for highway and city traffic, Ph.D. Thesis, Universität Duisburg-Essen, Standort Duisburg, October 2003.
[97] R. Barlović, T. Huisinga, A. Schadschneider, M. Schreckenberg, Open boundaries in a cellular automaton model for traffic flow with metastable states, Phys. Rev. E 66 (4) (2002) 6113–6123.
[98] S. Grabolus, Numerische Untersuchungen zum Nagel-Schreckenberg-Verkehrsmodell und dessen Varianten, Master's Thesis, Institut für Theoretische Physik, Universität zu Köln, 2001.
[99] S. Maerivoet, B. De Moor, Advancing density waves and phase transitions in a velocity dependent randomization traffic cellular automaton, 03-111, Katholieke Universiteit Leuven, October 2004.
[100] S. Maerivoet, Traffic Cellular Automata, Java software tested with JDK 1.3.1, URL: http://smtca.dyns.cx (2004).
[101] S. Krauß, P. Wagner, C. Gawron, Metastable states in a microscopic model of traffic flow, Phys. Rev. E 55 (304) (1997) 5597–5602.
[102] J. del Río, M. Lárraga, Transient situations in traffic flow: modelling the Mexico City Cuernavaca Highway, January 2005.
[103] T. Tokihiro, D. Takahashi, J. Matsukidaira, J. Satsuma, From soliton equations to integrable cellular automata through a limiting procedure, Phys. Rev. Lett. 76 (18) (1996) 3247–3250.
[104] K. Nishinari, Euler and Lagrange representation of traffic models, in: Proceedings of the Workshop on Traffic and Granular Flow '01, Nagoya University, Japan, 2001.
[105] J. Matsukidaira, K. Nishinari, Euler–Lagrange correspondence of cellular automaton for traffic-flow models, Phys. Rev. Lett. 90 (2003) 088701.
[106] K. Nishinari, D. Takahashi, A new deterministic ca model for traffic flow with multiple states, J. Phys. A: Math. Gen. 32 (1999) 93–104.
[107] K. Nishinari, A Lagrange representation of cellular automaton models of traffic flow, J. Phys. A: Math. Gen. 34 (2001) 10727–10736.
[108] H. Emmerich, T. Nagatani, K. Nakanishi, From modified Korteweg–de Vries equation to a second-order cellular automaton for traffic flow, Physica A 254 (1998) 548–556.
[109] K. Nishinari, M. Fukui, A. Schadschneider, A stochastic cellular automaton model for traffic flow with multiple metastable states, J. Phys. A: Math. Gen. 37 (2004) 3101–3110.
[110] C. L. Barrett, S. Eubank, K. Nagel, S. Rasmussen, J. Riordan, M. Wolinsky, Issues in the representation of traffic using multi-resolution cellular automata, LA-UR-95:2658, Los Alamos National Laboratory, TRANSIMS Report Series (1995).
[111] D. Helbing, M. Schreckenberg, Cellular automata simulating experimental properties of traffic flow, Phys. Rev. E 59 (1999) 2505–2508.
[112] W. Knospe, L. Santen, A. Schadschneider, M. Schreckenberg, Towards a realistic microscopic description of highway traffic, J. Phys. A: Math. Gen. 33 (2000) 477–485.
[113] W. Knospe, Synchronized traffic—microscopic modeling and empirical observations, Ph.D. Thesis, Universität Duisburg, June 2002.

[114] B. Kerner, S. Klenov, Microscopic theory of spatial-temporal congested traffic patterns at highway bottlenecks, Phys. Rev. E 68 (3).
[115] B.S. Kerner, S.K. Klenov, D.E. Wolf, Cellular automata approach to three-phase traffic theory, J. Phys. A: Math. Gen. 35 (2002) 9971–10013.
[116] T. Nagatani, Self-organization and phase transition in traffic-flow model of a two-lane roadway, J. Phys. A: Math. Gen. 26 (1993) 781.
[117] T. Nagatani, Traffic jam and shock formation in stochastic traffic-flow model of a two-lane roadway, J. Phys. Soc. Jpn. 63 (1994) 52.
[118] M. Rickert, K. Nagel, M. Schreckenberg, A. Latour, Two lane traffic simulations using cellular automata, Physica A 231 (1996) 534.
[119] P. Wagner, K. Nagel, D.E. Wolf, Realistic multi-lane traffic rules for cellular automata, Physica A 234 (1997) 687–698.
[120] P. Simon, H. Gutowitz, A cellular automaton model for bi-directional traffic, Phys. Rev. E 57 (2) (1998) 2441–2444.
[121] P. Gundaliya, V. Tom, S. Dhingra, Heterogeneous traffic flow modelling using cellular automata for an arterial, in: Proceedings of the Sixth International Workshop on Transportation Planning and Implementation Methodologies for Developing Countries (TPMDC04), Transportation Systems Engineering, IIT Bombay, 2004.
[122] C. Mallikarjuna, K. Ramachandra Rao, Traffic flow modelling on highways using cellular automata: A review, in: J. Bandyopadhyay, B. Maitra (Eds.), Proceedings of International Conference on Structural and Transportation Engineering (START05), Elite Publishing House, New Delhi, 2005, pp. 912–919.
[123] D. Helbing, B. Huberman, Coherent moving states in highway traffic, Nature 396 (738) (1998) 738–740.
[124] O. Biham, A.A. Middleton, D. Levine, Self-organization and a dynamical transition in traffic-flow models, Phys. Rev. A 46 (10) (1992) R6124–R6217.
[125] O. Angel, A.E. Holroyd, J.B. Martin, The Jammed Phase of the Biham–Middleton–Levine Traffic Model, March 2005.
[126] M. Fukui, Y. Ishibashi, Evolution of traffic jam in traffic flow model, J. Phys. Soc. Jpn. 62 (11) (1993) 3841–3844.
[127] J. Freund, T. Pöschel, A statistical approach to vehicular traffic, Physica A 219 (1995) 95–113.
[128] Y. Shi, Self-organization in BML traffic flow model: Analytical approaches, Commun. Theor. Phys. 31 (1999) 85–90.
[129] D. Chowdhury, A. Schadschneider, Self-organization of traffic jams in cities: effects of stochastic dynamics and signal periods, Phys. Rev. E 59 (2) (1999) 1311–1314.
[130] J. Esser, M. Schreckenberg, Microscopic simulation of urban traffic based on cellular automata, Int. J. Mod. Phys. C 8 (5) (1997) 1025–1036.
[131] P. Simon, K. Nagel, Simplified cellular automaton model for city traffic, Phys. Rev. E 58 (2) (1998) 1286–1295.
[132] G. Diedrich, L. Santen, A. Schadschneider, J. Zittartz, Effects of on- and off-ramps in cellular automata models for traffic flow, Int. J. Mod. Phys. C 11 (2) (2000) 335–345.
[133] H. Fukś, N. Boccara, Generalized deterministic traffic rules, Int. J. Mod. Phys. C 9 (1998) 1–12.
[134] H. Fukś, Exact results for deterministic cellular automata traffic models, Phys. Rev. E 60 (1999) 197–202.
[135] H. Fukś, N. Boccara, Convergence to equilibrium in a class of interacting particle systems evolving in discrete time, Phys. Rev. E 64 (1) (2001) 016117.
[136] H. Fukś, Critical behaviour of number-conserving cellular automata with nonlinear fundamental diagrams, J. Statist. Mech. Theory Exper. (5) (2004) p07005.
[137] N. Boccara, H. Fukś, Critical behavior of a cellular automaton highway traffic model, J. Phys. A: Math. Gen. 33 (2000) 3407–3415.
[138] N. Rajewsky, A. Schadschneider, M. Schreckenberg, The asymmetric exclusion model with sequential update, J. Phys. A 29 (1996) 305–309.
[139] M. Schreckenberg, A. Schadschneider, K. Nagel, N. Ito, Discrete stochastic models for traffic flow, Phys. Rev. E 51 (4) (1995) 2939–2949.
[140] A. Schadschneider, M. Schreckenberg, Garden of Eden states in traffic models, J. Phys. A 31 (1998) 225–231.
[141] A. Schadschneider, M. Schreckenberg, Car-oriented mean-field theory for traffic flow models, J. Phys. A 30 (1997) 69–75.
[142] A. Schadschneider, Analytical approaches to CA for traffic flow: Approximations and exact solutions, in: M. Schreckenberg, D. Wolf (Eds.), Proceedings of the Workshop on Traffic and Granular Flow '97, Springer, Berlin, 1997.
[143] Y. Georget, A Game of Life in C for X11, March 2002.